A STATISTICAL ANALYSIS OF PULSAR EVOLUTION

By

Fraser Ivor Gordon

Thesis

submitted to the

University of Glasgow

for the degree of

Ph.D.

Department of Physics and Astronomy

University of Glasgow

Glasgow

G12 8QW

Scotland

September 1990

ProQuest LLC.
789 East Eisenhower Parkway
P.O. Box 1346
Ann Arbor, MI 48106 – 1346

To my Father and Mother,

for everything.

You came upon me carving some little figure out of wood and you said 'Why don't you make something for me?'

I asked you what you wanted, and you said, 'A box.'

'What for?'

'To put things in.'

'What things?'

'Whatever you have,' you said.

Well, here's your box. Nearly everything that I have is in it, and it is not full. Pain and excitement are in it, and feeling good or bad and evil thoughts and good thoughts - the pleasure of design and some despair and the indescribable joy of creation.

And on top of these are all the gratitude and love I have for you.

And still the box is not full.

John Steinbeck

'East of Eden'

[Mandarin (1990)]

SUMMARY

Since the discovery of pulsars, and their identification with magnetised neutron stars, a vast amount of observational and theoretical effort has been directed at increasing our understanding of these objects. Not only do we study the basic physical processes at work behind the generation of the pulses [Ruderman(1979), Michel(1982) and refs. therein], but also the structure of the interior and crust of the neutron star [Greenstein(1975),Pines(1987)], the influence of a pulsar on a supernova remnant [Radhakrishnan(1982 and 1986), Pacini and Salvati(1987)] and the manner in which pulsars evolve. [Gunn and Ostriker(1970), Lyne et al(1985), Candy and Blair(1983),(1986), Chevalier and Emmering(1986), Narayan(1987) and Cheng(1989)]. It is this latter topic with which this thesis is concerned. Since our observed sample of pulsars now numbers over 500 we can use statistical methods to try and gain information from the accumulated data, which is extensive, since many different pulsar properties can be estimated or derived from the large observational database.

The observed population is primarily local, as most objects are visible due to their proximity to the Sun. The existence of a much larger galactic population is not doubted, and thus it is the properties of this parent distribution of pulsars that are primarily of interest. To infer such knowledge from a limited data sample requires identification and correct application of the selection effects responsible for limiting the available sample to that which is observed. This is an inherently statistical problem, and requires us to consider the pulsar population by means of a mathematical distribution function in the properties of pulsars (e.g. period, magnetic field). This replaces the discreteness of

the data by a continuous function. One cannot treat selection on an individual pulsar-to-pulsar basis, but only for the ensemble of observed objects.

In this thesis, this approach is exploited fully, and the time-dependent continuity equation in the pulsar distribution function is used as a starting point. This is solved, for a given evolutionary model, selection effects are applied, and the result is a predicted distribution for the observed pulsars in the $P,\dot{P}$ diagram. This is a new technique and although it reproduces the results of some other authors, is fundamentally superior in that it makes no assumption regarding the stationarity of the pulsar population, and is more logical in approach. The conventional stationarity argument assumes that the pulsar population is in a steady-state such that the birthrate equals the deathrate at all times. This is a restrictive constraint which can be shown to be not necessarily justifiable.

In Chapter 1 we introduce the basics of pulsar history, observations and terminology. The identification of pulsars with neutron stars is explained, then the various observational means of determining pulsar properties are dealt with. Next the nature and importance of selection effects are explained in turn, before an overview of the main observational data and a discussion of the outstanding features of these data.

The standard models for pulsar evolution are introduced in Chapter 2, through a review and criticism of the major, landmark papers such as Gunn and Ostriker(1970), Lyne, Manchester and Taylor(1985), Candy and Blair(1983),(1986), and Narayan(1987). This puts into context the nature of and difficulty with pulsar evolutionary problems.

Chapter 3 begins with a justification for the time-dependent nature

of our work, which is jointly a criticism of the inadequacies of the time-independent argument, and an exposition of the potential merits to be gained from abandoning the ubiquitous notion of stationarity. Then the continuity equation method is introduced and the means of solution described. The technique is next demonstrated by developing four simple models in the time-dependent approach, two with and two without field decay. These show the power of the method, the critical influence of selection effects and challenges some preconceived notions concerning the steady-state ideas. This work is not intended to reproduce the observational data but to be primarily demonstrative.

It is also shown in Chapter 3 how interesting inverse problems arise from the application of our method to simple models, and these can in principle be solved to yield information on the source distribution of intrinsic pulsar properties.

Thus it is possible to treat the first major model in Chapter 4. This is a model with no field decay and no alignment. Using the time-dependent method, we derive the $P,\dot{P}$ distribution predicted by this model. This is then compared with the observed $P,\dot{P}$ diagram using the chi-squared goodness-of-fit test. This test will be applied to all models in turn. This is similar to the work of Cheng(1989) but more analytically explicit. The flaws of not treating the data in this fashion can be exposed with this first model. This fails to provide a satisfactory fit to the joint $P,\dot{P}$ distribution but can account for the period histogram alone. Thus accepting a model on the basis of the good fit to the P distribution would be fallacious, since it cannot explain the more important joint distribution.

The field-decay type of model is examined in Chapter 5. Exponential decay of the magnetic field is the 'standard' explanation of pulsar

evolution by most authors. In our model, which is more detailed than those of Gunn and Ostriker(1969), Chevalier and Emmering(1986) and Lyne et al(1985), it is found that an acceptable fit can be made to the $P,\dot{P}$ diagram. A discussion of magnetic field decay of a neutron star is also included.

In Chapter 6 an alignment model is presented. By alignment, it is conventional to refer to the scenario where magnetic and rotation axes tend to align as time passes (alignment angle tends to 0°.) This features a new development, the beaming fraction (which represents the proportion of pulsars rendered invisible by geometrical orientation) now becomes period-dependent, since nearly-aligned (older) pulsars are harder to detect than others. To model this correctly requires a development of the formalism of Proszynski(1979) which has been absent from the literature. This links up with the use of the pulsewidth data as a diagnostic for pulsar evolution. It is found that an acceptable fit to the $P,\dot{P}$ diagram is again found for the alignment model. To attempt to further distinguish between field decay and alignment models it is proposed to utilise the information in the pulsewidth distribution, following the work of Candy and Blair(1983 and 1986). The predicted distribution of pulsewidths in the alignment model is found, but this does not resemble in detail the observed distribution. Similarly, the distribution of pulsewidths in the case where the angles do not evolve is derived.

The final chapter contains the conclusions of the thesis and ideas for topics of future research. These include the use of inverse problems in pulsar work, the development of a counter-alignment model, the application of the time-dependent continuity equation method to the problem of the cooling rates of white dwarf stars and inclusion of

positional coordinates in our method to model the migration of pulsars away from the galactic plane, including selection effects. A final interesting area of study would be the use of the time-dependent method to study a starburst scenario (all pulsars created in a short time interval), which can only be done using a time dependent method, as clearly no steady state in the observed pulsar population will result in this case.

PREFACE

This thesis is concerned with the question of radio pulsar evolution, that is explaining from theoretical considerations the form of the observed scatter plot of period and period derivative, the so-called $P,\dot{P}$ diagram. For this objective, a new method of deriving the predicted distribution of pulsar parameters such as P and $\dot{P}$ has been devised. It was found from existing literature that previous work was unsatisfactory either through an improper treatment or ignorance of selection effects, which we shall show to be extremely important, or utilised techniques that were difficult to follow or possibly inconsistent, to derive the pulsar birthrate, for example. The birthrate is an important prediction of any model, and is of wider astrophysical interest through its significance for galactic metal abundances and the strength and origin of the neutron star population.

All previous treatments had made the assumption that pulsar lifetimes were short enough that the population would be in a steady state. Our method, based on the solution of the time-dependent continuity equation in the pulsar distribution function, makes no such assumption, is logical in development and allows easy yet rigorous inclusion of the effects of selection. We use this method to develop different models of pulsar evolution which are compared statistically against the observed data to assess their relevance.

The work of Chapter 3 has been submitted as a paper to 'Astronomy and Astrophysics', entitled "On the evolution and birthrate of radio pulsars." It is intended to publish the work of Chapters 4-6 in the near future.

I am very grateful to Dr. Andrew Lyne of Jodrell Bank who kindly sent me a copy of his pulsar data catalogue, following a visit to

Glasgow University in 1987. Without his cooperation the work of this thesis would probably not have been possible.

The work of this thesis was carried out in the Department of Physics and Astronomy at Glasgow University, when the author was a postgraduate student in the astronomy group from October 1986 to August 1990. I must thank the head of this group, Prof. J.C. Brown for his guidance and supervision throughout this period, and for reading the thesis prior to submission. I am also indebted to Daphne, our hard-working secretary, who in addition to keeping the supplies of tea and coffee available, also has dealt with a multitude of assorted problems that I bothered her with.

My grateful thanks and appreciation go to John Simmons, my supervisor, who provided a steady stream of ideas and suggestions, some dreadful puns, and read through the draft version of this work. Good luck with the book John, I look forward to the sequel 'B.T.B.W.J.S.', due out in 2017 A.D., along with the squash ladder.

I would like to gratefully acknowledge the support of the Carnegie Trust for the Universities of Scotland, who provided a three-year scholarship which enabled me to carry out this research, and also the Computing Service of Glasgow University for their assistance.

I thank the members of the Astronomy Group for their friendship and numerous helpful discussions, especially Alec who started the interest in pulsars in the first instance, Prof. Sweet for ideas and expertise, Geoff who was always keen to visit the pub and in no particular order the Waster, the Whinger, the Slurper, The Quiet Man and The Turk.

Finally I must thank Laura for her love and companionship, and for encouragement and realism when the best-laid schemes were not going exactly as planned.

CONTENTS

CHAPTER 1

INTRODUCTION AND REVIEW OF OBSERVATIONS

1.1 INTRODUCTION

In this introductory Chapter we will outline a brief history of pulsar observations, recount the initial identification of pulsars with neutron stars and outline the observational characteristics associated with this class of objects. The nature of the selection effects that limit our ability to observe the pulsar population is then discussed, prior to an overview of the main features of the observational data. Finally, we outline why pulsars are important and interesting to study, and summarise the objectives of this thesis.

1.2 HISTORY OF PULSAR DISCOVERIES

The first pulsars were discovered in 1967 at Cambridge by Hewish and Bell (Hewish et al(1968)) during a study of radio scintillation associated with quasar surveys and detection. The pulsars appeared as unresolved, broadband sources of highly periodic radio emission, at high frequencies around 400 MHz, with a distribution on the sky that showed them to be primarily a galactic disc population with a scale height of $\approx$ 600 parsecs [see e.g. Narayan(1987), Morini(1981), Gailly et al (1978)] similar to O-type stars, and the majority could not be associated with any known objects.

Most of the ~ 500 presently known pulsars were detected in one of a number of major surveys, carried out at Jodrell Bank, Arecibo, Molonglo and Green Bank [Stokes et al(1986), Dewey et al(1985), Dewey et al (1988), Davis et al(1985), Damashek et al(1982), Large and Vaughan(1977) and Clifton and Lyne(1986)]. Depending on the aims and constraints of each survey and varied observing techniques, these were sensitive to different areas of the sky, different period ranges

or particular types of pulsar.

The first pulsar discovered to coincide with a known object was PSR0532 in the Crab nebula which could be identified with the famous 'south-proceeding star' which had been observed at optical frequencies. Here '0532' refers to the right ascension of the pulsar, the full name including the declination as well. Under this universally accepted scheme the Crab pulsar becomes PSR0532+21. The Crab and Vela pulsars were amongst the first to be discovered [PSR0531+21 and PSR0833-45] and were identified as the power sources in the respective nebulae. However, only four pulsars have been found with a definite association with supernova remnants, and approximately 90% of all supernova remnants show no evidence for central pulsar activity. [Kassim and Weiler(1990)].

The first binary pulsar was discovered in 1974 [PSR1913+16, Hulse and Taylor(1975)] with an orbital period of under 8 hours. This system was soon realised to be an important 'laboratory' for testing general relativistic predictions which were impossible terrestrially, e.g. testing of orbital periastron precession due to highly accurate pulse timing measurements. It was also possible to accurately estimate the neutron star masses. Eventually this system was identified as a progenitor for a possibly important source of gravitational waves in the Universe [Schutz(1987),Schutz(1989)]. There are now thirteen binary pulsars [Lyne(1989)], and they typically have periods much shorter than those of single radio pulsars.

A millisecond pulsar [PSR1937+21] was discovered in 1982 [Backer et al(1982)] with a period of only 1.56ms. This is still the 'fastest' known pulsar. Its discovery aroused great excitement in the astronomical community since its low period could be used to infer properties of

neutron star behaviour and its spin-down rate was unprecedently low, making it an exceptionally reliable 'cosmic clock' [Taylor(1987)].

The most recent developments include the search for a pulsar in the aftermath of SN1987A in the Large Magellanic Cloud, which, if discovered, would be the youngest neutron star observed, and allow unique insight to the first stages of pulsar evolution and the interaction with the surrounding nebula. Also a unique pulsar [PSR1957+20] nicknamed the 'black widow' pulsar has been found which is an eclipsing binary pulsar, but appears to be ablating its binary companion through its own energetic output as the companion attempts to accrete matter onto the pulsar surface [Michel(1989)].

1.3 PULSARS AS NEUTRON STARS

Work in the field of pulsar evolution could be said to have commenced with the papers of Gold(1969) and Gunn and Ostriker(1969), which identified the pulsars as rotating, magnetised neutron stars, although a pre-discovery paper by Pacini (1968) had suggested an energetic neutron star as the power source for the Crab Nebula. The observations of a wide range of periods, and small, but steady positive period derivatives implying slow spin-down of the star, could rule out alternative candidates such as white dwarfs and binary objects. This was because the period range was incompatible with vibrational excitation frequencies predicted for both neutron stars and white dwarfs, and the period derivatives were positive rather than the negative values required for binary motion. The Crab pulsar also appeared to provide a means of supplying energy to the surrounding nebula, and its inferred spindown luminosity $I\omega\dot{\omega}$ (with $\omega = 2\pi/\text{Period}$) closely matched the observed output of the supernova remnant, for the canonical value of moment of inertia I expected for a neutron star.

Assuming that magnetic dipole radiation was the mechanism by which the star was losing rotational energy led to a magnetic field strength of $\sim 10^{12}$ Gauss, again consistent with values estimated from flux-conservation during collapse of a progenitor star.

The possibility of creating neutron stars in supernovae had been raised by Baade and Zwicky (1934) but not until then considered seriously. This interpretation of pulsars gained considerable support both observationally and theoretically as subsequent discoveries of new objects added to the data set, and major papers by Ostriker and Gunn(1969), and Gunn and Ostriker(1970) showed how the basic features of pulsar behaviour could be explained under an extended version of the Gold/Pacini model. Despite being based on a paucity of data (see later) this interpretation was largely reinforced rather than contradicted as more pulsars were discovered.

1.4 OBSERVATIONAL CHARACTERISTICS

1.4.1 Periods and period derivatives.

The primary characteristic observable was the period P of each pulsar, which had a very high stability when averaged over a number of cycles. The periods of the first pulsars were found to be in range 33ms (Crab) up to a few seconds. Timing measurements on the arrival times of the actual pulses soon revealed that the periods of the pulsars were in fact increasing steadily and a period derivative ($\dot{P}$) could be defined and measured, if sufficient observational data were available to eliminate contributions from the Earth's motion etc. The periods were found to be lengthening at a slow rate, of the order of nano-seconds per year but $\dot{P}$ varied over several decades in size for the observed population. The information obtained from such studies is best displayed in the form of a scatter plot of $\dot{P}$ against P , the

so-called P,$\dot{P}$ diagram. [Figure 1.1]. The content of this will be discussed in Section 1.6. Histograms of the period and period derivative data are shown in Figures 1.2 and 1.3 respectively.

If it is assumed that a pulsar moves through space at a constant velocity, then $\dot{P}$ is a true measure of its spin-down rate. There is some doubt over the accuracy of this for globular cluster pulsars where the density of stars is much higher, and spurious $\dot{P}$ values may be observed, due to the gravitational acceleration of the pulsar and the resulting Doppler contribution to the observed period and period derivative. A recent measurement of a negative $\dot{P}$ [Wolszczan(1989)] casts doubt [Lyne(1989d)] over our ability to know the true spindown behaviour of globular cluster pulsars.

1.4.2 Pulse profiles, pulsewidths and polarisation.

Although individual pulses may vary in shape as they arrive, the overall long-term average is found to be characteristic of the pulsar, and its properties can be studied. It is fair to say that pulse profiles are as individual as fingerprints, in that no two appear to be identical. [Lyne and Manchester(1988)]. These pulse profiles have widths (usually measured at 10% or 50% of the peak intensity) which are small compared to the pulsar period, hence the duty cycles, defined as the ratio of pulsewidth to period, are typically a few per cent.(Henry and Paik(1969), Prosynski(1979)). The observed distribution of pulsewidths is shown in Fig. 1.4.

Substantial degrees of linear polarisation have been observed (up to 50%) within the pulses, and the instantaneous plane of polarisation is found to vary smoothly across the profile, although many pulsars show complicated variations on this theme. This feature led Radhakrishnan and Cooke(1969) to propose a model for pulsar emission in a highly

directional beam of radiation centred on the magnetic polar cap of a rotating neutron star. The plane of polarisation then became related to the projected direction of the magnetic field at the point on the star directly on the line of sight. The outstanding consequence of this model was that for realistic parameters of the beam, the majority of hypothetical galactic observers would not in fact be able to observe the pulsar, since the cone would not sweep through all directions in space. This leads immediately to the concept of 'beaming fraction' (and its reciprocal, the beaming factor) which estimates which fraction of all such objects will be potentially observable to an observer due to the geometry of the source. Such estimates will clearly be relevant to evolutionary models, particularly if the beaming fraction depends on other pulsar parameters and is time-dependent. We shall return to the question of pulsewidths and their importance in Chapter 6.

1.4.3 Dispersion measures and distances.

The presence of free electrons in the interstellar medium allows the dispersion measures to be used as pulsar distance indicators, given a model for the electron distribution in the galaxy. The dispersion measure relates the delay in arrival time for one pulse observed at two frequencies to the integrated electron distribution along the line of sight and the two frequencies. The electron density can be estimated from distances for the few pulsars with independent estimates of their distances, from neutral hydrogen absorption data or by using the pulsars themselves to calibrate the interstellar distribution of free electrons. [Gailly et al(1978), Arnett and Lerche(1981), Harding and Harding(1984), Lyne et al (1985).]

1.4.4 Flux densities and spectra.

Most pulsars have spectral indices in the range [-2,-1] for the radio

portion of the spectrum. There is a turnover at the low frequency end. [Malofeev and Shitov(1981)]. Survey frequencies have to cope with increased background noise at lower frequencies and the fall in intensities at the high frequency, usually resulting in observing at 400 Mhz or so. The fluxes are typically of order 100 mJy, and the faintest pulsars usually have flux densities around 1-10mJy.

The only pulsars observed at other wavelengths are the Crab, Vela and PSR1509-58, all three embedded in supernova remnants. These have been detected in both x-ray and γ-ray wavelengths, and the first two also are optical pulsars.

1.4.5 Luminosities.

A luminosity can be defined as $L_{400} = S_{400}d^2$ where S_{400} is the flux density at 400 MHz and d the distance inferred for the pulsar. These luminosities were found to be several orders of magnitude less than the inferred 'spin-down' luminosity $L_{sd} = I\omega\dot{\omega}$ found from the observed period and period derivative, which showed that the pulse emission process did not contribute significantly to the overall energy budget of the neutron star. An alternative definition of luminosity, used by Manchester and Taylor(1977) involves the assumption of a beam size for the pulsar, but the most common usage is that defined as above.

1.4.6 Spatial distribution.

The observed pulsars form predominantly a local population. The majority of objects are clustered in the galactic plane, and a vertical scale height of $\triangleq$ 600 pc is typical for the observed sample. [See Morini(1981), Gailly et al (1978), Narayan(1987)]. See Taylor and Stinebring(1986) for plots of the pulsars in galactic coordinates, and the local distribution in the galactic plane.

1.4.7 Pulsar kinematics.

Although the pulsars had been identified as primarily a galactic disc distribution the distribution in galactic latitude suggested that pulsars were being expelled from the plane with unusually high velocities. The proper motions of several pulsars were observed by Lyne et al (1982) and they found that most of their sample were moving out of the plane at velocities of several hundreds of kms^{-1}. Other work by Cordes [Cordes(1986) and Cordes(1987)] using interstellar scintillation studies dealt with a larger sample but reached slightly different conclusions, especially regarding the number of low-velocity objects. The implications of these observations will be discussed in Section 1.6.7.

1.4.8 Pulsars and supernovae.

It is of interest to note that the pulsars thought to be the youngest are those associated with the remnants of the supernovae explosions that created the neutron star, but only 4 out of ≈ 300 galactic supernova remnants (SNRs) have visible pulsars, although approximately 10% show Crab-like 'plerion' structure indicating the possible presence of a pulsar which cannot otherwise be seen, due to the directional emission. The remainder, about 90% of the total, are shell-like and hollow in appearance and give no indication of rapidly rotating neutron stars at all, though a slowly rotating neutron star may not give rise to observable effects. Thus it is clear that not necessarily all supernovae create neutron stars, and in turn a neutron star may not be a pulsar. The estimated observed lifetime of an SNR is $\sim 10^{4-5}$ years and that for pulsars considerably longer such that most pulsars will not show evidence of their formation event. See Radhakrishnan and Srinivasan(1981).

1.4.9 Other pulsar phenomena.

There is in fact an astonishing diversity of observed pulsar phenomena. Certain pulsars were seen to 'glitch', i.e. discontinuously decrease their period before 'relaxing' to the previous value, by a process thought to be a neutron 'starquake', and a potentially fruitful means of probing the relatively unknown interior structure of neutron star. These 'pulsar glitches' [Boynton et al(1971), Reichley and Downs(1969),(1970), Papaliolos et al (1971), Scargle and Pacini(1971) and Radhakrishnan and Manchester(1969)] are not thought to affect the long-term evolution of the star. At the level of pulse micro-structure and pulse-shape morphology there are several puzzles to be solved, but since the pulse emission is not believed to be fundamental to the spin-down, we can ignore it in this work. It is intended to treat the large-scale behaviour of the pulsar, not the details of emission processes and pulse micro-structure. [See Section 1.8 for the objectives of this thesis.]

1.5 SELECTION EFFECTS

1.5.1 Introduction.

It should be emphasised at this stage that there is an important distinction between the intrinsic pulsar population in the galaxy and that which we infer from observations, which are subject to a variety of selection effects. This means that in general the observed sample is a statistically biased sample of the parent population, which in turn means that quantities of importance inferred for the observed sample (such as mean magnetic field, or typical pulse shape e.g.) will differ from those same quantities deduced by a hypothetical observer who can see all the pulsars in the galaxy. Therefore, to properly conduct an analysis of pulsar distributions requires rigorous treatment of

selection effects to correct for these biases and ensure our inferences are not spurious. [Vivekanand et al(1982), Narayan(1987), etc.] The main selection effects are the following.

1.5.2 The Malmquist Bias.

In Figure 1.5 luminosity is plotted against distance for the observed pulsars. At larger distances there is a clear tendency for only the most lumininous pulsars to be observed. This is a manifestation of the Malmquist Bias, an effect named after its discoverer, who noticed its importance in the field of stellar classification. It is also a serious obstacle to determining distances of galaxies in cosmology. It arises through the inability of telescopes to detect or record objects which are too faint to cross some flux threshold characteristic of that instrument. Thus any data samples from that telescope will be flux-limited, i.e. all objects will have greater than some minimum flux density. The principal effect of the Malmquist Bias is to raise the mean luminosity of the observed sample above the mean of the population as a whole. Of more relevance to the pulsar population is the associated bias that may be present in the period and period derivative data. This can arise if the luminosity depends on the period and period derivative, as proposed by several authors. [Proszynski and Przybcien(1984), Stollmann(1987b), Vivekanand and Narayan(1983)]. This means immediately that the $P,\dot{P}$ data for the sample of observed pulsars is biased away from the true, intrinsic distribution. A further consequence will be that any quantities estimated from P and $\dot{P}$, such as mean magnetic field strength, will also be unreliable indicators of the true typical value. The importance of this has not, we feel, been given sufficient attention in the literature.

1.5.3 Beaming effects.

As pointed out above, not all pulsars are potentially visible to a particular observer. The beaming fraction estimates the fraction of pulsars that are favourably orientated, and depends on the geometry of pulsar emission. If this geometry were to alter through a pulsar's lifetime by means of alignment (or counter-alignment) of magnetic and rotation axes, for example, then the beaming fraction will then be a variable quantity which must be accounted for in any analysis of evolution, by which we mean a theoretical prediction of the pulsar distribution in P and $\dot{P}$ which is subsequently compared statistically against the observations, see Section 1.8.

1.5.4 Survey sensitivity.

Different surveys obtained different sensitivities to pulsar detection, by virtue of different observational techniques, observing frequencies and sampling rates [Lyne(1989b)]. Also the background sky temperature varies with position and can degrade sensitivity to certain portions of the sky, particularly in the direction of the galactic centre. So the minimum flux threshold is not a constant for all samples, but depends on the survey in question. More details are discussed in Lyne et al(1985). This means that pulsars discovered by one survey may not have been found by a second survey in the same area of the sky, but with a different sensitivity.

1.5.5 Period-dependent selection.

There is an additional factor which inhibits detection of short period pulars and is a consequence of the standard detection methods employed by the major surveys. The observed pulsewidths are broadened due to a small time delay in the integration process and a period dependent factor of the form

$f = 1/(1 + 0.25/P^2)^{1/4}$ is introduced. [Lyne et al(1985)]. This effectively alters the beaming fraction obtained from purely geometrical considerations.

1.6 DISCUSSION OF THE OBSERVATIONAL DATA.

1.6.1 The $P,\dot{P}$ diagram.

The $P,\dot{P}$ diagram is shown in Fig. 1.1., for 368 pulsars with known $\dot{P}$ values. It is clear that there is a tendency for long-period pulsars to have smaller values of $\dot{P}$ but the large scatter in both P and $\dot{P}$ makes the overall correlation fairly small between $\dot{P}$ and P. The Pearson and Spearman correlation coefficients defined in Appendix A4 can be used to quantify this, and in fact it is found that the Pearson coefficient $\rho_1 = 0.30$, with associated probablity $p_1 = 2.4\times10^{-9}$, and Spearman's $\rho_2 = 0.06$, with $p_2 = 0.21$. , confirming our visual impressions. However, these are small correlation coefficients, indicating a weak dependence. The very small value of ρ_2 tells us that it is not unreasonable to assume that P and $\dot{P}$ are uncorrelated as a first approximation.

There are several salient features relevant to the question of evolution. Major papers studying the $P,\dot{P}$ diagram include Lyne et al (1985), Phinney and Blandford(1981), Lyne et al(1977), Radhakrishnan(1982), Van den Heuvel(1984) and Vivekand et al(1982). The pulsars found in the top left hand corner have some of the fastest periods and these also have the largest period derivatives, and are those which are seen to be associated with supernova remnants. These also are the most 'active' objects, since they can be observed at other wavelengths. There are no pulsars found in the bottom right and it is possible to draw a line separating this region from the occupied area of the diagram, the 'deathline' as it is commonly called. This has been argued to be a threshold for pulse production to cease,

such that 'dead' pulsars occupy the region below the deathline. [Ruderman and Sutherland(1975) and Stollmann(1987)].

There are also a number of pulsars with short periods and low spin-down rates which occupy the lower left corner. It seems significant that the majority of these are binary pulsars and have possibly undergone a different evolutionary history from the standard pulsars in the rest of the $P,\dot{P}$ plane. [Alpar et al(1982), Van den Heuvel(1984)]. It is possible that these pulsars, having spun down conventionally, were 'resurrected' by undergoing a spin-up phase during which they increased their angular momentum by accreting matter from their less massive companion stars. The eventual demise of the companion resulted in a fast pulsar orbiting another compact object. The binary nature of these objects is inferred from the timing observations- a regular Doppler variation in the value of $\dot{P}$ reveals the presence of an unseen orbiting companion. It would be dangerous to assume that the binary pulsars could be easily explained by the same theory that governs the single objects, since they may have experienced a completely different evolutionary history.

The millisecond pulsar lies to the bottom left of the diagram, with the fastest period of 1.56 msec. PSR1953+29 has the smallest $\dot{P}$ of $\triangleq 10^{-20}$ ss^{-1}, and is a binary pulsar.

1.6.2 The luminosity data.

The data for L_{400} (as defined in Section 1.4.5) are displayed in a histogram in Fig. 1.6. There is a large spread of 4 decades in the values. A median value of ~100 mJykpc^2 is found for this sample. The alternative definition used by Manchester and Taylor(1977), using an assumed circular conical beam, giving L, can be compared directly by plotting the two values against one another, as in Fig.1.7. There is good agreement, the correlations for the sample of 301 objects being $\rho_1 = 0.95$ and $\rho_2 = 0.95$ (Pearson and Spearman coefficients), both highly significant.

There has been some discussion in the literature over the discrimination of pulsars into two types, often based on the luminosity histogram, which shows a 'deficit' of pulsars at $\log(L \text{ ergs}^{-1}) \triangleq 27.5$. Pineault (1986) and other authors have argued that this is evidence of two classes of pulsars with differing luminosity characteristics. Since we do not know what shape of distribution to expect for luminosity data, we prefer to treat all pulsars as a single class, and expect a more complete sample will remove any curious artefacts from the data histogram, or confirm the 'two-population' hypothesis.

We should note at this point the somewhat arbitrary definition of pulsar luminosities. It is not possible to know for sure the actual power output of any pulsar, but L_{400} gives an approximate estimate of it. The uncertainties in the distance estimates carry forward to the luminosity values too.

We have argued above that the flux-limited nature of pulsar surveys will introduce a bias to the observed data, which will have to be corrected for in all conclusions we reach based on the known pulsar sample. This can be demonstrated very easily with a simple example.

1.6.3 Demonstration of the Malmquist bias.

We can demonstrate the effect of the Malmquist bias very simply and analytically as follows. We assume that the intrinsic distribution in pulsar luminosities (that of all pulsars in the galaxy) is given by a log-normal. This means that the quantity ln(L) is distributed as a univariate normal, or Gaussian. Let μ be the mean and σ^2 the variance of this distriubtion, denoted N(z) where z = ln(L). This implies that the number of pulsars with ln(L) in the range z to z+dz will be N(z)dz. Therefore

$$N(z) = \frac{N_0}{\sqrt{(2\pi)\sigma}} \exp\left[\frac{-(z-\mu)^2}{2\sigma^2}\right] \qquad (1.1)$$

where N_0 is the total number of pulsars in the population.

Now we assume that the galaxy consists of an infinite planar disc.

A pulsar survey with minimum flux threshold F_{min} will detect pulsars out to a distance given by r_{max}, where $r_{max}^2 = \frac{\exp(z)}{4\pi F_{min}}$ (1.2)

So the observed distribution in z will be given by:

$$N_{obs}(z) = \int_0^\infty N(z)\, H(\exp(z)-4\pi r_{max}^2 F_{min}).2\pi r.\rho(r).dr \qquad (1.3)$$

So the number of pulsars observed in z, z+dz is $N_{obs}(z).dz$

We will assume for simplicity that $\rho(r)$ is uniform, i.e. $\rho(r)=\rho_0$, the spatial density of pulsars in the disc. So we obtain

$$N_{obs}(z) = N(z).\pi\rho_0 r_{max}^2 = N(z).\rho_0.\exp(z)/4F_{min} \qquad (1.4)$$

By theorem 1 in Appendix 3A, this is a second normal, with new mean given by $\mu' = \mu + \sigma^2$, and the same variance. Thus the observed mean is *higher* than the intrinsic mean, so that the observed sample is biased to higher luminosity objects. Alternatively, we could derive the

expression for $E_{obs}(z|r)$, the expectation value of z at fixed r.

This is defined as:

$$E_{obs}(z|r) = \int_{-\infty}^{\infty} \frac{N(z,r).z.dz}{N(r)} \qquad (1.5)$$

This turns out to be :

$$E_{obs}(z|r) = \mu + \frac{2\sigma^2.\exp(-\gamma^2)}{\mathrm{erfc}(\gamma)} \qquad (1.6)$$

$$\text{where } \gamma = \left[\frac{(\ln(4\pi r_{max}^2 F_{min}) - \mu)}{\sqrt{2}\,.\,\sigma} \right] \qquad (1.7)$$

and erfc is the complement to the standard error function erf, such that erfc(0) = 1 and erfc(∞) = 0 .

(1.6) is a monotonic increasing function of r, so at greater distances only the very brightest pulsars are detected. This shows simply the effect that luminosity selection can have on pulsar samples.

1.6.4 Pulsar luminosity laws.

Several authors have pointed out the likely dependence of luminosity on period and period derivative. [Proszynski and Przybcien(1984), Stollmann(1987), Vivekanand and Narayan(1981),(1983)]. This may be a direct effect, or possibly due to a dependence on magnetic field strength, which in the standard model is given by $\sqrt{(P\dot{P})}$, so the dependence is carried over to P and $\dot{P}$. Of particular interest is the direct effect on the observed distribution of period and period derivative of a power law of the type found by Proszynski and Przybcien(1984);

$$L = \Delta\, P^{\alpha}\dot{P}^{\beta} \qquad (1.8a)$$

or more conveniently $\ln L = \ln\Delta + \alpha \ln P + \beta \ln\dot{P}$ (1.8b)

for constants α, β and Δ. On the basis of a regression least-squares fit they found the values $\alpha = -1.04\pm0.15$, $\beta = 0.35\pm0.06$ and $\ln(\Delta) =$

16.0±2.0, where earlier work on a smaller sample gave Vivekanand and Narayan (1981) the results $\alpha = -0.86\pm0.2$, $\beta = 0.38\pm0.06$ We repeated this analysis for 351 pulsars from the data in the pulsar catalogue of Manchester and Taylor and the following values found: $\alpha = -0.9\pm0.2$, $\beta = 0.35\pm0.04$ and $\ln(\Delta) = 15.8\pm1.8$. If attention is restricted to the sample of 242 pulsars with fluxes above 10 mJy, then slightly different results are found: $\alpha = -0.87\pm0.18$, $\beta = 0.43\pm0.03$, and $\ln(\Delta) = 19.3\pm1.5$. This is notable for the much higher value of Δ that is found compared to the original fit, showing conclusively the Malmquist bias in action.

Using the Manchester and Taylor(1977) alternative values of L in the regression, the following values are found for α,β and Δ : $\alpha = -1.16\pm0.2$, $\beta = 0.25\pm0.04$ and $\ln(\Delta) = 12.7\pm2.1$ for a sample of 195 pulsars. These are not substantially different, so we proceed by restricting attention to L_{400} from now on. These results have lent support to the model in which the true values of α and β are -1 and 1/3 respectively, so that $L_{400} \propto (I\omega\dot{\omega})^{1/3}$, i.e. proportional to the cube root of the spindown luminosity [Proszynski and Przybcien(1984) and Narayan(1987)].

However, these fits fail in a fundamental way to take account of the bias introduced into the data by the presence of such a power law : clearly certain regions of the $P,\dot{P}$ plane (depending on α,β) will be discriminated against through the Malmquist effect and the subsequent determination of α,β from a sample of pulsars biased by the very law that is being quantified. It is expected that the true values of α,β may be substantially different from those obtained by the Proszynski and Przybcien analysis. This inherent biasing cannot be dealt with unless we know the underlying intrinsic distribution in $P,\dot{P}$ and L which is impossible without a model for pulsar evolution.

In addition, a law such as (1.8) cannot exactly explain the scatter in

the data if Δ is a constant for all pulsars. It is likely that the uncertainties inherent in the evaluation of luminosity (principally through the distance estimates) contribute to this scatter to a large extent. For realistic models, some intrinsic variation in the parameter Δ is desirable. Most authors, however, adopt this type of luminosity law and thus introduce a bias into the $P,\dot{P}$ distribution, but probably different from the actual bias that is present.

Therefore, when interpreting the $P,\dot{P}$ diagram it is essential to consider not just evolutionary effects but also selection in discussing the significance of the various 'populated' regions in that plane.

1.6.5 Scatter diagrams.

An alternative means of looking at the dependence of luminosity on period and period derivative is to study directly the scatter plot for L vs P and L vs $\dot{P}$. These show considerable scatter, and the correlations are as follows (see Figs 1.8 and 1.9):

For L vs P $\rho_1 = -0.21$, $p_1 = 3.1\times10^{-5}$; $\rho_2 = -0.24$, $p_2 = 2\times10^{-6}$ and for L vs $\dot{P}$ $\rho_1 = 0.24$, $p_1 = 5.3\times10^{-6}$; $\rho_2 = 0.29$, $p_2 = 6.9\times10^{-8}$, where ρ_1=Pearson's correlation coefficient and ρ_2 = Spearman rank-order coefficient of correlation. The negative value of ρ for L vs P supports the idea of a negative value of α. Drawing firm conclusions from such diagrams is not possible, given the discussion on selection effects above, but we can see there is a tendency for lower luminosity pulsars to have longer periods and smaller period derivatives. This tentative conclusion is supported by the correlations calculated from these data. The Spearman coefficient is a non-parametric statistic, which is insensitive to the form of the underlying distributions, thus is a reliable indicator of a genuine correlation.

One other way of assessing the dependence of the luminosity on P

and $\dot{P}$ is to find the correlations of P and $\dot{P}$ with r, the distance to the pulsar, which generally reinforce those from the previous diagrams. It is found that the longer period pulsars are generally less luminous (and can only be seen at nearby locations) and small period derivatives are similarly subject to being detected only at close distances. The correlations are:

For P vs r : $\rho_1 = -0.11$, $p_1 = 0.02$; $\rho_2 = -0.18$, $p_2 = 1.4\text{x}10^{-4}$ and

for $\dot{P}$ vs r : $\rho_1 = 0.19$, $p_1 = 0.02$; $\rho_2 = 0.25$, $p_2 = 1.9\text{x}10^{-6}$.

The graphs of $E_{obs}(L|r)$, $E_{obs}(P|r)$ and $E_{obs}(\dot{P}|r)$ are in Fig 1.10. The Malmquist effect is seen explicitly on $E_{obs}(L|r)$, and corresponding behaviour might be anticipated for P and $\dot{P}$, i.e. we would interpret a steady rise in $E_{obs}(P|r)$ as clear evidence for a positive value of α. To calculate these quantities, the data is binned in r and in each bin the mean value of P, $\dot{P}$ and L is found. Clearly there is less obvious dependence on r than might have been expected from the regression result. This presentation averages over the scatter in the previous plots, but possibly for that reason gives a less emphatic result, which will depend on what binning scheme is used.

Emmering and Chevalier(1989) have recently adopted the Proszynski and Przybcien law as a necessary feature of their models, in that it must be reproduced by any pulsar model in addition to satisfying other demands related to the P and $\dot{P}$ distribution. Thus the predicted distribution of P,$\dot{P}$ and L must give rise to a regression law similar to that of (1.8b) with the appropriate α and β values being obtained. This allows the luminosity data to be included in any model-fitting scheme in an indirect way.

Finally, the scatter of the luminosity data can be emphasised by re-plotting the P,$\dot{P}$ diagram but with each pulsar represented by a

square whose area depends on the luminosity. To avoid a clutter of points, only a quarter of the sample is used, but it can be seen there is considerable spread in luminosity in all regions of the $P,\dot{P}$ plane. This is shown in Figure 1.11.

1.6.6 Summary of the importance of luminosity.

The importance of these results must be reiterated. They show that the luminosities of the observed sample do depend on P and $\dot{P}$ according to the law found by Proszynski and Przybcien(1984) but this law will not necessarily govern the whole pulsar population. The law input to a pulsar model should not be the same as the one deduced from the regression fit. It can be shown that, if the underlying distribution in $P,\dot{P}$ and Δ is multi-variate normal then a regression done on the corresponding observed sample will recover the true values of α and β and a higher than true value of Δ- the Malmquist bias acts only to change Δ. This is however an idealised case and does not correspond to an evolutionary model. A further point to note is that this 'bias' in the data will be carried forward to other conclusions drawn from any analyses. For example, the estimation of magnetic field strengths from $\sqrt{(P\dot{P})}$ will give a biased result so that the mean inferred for an observed sample will be different from that of the entire population.

1.6.7 Pulsar kinematics.

The kinematics of pulsars have been studied notably by Lyne et al(1982) , Cordes(1986) and Cordes(1987). The Lyne sample is smaller (26 pulsars), and looked at the proper motions using interferometry, whereas Cordes studied the interstellar scintillation patterns attributed to the pulsar transverse velocities. Both found high transverse velocities of the order of hundreds of km/sec and the majority of

objects heading out of the plane of the galaxy. An additional feature was an apparent correlation between transverse velocity and $P\dot{P}$, proportional to the square of the magnetic field strength in the standard model. This is relevant for the question of the asymmetry of the supernova explosion which created the 'kick' to eject the pulsar from a binary system.

1.7 THE IMPORTANCE OF PULSARS

1.7.1 Evolutionary considerations.

The outstanding problems of evolution were soon identified: how do pulsars spin down? ; how often are they created, and where?; what happens to old pulsars?; and later binary pulsars caused these questions to be addressed once more after the discovery of PSR1913-16 in 1974. We shall show later how the question of field decay in neutron stars may well be resolved by pulsar evolutionary studies, by modelling the distribution of pulsars in P and $\dot{P}$, and putting constraints on the parameters of simple field decay laws. Similarly, we may be able to infer whether it is necessary for pulsar alignment or counter-alignment to occur to explain the observations, again by modelling the consequences for the observed $P,\dot{P}$ population and using the pulsewidth data.

A key aim of evolutionary studies is to obtain estimates of the pulsar birthrate and population in the galaxy, which would have relevance for understanding the fates of intermediate mass stars (say 3 - 6 solar masses), abundances of iron-peak elements and the galactic mass distribution. [see Ostriker et al (1974), Hills(1978)].

1.7.2 Nuclear matter and the neutron star equation of state.

Pulsars were also realised to be extremely useful tools for the study of matter at nuclear densities, unobtainable on Earth, and finding the

equation of state under the extreme conditions in neutron star interiors. Pulsar evolution has importance for the study of nuclear matter through estimating timescales for the decay of neutron star magnetic fields, which are closely related to the electrical conductivity of this terrestrially-unobtainable state of matter. The equation of state (EOS) of neutron star material can be constrained by

(a) observations of the fastest pulsars with millisecond periods, by applying our knowledge of the Chandrasekhar-Friedman-Schutz (CFS) instability for rapidly rotating stars, e.g. Lindblom(1987), Friedmann(1983) and Friedmann et al(1987) and also

(b) by interpreting data from pulsar glitches (sudden spin-up phases in the pulsar's behaviour with near-discontinuous jumps in the period) attributed to neutron star-quakes and the subsequent relaxation in period gives some insight into the properties of the neutron star crust and interior structure, which is believed to be a neutron superfluid.

1.7.3 Interstellar electrons and magnetic fields.

The probing of the interstellar distributions of both electrons and magnetic fields can be aided by pulsar studies. Using the pulsars to find the electron densities along the lines-of-sight has been done by Harding and Harding(1984), whereas Lyne(1989a) has used pulsar rotation measures to infer averaged magnetic field strengths in interstellar space.

1.7.4 Supernova remnants

The role played by pulsars in the morphology of supernova remnants (SNRs) also tells us about their formation [Radhakrishnan(1982,1986), Radhakrishnan and Srinivasan(1981).]. The supernova rate must also fit in with our ideas of pulsar creation and generation of heavy elements.

1.7.5 Gravitational wave sources.

Pulsars are potential sources of gravitational radiation [Smarr(1979), Thorne(1988) and Schutz(1989)]. A pulsar with a permanent quadrupole moment, perhaps a 'lumpy' pulsar, will generate gravitational waves at the rotational frequency. For some of the fastest pulsars, this may be detectable by future generation detectors. The strength of such emission and the degree of asymmetry can be constrained by the inferred spindown luminosity for particular pulsars, which suggests only small degrees of 'flattening' or oblateness for pulsars such as the Crab and PSR1937+21.

The binary pulsar systems (now 13 in number) are progenitor systems for the celebrated 'coalescing binary' class [Krolak and Schutz(1988), Krolak(1989), Schutz(1989)] of gravitational wave sources whose event rate will be of importance in advance of the construction of the proposed LIGO (laser-interferometer-gravitational wave observatory) detectors, and can be estimated through study of the pulsar population, since the pulsar birthrate will ultimately determine how often such coalescences take place.

1.8 OBJECTIVES OF THE THESIS

It is our intention in this work to present a new method for the study of pulsar evolution. This will be based on the solution of the time-dependent continuity equation in the pulsar distribution function. For any given model, which in raw form constitutes a source function governing the distribution of pulsar properties at birth, and a set of dynamical equations describing the time evolution of the variables (e.g. period P, magnetic field strength B and luminosity L) the method will produce the theoretical joint distribution expected on the $P,\dot{P}$ plane. This will be an analytical expression, which must be compared

statistically with the observed $P,\dot{P}$ diagram. The distribution of all the variables can be found but only that for P and $\dot{P}$ will be analysed in detail.

This method will not assume (a priori) stationarity in the pulsar population, a virtually universal assumption in the literature. We will demonstrate how a steady-state is not necessarily justified by observations, and may not be relevant for certain models. Our method, valid under less restrictive constraints, is thus more generally applicable.

Our basis for the comparison of the $P,\dot{P}$ distributions (observed and predicted) will be the chi-squared goodness-of-fit test, operating with the null hypothesis that the two distributions (predicted and observed) are in fact the same. For a given predetermined level of significance, that will indicate an acceptable fit, each model will be best-fitted by varying its parameters until the chi-squared statistic is minimised. This multi-dimensional optimisation operation over the parameter space will yield the most closely-matched prediction to the actual observations. If this fails to satisfy our criteria of significance, the model will be rejected as incompatible with the observed $P,\dot{P}$ diagram.

In this way, we will rigorously compare different models. Unsatisfactory models will be identified, and can be rejected. Models which fit to an acceptable level must be subjected to further tests to check if either can be taken as a more realistic representative of the observations. A similar but less explicitly analytic approach has recently been used by Cheng(1989) to analyse the $P,\dot{P}$ diagram. Other authors have adopted the chi-squared test as well, including Emmering and Chevalier(1989) and Narayan and Ostriker(1990).

We shall in later chapters compare the observed distribution in P and $\dot{P}$ against those predicted by pulsar models. This will involve dividing the P,$\dot{P}$ plane into boxes and comparing the observed and predicted box occupancies by a χ^2 test. Ideally one should test for the distribution of luminosity as well but the present low number of known pulsars does not allow for sufficient numbers in the cells for the chi-squared test to be valid. The necessary three-dimensional bin scheme would be grossly underpopulated rendering the statistical approach invalid. Failing this, the fitting of the joint P,$\dot{P}$ distribution will suffice, and this is justified when we regard the luminosity data as only secondary in importance to that for period and period derivative, since these latter are essentially directly observed, not derived quantities, and so deserve a greater weighting in any model-fitting procedure. The three-dimensional fitting is discussed in Chapter 7 as a topic of future research.

FOOTNOTE: Other selection effects relevant to the P,$\dot{P}$ diagram.

We shall not attempt to model all known selection effects, The complicated nature of these requires a more numerical approach. We have included the principal contributing effects. Other factors limiting our knowledge of the P,$\dot{P}$ diagram are:

(1) Sensitivity of surveys to broad pulses- it is easier to detect narrow profiles. In fact the signal-to-noise ratio rises as $\sqrt{\omega}$ where ω is the pulsewidth. This could, however, be easily incorporated into our analysis. However, any systematic variation of ω with P and $\dot{P}$ could be important for model fitting and should be included.

(2) Pulse nulling can be important for longer period pulsars, which spend time in a null state, preventing straightforward detection. There is in fact a large area of the P,$\dot{P}$ plane occupied by 'nullers'.

(3) Pulsars located in the galactic plane suffer from pulse broadening and signal scattering, inhibiting detection of the younger objects expected to reside in these regions.

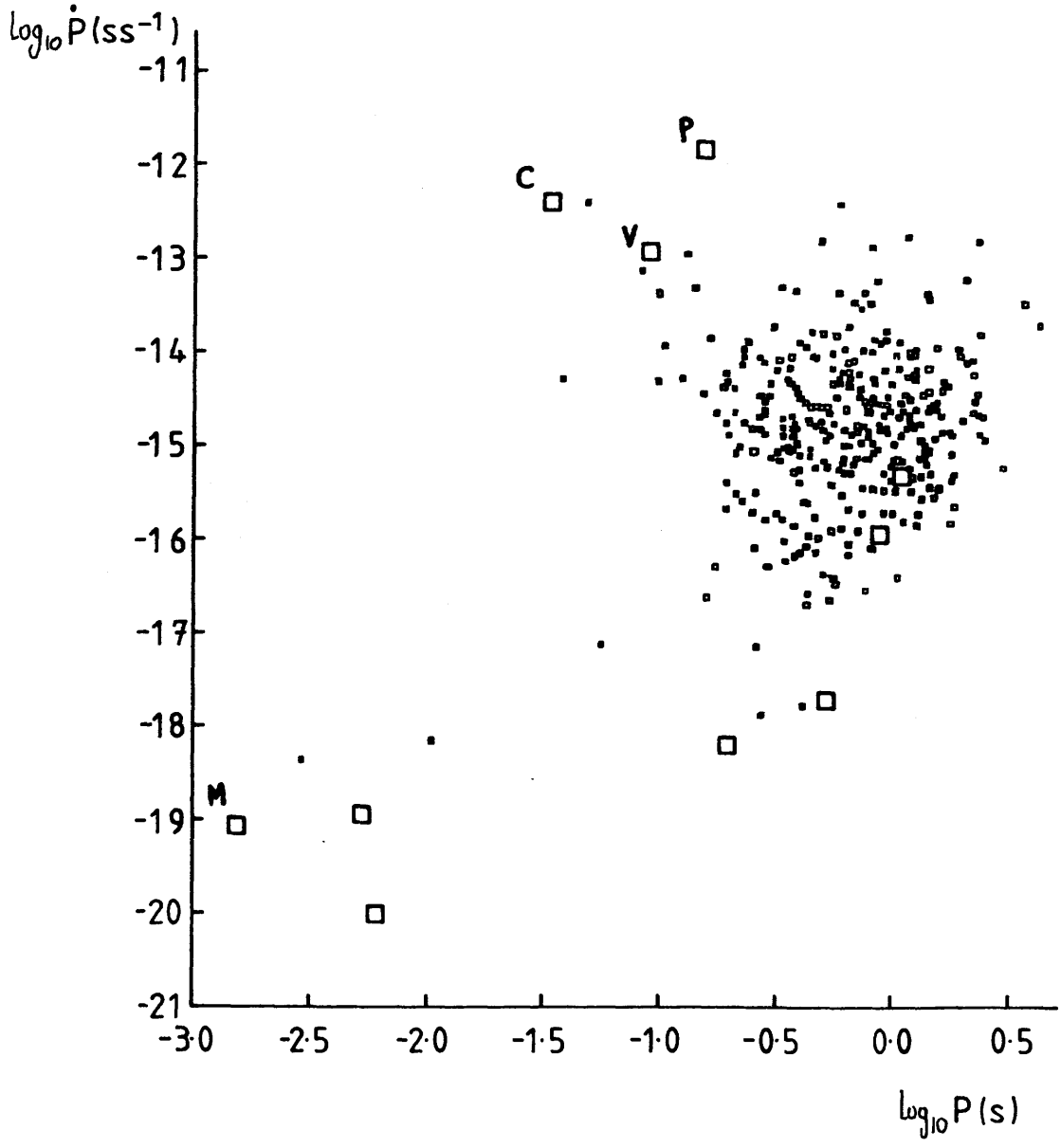

FIGURE 1.1

The P,$\dot{P}$ diagram for 368 observed pulsars, from the catalogue of Lyne, Manchester and Taylor, updated with the recent determinations of $\dot{P}$ from Stokes et al(1988). The binary pulsars are shown as small squares, as are the young pulsars in supernova remnants, the Crab, Vela and PSR1509-58, (C,V and P respectively), and the millisecond pulsar PSR1937+21 is shown by M.

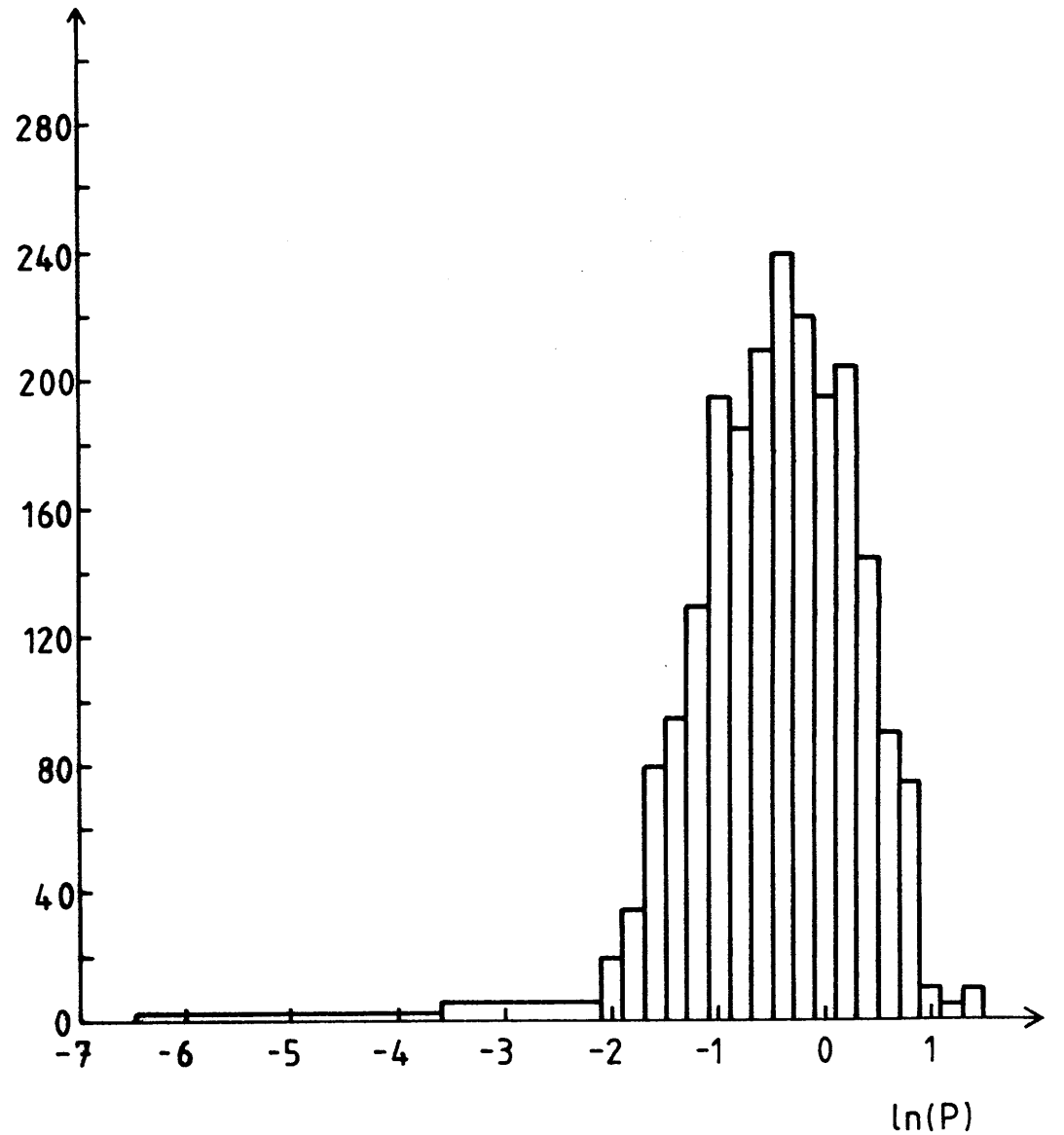

FIGURE 1.2

The histogram of observed periods for 444 pulsars from the Lyne, Manchester and Taylor catalogue. The bins are even in ln(P) between -2.1 and 1.5. Arbitrary units are used on the vertical scale.

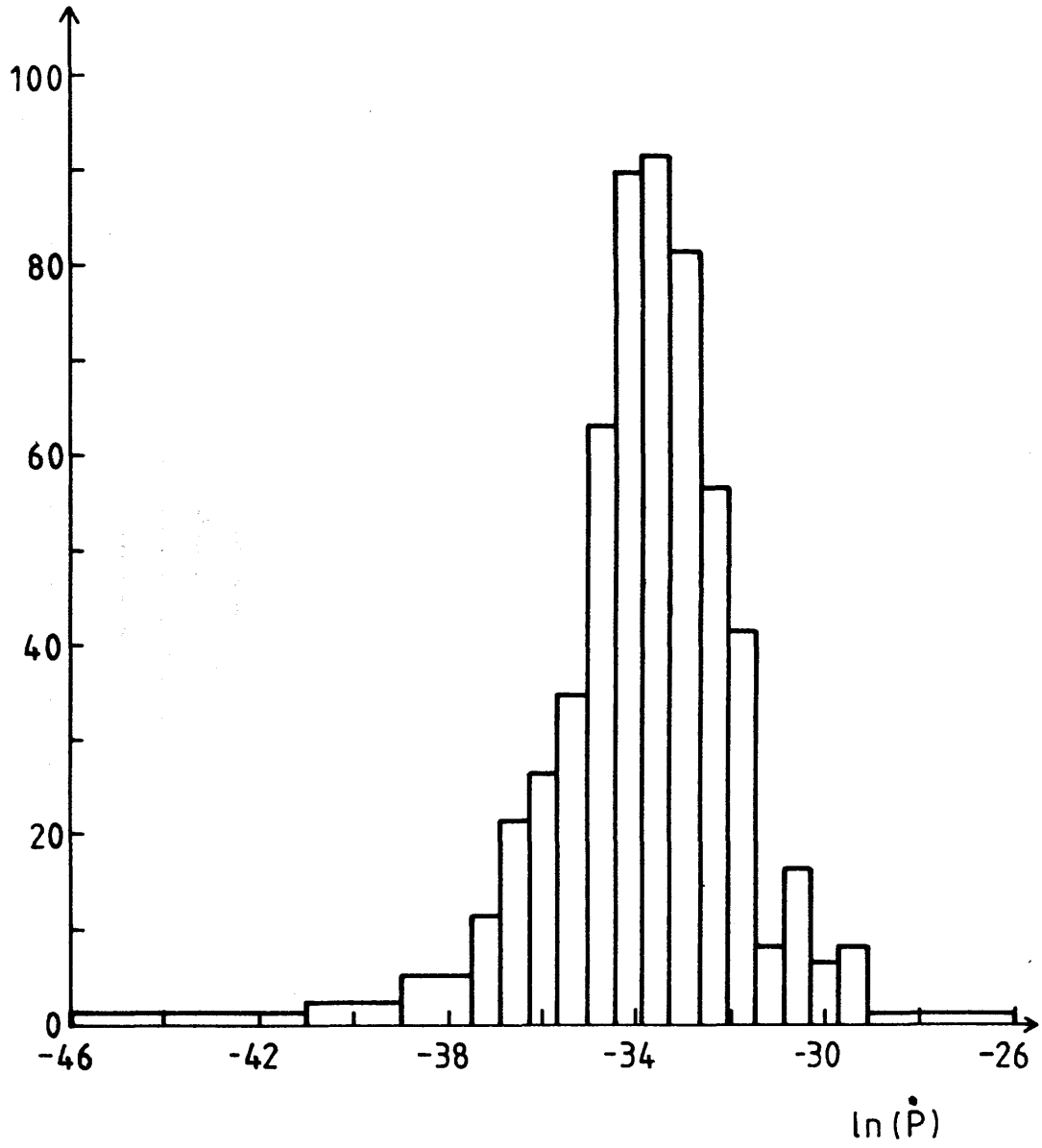

FIGURE 1.3

The histogram of period derivative for 360 observed pulsars, from the Lyne, Manchester and Taylor catalogue, supplemented by the data of Stokes et al(1988). The bins are even in $\ln(\dot{P})$ between -37.5 and -29.1.

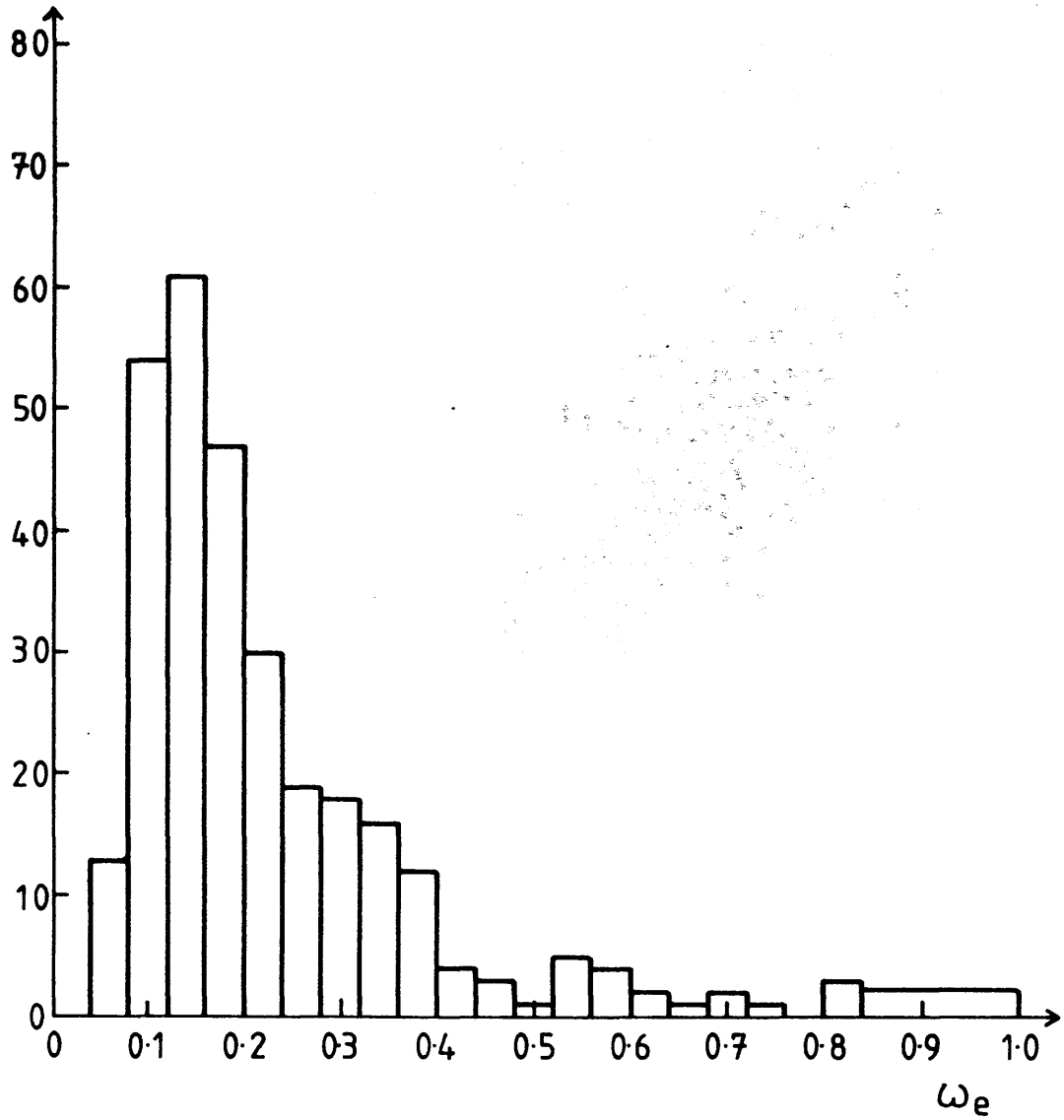

FIGURE 1.4

The histogram of observed pulsewidths for 309 pulsars, from the catalogue of Lyne, Manchester and Taylor. The pulsewidths plotted are equivalent widths, in units of radians.

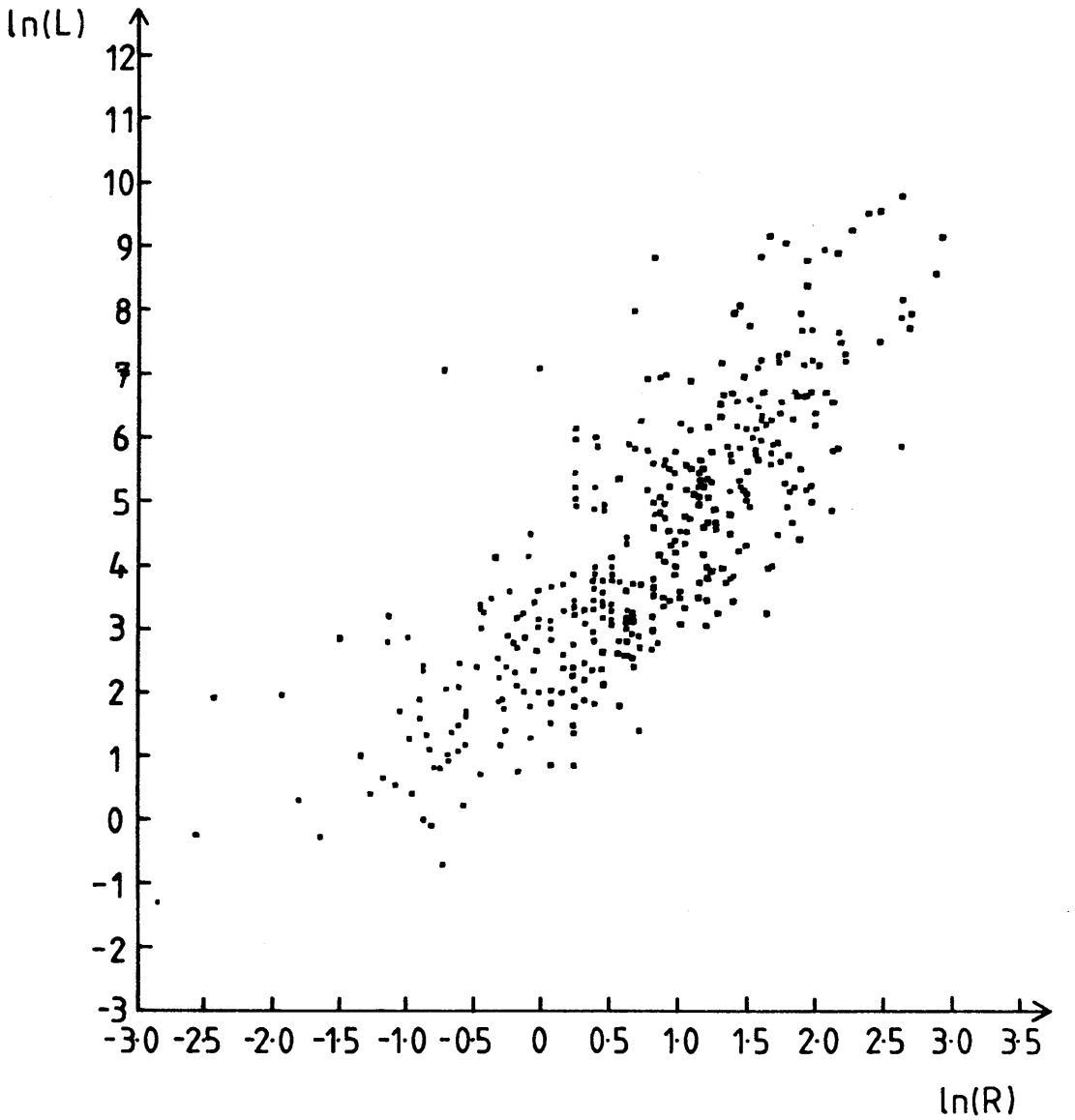

FIGURE 1.5

Diagram of luminosity (L_{400}) against distance for 388 observed pulsars. L_{400} is in mJykpc^2, r in kpc. Distances are calculated from pulsar dispersion measures, luminosities from $S_{400}*d^2$.

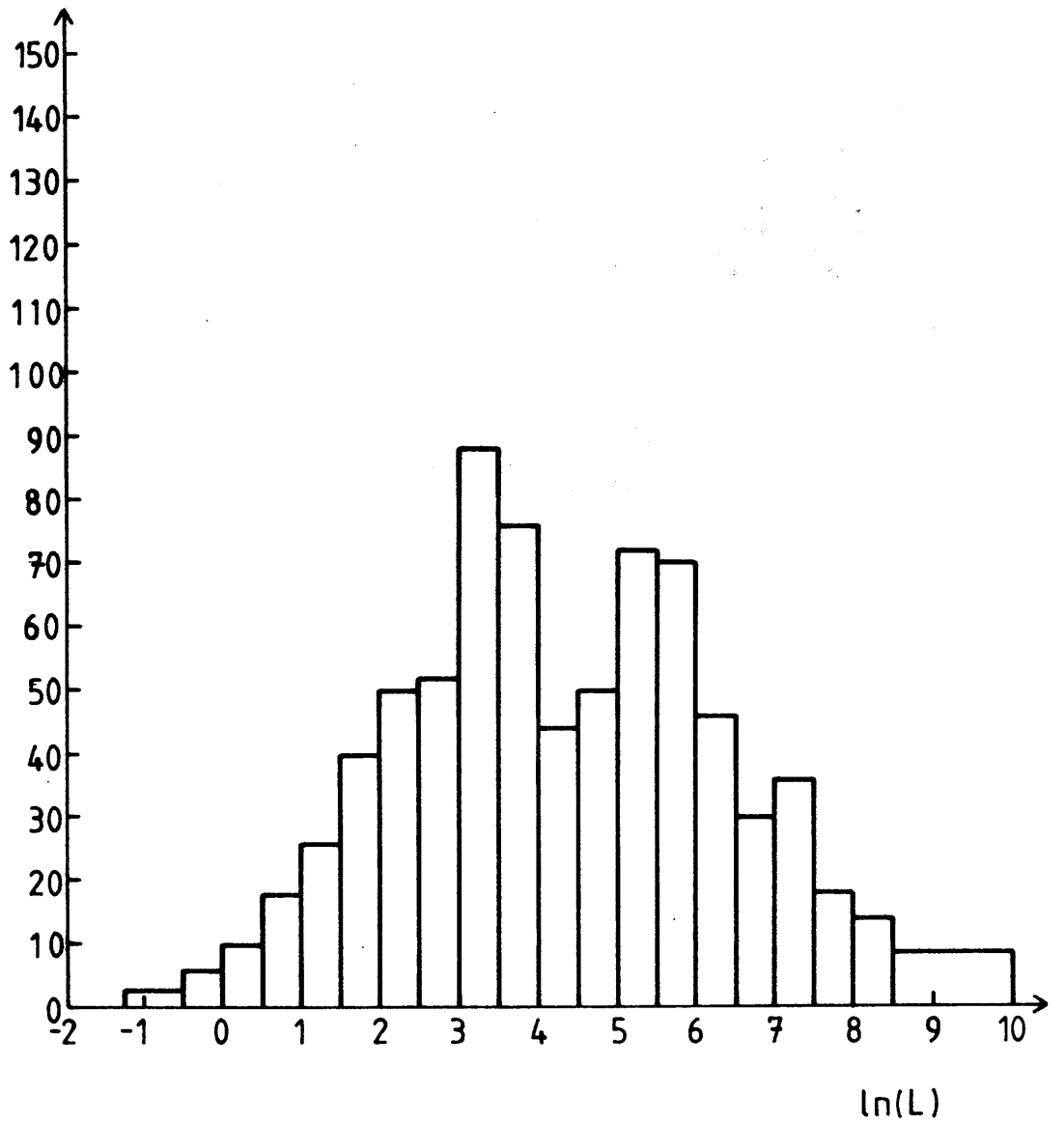

FIGURE 1.6

The histogram of observed luminosities for 388 pulsars from the Lyne, Manchester and Taylor catalogue. Here luminosities are L_{400} as defined in Section 1.2.5 in units of mJy.kpc^2.

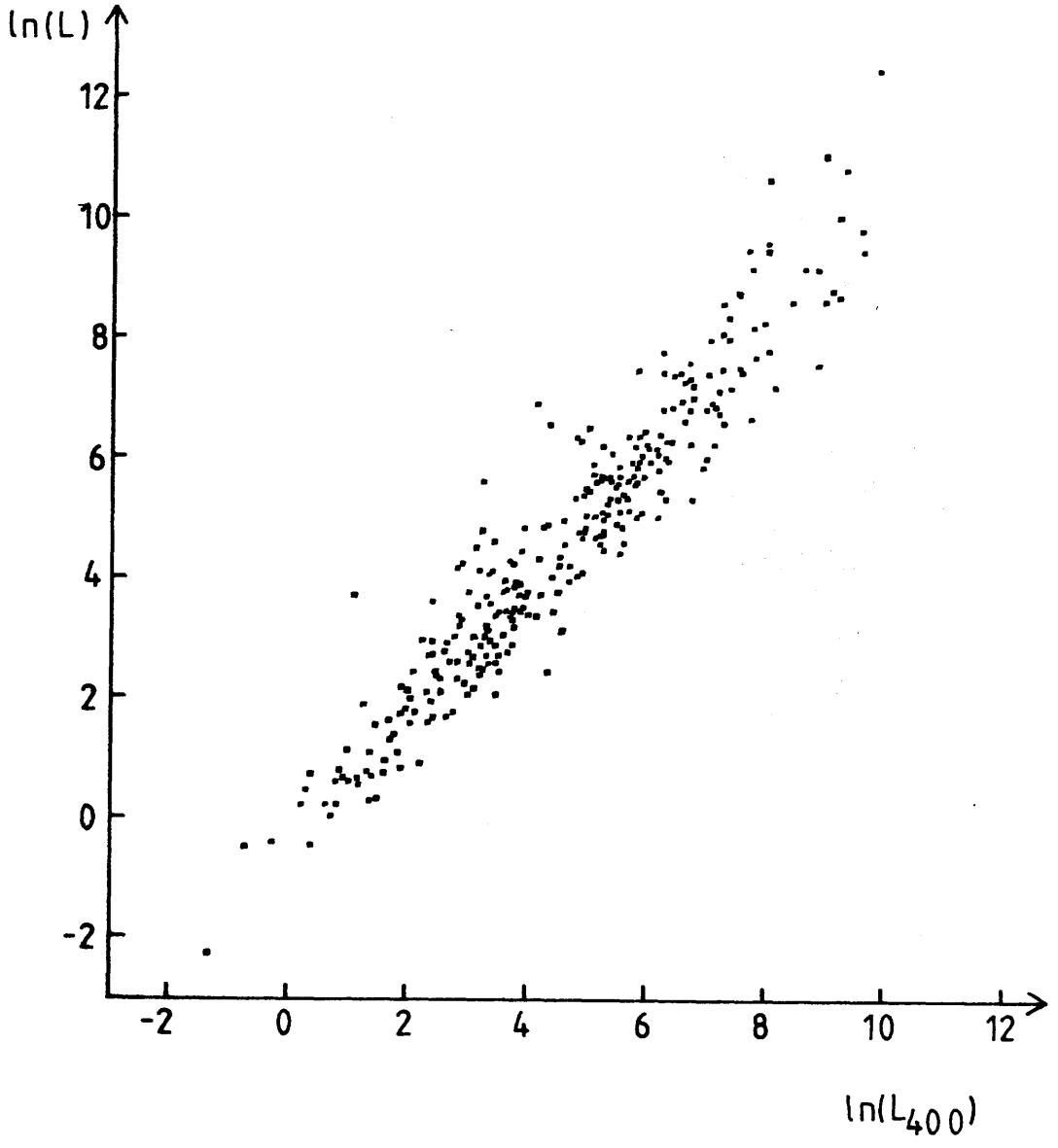

FIGURE 1.7

Scatter diagram of L versus L_{400} for 301 observed pulsars, in units of mJykpc^2. Here L is calculated by the Manchester and Taylor(1977) method and L_{400} as defined in Section 1.2.5. Both are in units of mJy.kpc^2. The correlations are ρ_1 = 0.955 and ρ_2 = 0.951 where ρ_1, ρ_2 are the Pearson and Spearman correlation coefficients as defined in Appendix A4, and discussed in Section 1.6.2..

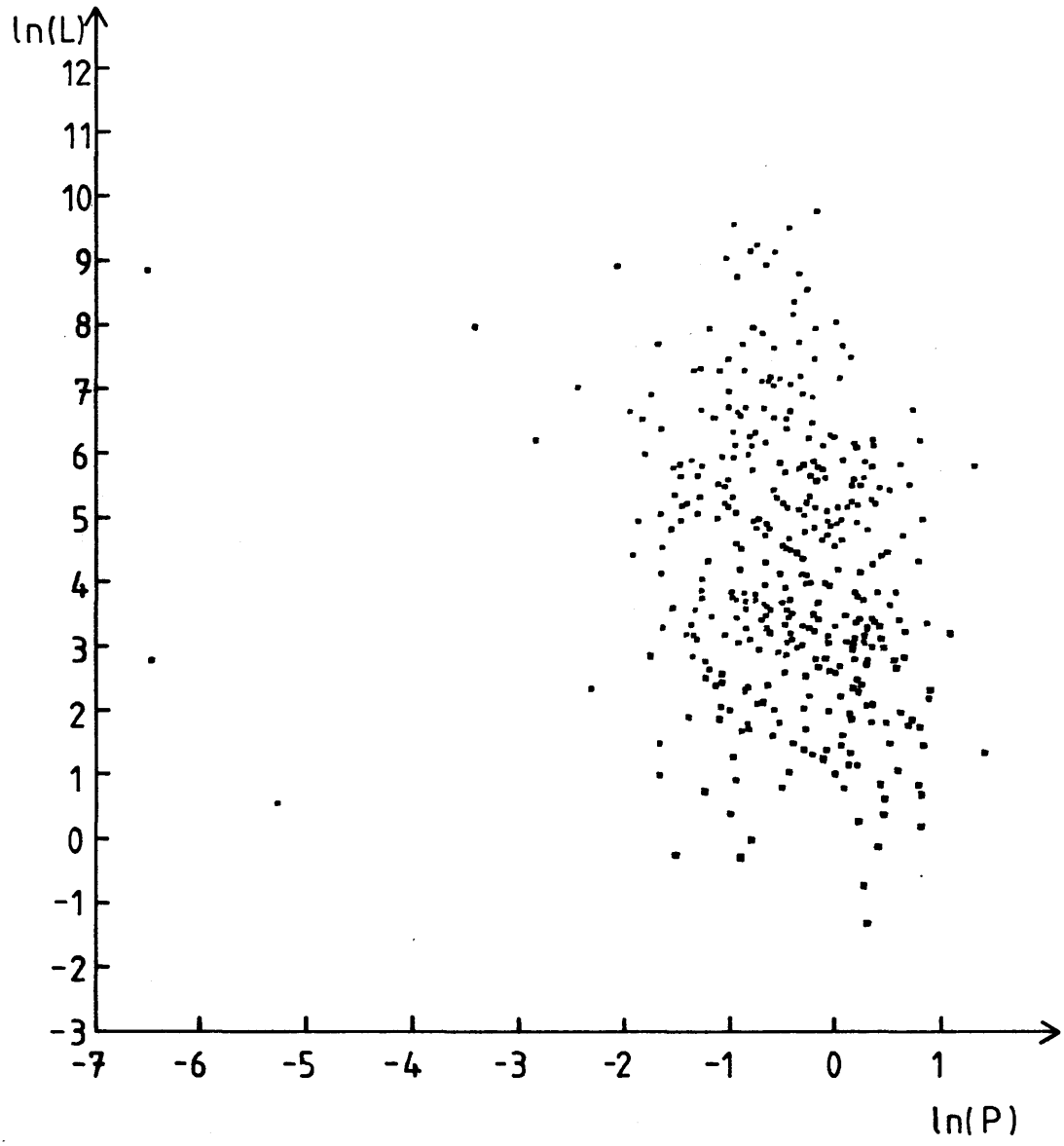

FIGURE 1.8

Scatter plot of luminosity (L_{400}) against period for 388 observed pulsars, with the data from the catalogue of Lyne, Manchester and Taylor. P is in seconds, L in mJykpc^2.

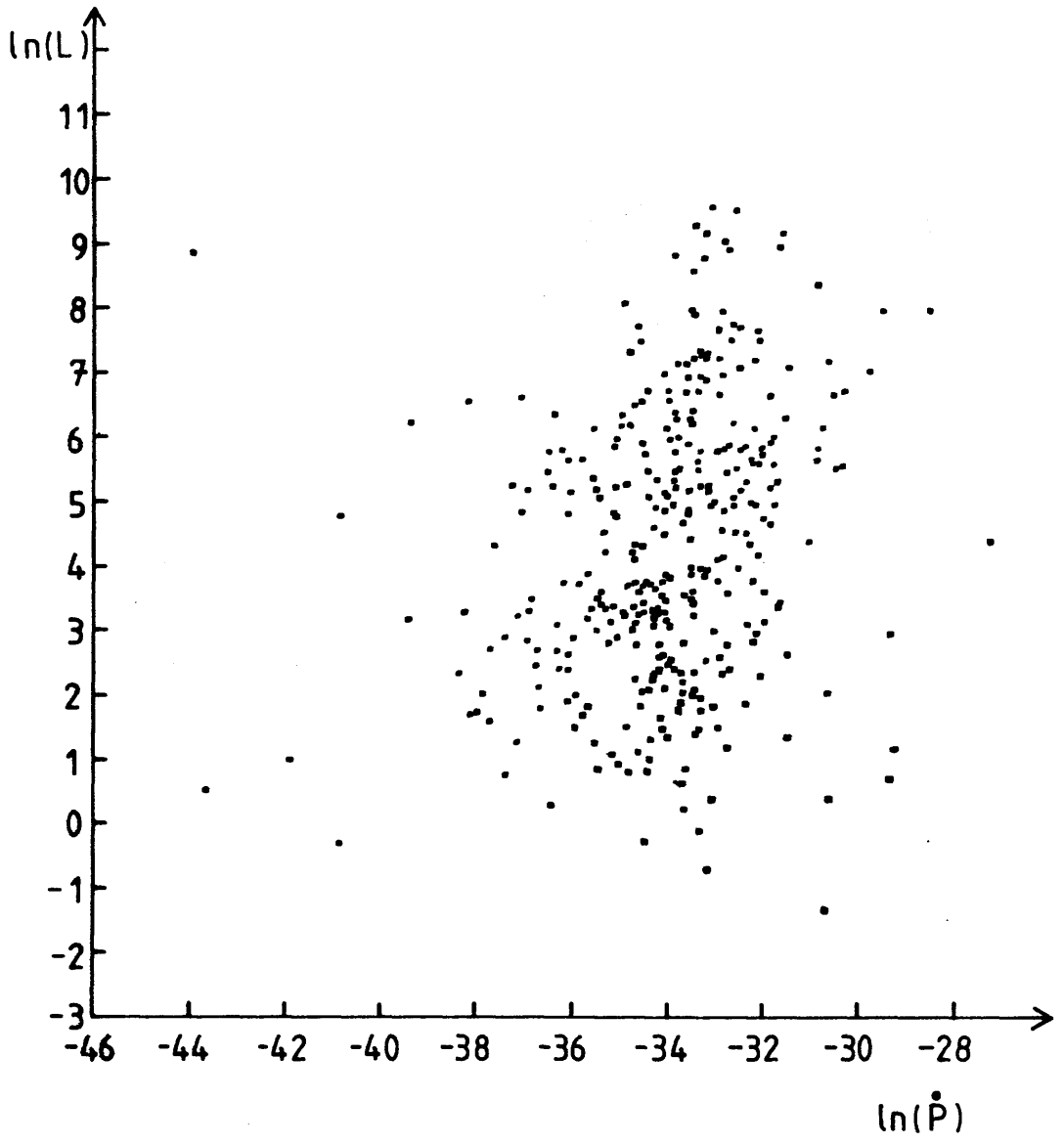

FIGURE 1.9

Scatter plot of luminosity (L_{400}) against period derivative for 351 oberved pulsars, with data taken from the catalogue of Lyne, Manchester and Taylor. $\dot{P}$ is in ss^{-1}, L in $mJykpc^2$.

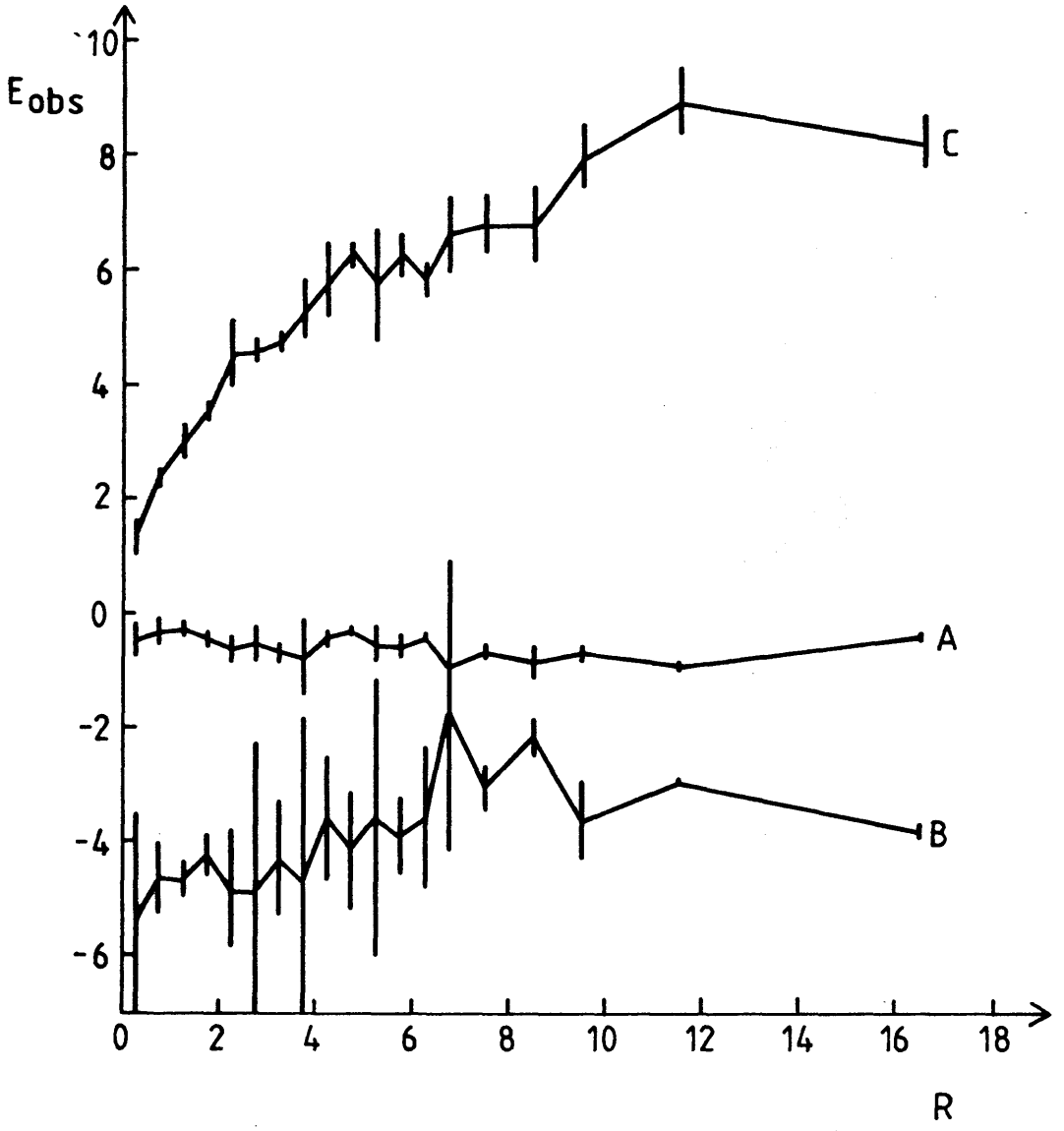

FIGURE 1.10

Plot of the expectation values of P,$\dot{P}$ and L conditional on distance R, formally $E_{obs}(P|r)$, [curve A], $E_{obs}(\dot{P}|r)$ [curve B] and $E_{obs}(L|r)$, [curve C]. Units are P in seconds, $\dot{P}$ in 10^{-10} seconds per year, and L in mJykpc^2, and R is in kpc.

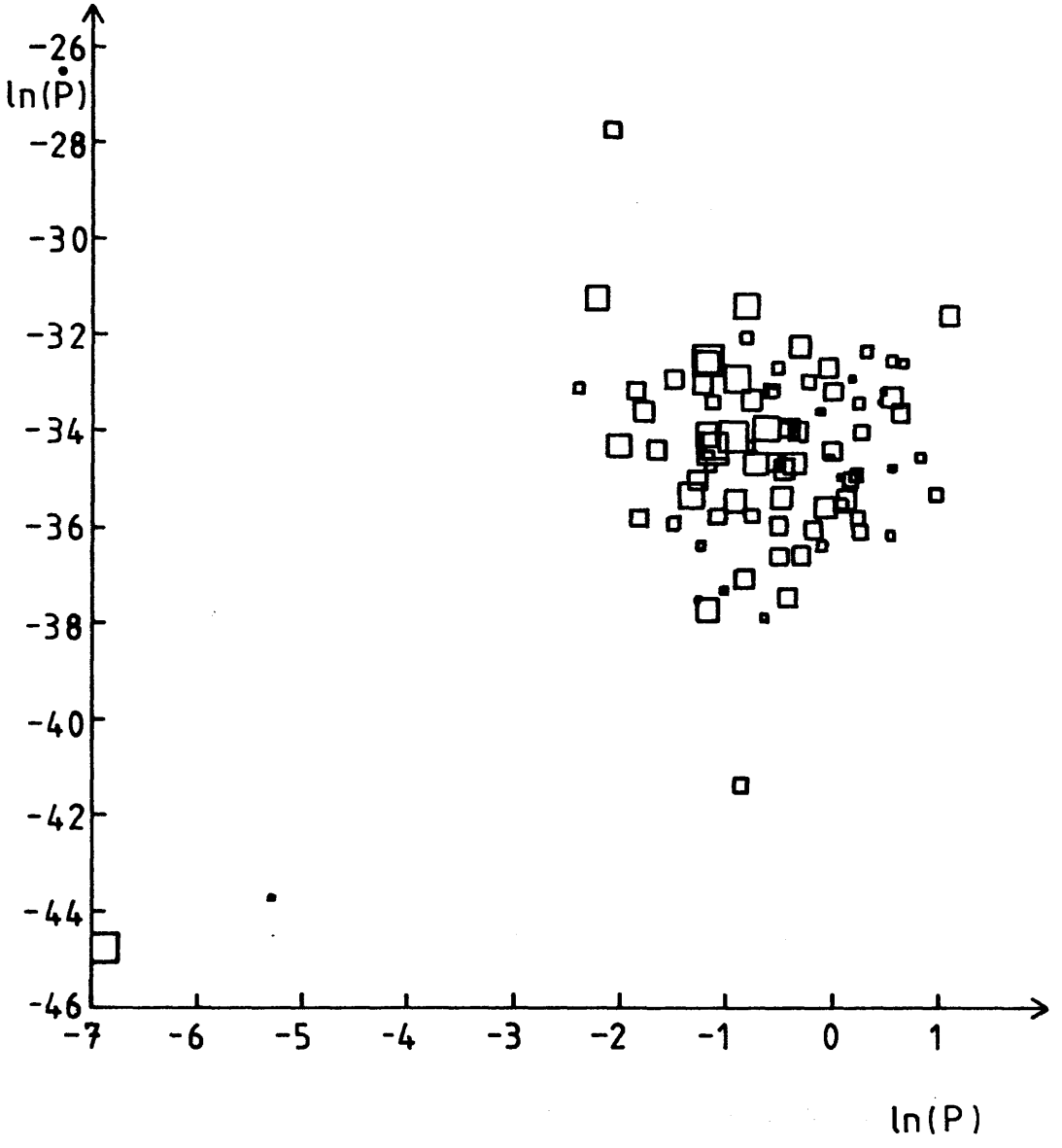

FIGURE 1.11

The P,$\dot{P}$ diagram of Figure 1.1 with the luminosity of each pulsar indicated by the size of the square. The area of the square is proportional to the natural logarithm of the luminosity in mJykpc^2. For the central densely occupied region, only one quarter of all pulsars are indicated for clarity.

CHAPTER 2

REVIEW OF PULSAR EVOLUTION THEORY

2.1 INTRODUCTION

In this Chapter we will firstly look briefly at the properties of neutron stars, both observed and theoretically predicted. Then we shall introduce the standard models proposed to explain the evolution of pulsars, and show qualitatively the effects these models have on the predicted distributions of pulsars in the $P,\dot{P}$ plane. Next we review and discuss critically in turn the major papers of Gunn and Ostriker(1970), Lyne, Manchester and Taylor(1985), Candy and Blair(1986) and Narayan(1987), hereafter GO, LMT, CB86 and N87 respectively. These are representative of the standard evolutionary ideas and although there are many other works of great importance [Beskin(1984), Chevalier and Emmering(1986), Fujimara and Kennel(1980), Phinney and Blandford(1981), Cheng(1989), Narayan and Ostriker(1990)] we choose to concentrate attention on these particular papers, as they especially are recognised as seminal contributions to our understanding of the problems of pulsar evolution.

2.2 NEUTRON STAR PROPERTIES

2.2.1 Masses, radii and magnetic fields

Our knowledge of neutron star masses and radii is generally obtained by construction of models for neutron star matter, subject to various equations of state [EOS] and integrating up the structure equations to create a 'star'. [See e.g. Arnett and Bowers(1977), Baym and Pethick((1979), Freidman et al(1986)]

However, the neutron star equation of state is not well-known, and a variety of different EOSs have been proposed [e.g. Bethe and Johnson(1974), Pandharipande and Smith(1975), Friedman and

Pandharipande(1981), Baym et al (1971), Glendenning(1988)] which lead to different predictions for maximum masses and mass-radius relations. The effect of rotation can also alter the accuracy of a neutron star model which is normally calculated under non-rotating conditions. It is also impossible to predict with certainty which stars will create neutron stars, and to model the collapse accurately enough that the distribution of neutron star properties be deducible from those of the progenitor population. Given these restraints, it is sometimes easiest to invoke 'Occam's razor' and assume that all neutron stars are roughly the same mass and of the same radius. It would, however, be naive to adopt the parameters deduced for, say, the Crab pulsar as 'typical' for the entire population, even though they may be well-observed. For our purposes, we are concerned with the distribution of magnetic field as well as moments of inertia (see Section 2.3). It is simplest to attribute all the unknown spreads in these quantities into a single quantity, which we will usually take to be the magnetic field strength. We shall see that this distribution is quite crucial to the models that we shall develop in Chapters 4-6.

In fact pulsar observations can further our knowledge of neutron stars in two ways- binary pulsars allow a determination of the mass function, which in the case of 1913+16 has produced unambiguous mass determinations for both components. The fastest pulsars can constrain neutron star EOS's through the Chandrasekhar-Friedman-Schutz instability, which limits the rotational frequency of pulsars at a value dependent on the equation of state.

2.2.2 Pulsar magnetospheres.

The identification of pulsars as magnetised neutron stars led to intense theoretical activity directed towards understanding the global

dynamics of such a system. Goldreich and Julian (1969) showed that there would be a magnetosphere surrounding the star, consisting of plasma material ripped from the surface by the electric field. This plasma magnetosphere would extend out to the light cylinder which is situated at a radial distance where the corotation velocity equals the speed of light. However, it was found impossible to develop a model where self-consistency was maintained between the inflowing and outflowing currents, even for the aligned rotator model in which rotation and magetic axes are collinear. The conditions necessary for emission to take place could be deduced, but to create these conditions by means of current flows and particle motions proved too difficult and working models would instead make idealised assumptions or use specialised approximations to make progress. The most notable recent attempts to solve these problems are those of Mestel and his collaborators [Mestel(1984), Mestel et al(1985), Fitzpatrick and Mestel(1988a) and Fitzpatrick and Mestel(1988b)] which have made progress towards the solution of the aligned rotator problem from a classical standpoint. They use a partly iterative procedure and global constraints on the system to find plausible magnetic field distributions and particle flows, then use these as the source of new electric and magnetic fields which are to be compared to those adopted at first. They also require that the dipole moment of these currents in the magnetosphere is cancelled by that of the neutron star itself, and that electrons may cross field lines well past the light cylinder before returning to the star. This model may be generalised to include the quantum effects of a dense mixed plasma.

Since the energies involved in the pulse emission process are several orders of magnitude down on the overall energy of the system as a

whole, it is safe to say that the pulsar phenomenon is merely a diagnostic for the more fundamental behaviour and energy budget of a rotating, magnetised neutron star that as yet we have not managed to pin down. The evolutionary path of a pulsar is thus not significantly affected by the details of pulse emission, but the observation of the pulses gives us the clues necessary to study the same evolution. Comprehensive reviews of the work on pulsar magnetospheres were made by Ruderman(1979) and Michel(1982).

2.3 EVOLUTIONARY MECHANISMS

2.3.1 Magnetic dipole radiation.

Classically, the electromagnetic field of a spinning dipole, in the wave zone, is that of magnetic dipole radation at the rotational frequency, with a power dependence on the 4th power of the frequency [Lorrain and Corson(1970)]. The success of the work of Ostriker and Gunn(1969) and Gunn and Ostriker (1970, hereafter GO) suggested that magnetic dipole radiation was a strong candidate as a means of dissipating the rotational energy in the form of intense electromagnetic waves at the rotational frequency. This predicted a simple model-dependent relationship between $\dot{P}$ and P as follows:

$$\dot{P} = \frac{2\,\pi^2 B^2 R^6 \sin^2\theta}{3\,I\,c^3\,P} \qquad (2.1)$$

where B= surface magnetic field strength (Gauss)

I= moment of inertia (gcm^3)

R= radius of neutron star(cm)

c= speed of light (cms^{-1})

θ= angle between magnetic and rotation axes

In its generalised version

$$\dot{P} = k\,P^{2-n} \qquad (2.2)$$

the so-called braking index n can take on different values. ($n=3$ gives the above case (2.1)). We can often group all the other factors together into k, which we call the magnetic torque. The simplest application of this would treat k as a constant characteristic of each pulsar. The trajectory of the pulsar on the log(P),log($\dot{P}$) plane would be a straight line given by:

$$\log(\dot{P}) = \log(k) + (2-n)\log(P) \qquad (2.3)$$

with gradient $2-n$. Unfortunately, the observed pulsars cannot, in general, be given trajectories, since $\ddot{P}$ is not known for them. n is related to P,$\dot{P}$ and $\ddot{P}$ by the following expression:

$$2-n = P.\ddot{P}/ (\dot{P}^{2}). \qquad (2.4)$$

Thus this relation is not directly testable except for a few of the fastest pulsars, and the results are ambiguous, as the sign of $\ddot{P}$ is observed to be both positive and negative for different pulsars. This may be due to observational uncertainties in the measuring of $\ddot{P}$. At present, we must use less direct methods to test the law given in equation (2.2)

A consequence of equation (2.1) is that the age of the pulsar is given (when $n = 3$ for the GO model) by the so called characteristic age τ_c, defined by:

$$\tau_c = P/2\dot{P} \qquad (2.5)$$

if the initial spin period is negligible in comparison to P, and

$$\tau_c = P_i/2\dot{P}_i + P/2\dot{P} \qquad (2.6)$$

where P_i and $\dot{P}_i$ refer to the initial (birth) values of P and $\dot{P}$. This will be equal to the true age of the object, provided both k and n are constant in time. [See GO, Chevalier and Emmering(1986)].

However, if the variables B and θ were to change with time i.e. through decay of the magnetic field or alignment/counter alignment

between the axes then the subsequent trajectory of the pulsar on the $P,\dot{P}$ plane will be very different. Also from (2.1) we see that $P\dot{P}$ gives an estimate of B^2, again assuming canonical values for I and R, if magnetic dipole radiation is responsible for the spin-down.

2.3.2 Alternatives to magnetic dipole radiation.

Not all authors assume that magnetic dipole radiation is the cause of pulsar spin-down. Notable amongst these are Beskin et al(1983), Beskin et al(1984) and Cheng(1985). The Beskin work uses a longitudinal current flow as means of dissipating energy, and approximates a solution to magnetospheric problems. This also acts to counter-align pulsars as they age, but has similar overall consequences for the distribution of pulsar periods as the standard field decay models, without any decay taking place.

Cheng has developed a model based on the capture and ionisation of interstellar grains as a means of providing closure of currents, which is a problem in all magnetospheric models. It also explains the correlation between transverse speed and $P\dot{P}$, since fastest pulsars capture more grains and spin down more efficiently.

2.3.3. Field decay and torque decay.

The necessity for torque decay, i.e. the increasingly inefficient spin-down of pulsars, to explain the lack of long period pulsars was first invoked by Gunn and Ostriker and since then by many pulsar modellers. Such a model also allowed pulsars to 'die' quietly either through a luminosity that faded with B or by crossing a deathline where potential gaps in the magnetosphere fell below a threshold for pulse production. Observationally, the deathline is an arbitrary cutoff, with no pulsars to the right (longer period side) of it [See Figure 4.1]. As we shall attempt to show in future chapters, the period

distribution by itself does not imply or require torque decay for its explanation if selection effects are treated properly. The correct approach is to work from the $P,\dot{P}$ diagram i.e. the joint distribution of pulsars in P and $\dot{P}$ from which conclusions can more reliably be drawn. In fact several models can successfully [See chapters 4-6] reproduce a period distribution but not the joint $P,\dot{P}$ distribution that is observed. It is an aim of this work to demonstrate that the correct way to compare and test models of pulsar evolution is to use joint distributions of P and $\dot{P}$ and this has not been done by previous authors in a consistent manner.

For simplicity, theoretical treatments of the case where the magnetic field B decays have assumed an exponential fall in B with an e-folding time of τ, typically in range 10^5 to 10^7 years. This makes easy an analytic development. Recently, Narayan and Ostriker(1990) have used a power-law dependence for the magnetic field decay and achieved satisfactory results.

The theoretical situation and observations from other sources, however, indicate a substantially different picture. Her X1, a galactic Xray source, is widely believed to be a neutron star of age $\sim 5\times10^8$ years. Cyclotron lines have been identified in the spectrum of HerX1 which indicate a magnetic field of $\sim 5\times10^{12}$ Gauss,[Trumper et al(1978)], a value incompatible with decay of the field on a timescale of 10^6-10^7 years. Theoretical studies of neutron star fields are subject to uncertainty regarding the interior conditions, specifically the conductivity of the matter in the star. If Ohmic dissipation of currents can not take place in superconducting matter then typical decay timescales may be as long as a Hubble time, in any case $>>10^6$ years. In particular the form of any decay is believed to follow a distinctly

non-exponential decrease, a more steady decline being anticipated, [Sang and Chanmugam(1987), Chanmugam and Brecher(1987) and Ewart et al(1975)]. The conclusion that is inescapable from these papers is that, over the duration of a 'kinematic' lifetime of a pulsar, no significant decay may take place. This fails completely to tally with pulsar models which require torque decay on kinematic age timescales $\triangleq 10^6$ years, and casts some doubt over these models. Kundt has also questioned the observational evidence for field decay [Kundt(1981) and Kundt(1988)].

In addition, Kulkarni(1986) observed the companion stars to the two binary pulsars PSR0655+64 and PSR0820+02 and found them to be white dwarf stars. He found that the companion of 0655+64 was as old as 10^9 years, on the basis of standard cooling curves, thus creating a contradiction that the pulsars's magnetic field ought to have long-since decayed, as the neutron star is at least as old as the white dwarf. Kulkarni's solution was to propose two components to the pulsar magnetic field, only one of which decayed in the 'normal' way, the other being a core field, stable over much longer timescales.

An alternative viewpoint on pulsar magnetic fields has been put forward by Blandford et al(1983) and Applegate et al(1984). They suggest that the pulsar fields are not fossil fields, but are generated by the pulsar after its creation through a thermal flux. The ability to do this depends on the amount of differential rotation in the interior of the star, which implies that faster pulsars will create their own fields much more swiftly than the rest. This explains the strong field of the young Crab-like pulsars, and ties in interestingly with the injection hypothesis of Narayan(1987) (see Section 2.7) in that the slower pulsars will take longer to create their fields, and will

'turn-on' later as pulsars after about 10^4 years.

It should be noted that if observations do demand less efficient spin-down as pulsars age, it is the torque that is inferred to decay, which can occur without any diminution of the magnetic field, as we shall go on to examine.

2.3.4 Alignment and counter-alignment.

An alternative means of producing torque decay is the alignment between spin and magnetic axes of the star. Since the classical expression for the dipole radiation contains a $\sin^2\theta$ factor, this would tend to zero as alignment ocurs. This would be brought about by electromagnetic torques, one component of which causes the spindown. In an early paper, Davis and Goldstein(1970) showed that a classical dipole in a vacuum would align on the same timescale as rotational energy was lost. However, since our ability to model the electric and magnetic fields in the near-pulsar enviroment is limited, the strength and sense of such a torque cannot be reliably predicted. This means that the pulsar may even counter-align i.e. the axes tend to move until they are perpendicular, [Beskin et al(1984)]. Thus theory again cannot currently provide a reliable mechanism, so there is freedom to choose different 'parametric' models for alignment. In the model of Goldreich and Julian even an aligned pulsar can spin itself down through a unipolar induction mechanism but this is subject to the same inconsistencies of all attempts to explain the magnetospheric structure. This difficulty was realised early on by GO who attempted a calculation of the aligning torque but showed the estimate of the crucial component was unreliable. Again, exponential alignment is frequently invoked in the form of the law

$$\sin(\theta) = \sin(\theta_0)\exp(-t/\tau) \qquad (2.7)$$

[Jones(1976), Jones(1981), Candy and Blair(1983), CB86] and timescales of exactly the same range as for field decay are deduced. Jones based his model of alignment on a torque from current flows between polar cap and magnetosphere in the pulsar, which acts provided a temperature-dependent dissipative torque can be neglected.

The alignment of pulsars has important consequences for the beaming fraction which will evolve with time. (see Chapter 6).

Both field decay and alignment, because of the decay in the spindown torque, lead to the characteristic age being greater than the true age of the pulsar. This could explain the high values of $P/\dot{P} \sim 10^8$ years and match them with the kinematic ages.

2.3.5 Deathlines.

In a number of models, a cutoff line in the $P,\dot{P}$ plane has been suggested. Below this line lies a region of the $P,\dot{P}$ plane in which the pulsar fails to function as before, effectively dies, and becomes invisible to any observer. This can be related to conditions in the magnetosphere, such that potential gaps are maintained of sufficient strength to allow pair production to continue. [See Ruderman(1979), Ruderman and Sutherland(1975), Stollmann(1987b), Michel(1982) for details.] Pulsars crossing such a deathline would enter the imaginatively entitled 'pulsar graveyard', where they would be confined to obscurity unless spin-up via a binary companion granted them a new active phase. Some models do not invoke a deathline, notably LMT, which relies on older pulsars fading gradually through luminosity decay.

2.4 THE WORK OF GUNN AND OSTRIKER

2.4.1 Review of papers.

Ostriker and Gunn(1969) and Gunn and Ostriker(1970), hereafter OG and GO, the two papers by Gunn and Ostriker, laid down ideas which have been remarkably enduring in their longevity and several subsequent models developed from the conclusions reached in this early work. For the purposes of review, we will treat them together. OG developed a model for pulsar evolution with theoretical predictions of pulsar behaviour and GO analysed this model in comparison to the actual data available. Despite using the limited data of the day, a mere 41 pulsars, only 14 of which had known values of $\dot{P}$ they were led to the following evolutionary scenario:-

1) Pulsars were born at short periods with a Gaussian distribution of $\ln_e(B)$, in the galactic plane, with a 'kick' velocity of ~100 km/s

2) Period evolution takes place according to $\dot{P}=A\ B^2/P$ and luminosity L = constant.B^2, for constant A.

3) About 1/4 - 1/6 of all potentially visible pulsars are seen by observers on Earth.

4) Magnetic fields decay exponentially on e-folding times τ ~4 Myrs.

5) Pulsars are associated with Type II supernovae and are produced from stars with masses greater than 4 solar masses.

The subsequent discovery of more pulsars appeared to lead to similar conclusions on the distribution of periods, culminating in LMT(1985) which is effectively a reworking of GO using the up-to-date data. It is important to look closely at the methods used and to assess their relevance and accuracy.

OG considered the dynamics of a rapidly spinning neutron star subject to both magnetic dipole and gravitational quadrupole radiation.

They also consider the origin of relativistic particles in the magnetosphere, but for our purposes only part of this paper is relevant. Using the work of Canuto(1969), Solinger(1969) and Hartle and Thorne(1968) on neutron star properties as a basis, they predict decay timescales of the magnetic field in the neutron star and solve the equation of motion for the star to give its spin-down behaviour. They found that an object such as the Crab could be matched exactly in age with the 1054A.D. supernova if a reasonable amount of energy had been lost in gravitational radiation. Since the gravitational radiation luminosity depends on a higher power of the rotational frequency than the magnetic dipole radiation luminosity, (ω^6 compared to ω^4, where $\omega = 2\pi/P$), it can safely be ignored after the earliest of times. They introduce the quantity 'terminal period' which is the maximum period a pulsar may reach through spindown if the field decays, and depends on both τ and the initial value of B.

OG also points out the possibility of alignment taking place, but show that the necessary calculation cannot give a reliable expression for the alignment torque due to our ignorance of the conditions in the magnetosphere at the stellar surface. The presence of a significant quadrupole field can dominate over this so the theoretical situation is complicated.

In GO, an analysis of the data is carried out, despite the paucity of known $\dot{P}$ values. Their initial assumption is that the observed period distribution in not seriously biased by selection effects in the regions occupied by the majority of observed pulsars. A log-normal distribution in initial magnetic field is assumed, and a luminosity law where the luminosity is proportional to the square of the magnetic field. This corresponds to $\alpha = \beta = 1$ in equation (1.8a). Pulsars are

assumed to be distributed uniformly in the galactic plane. They derive, by a most tortuous method, the predicted distribution in P_t, the terminal period, including the selection due to the flux-limitation of the surveys. They then 'fit' their distributions (apparently eyeball fits) to the observed P_t data (a histogram of 14 pulsars) estimating 'best-fit' values for the parameters, which are the mean and variance in initial magnetic field, (the decay timescale being provided by theory), finally deriving a period distribution which is claimed to be a good fit to the data.

To derive a birthrate, a further analysis of the distance data is required so that a mean distance parameter can be deduced. Also the pulsewidth data is analysed and a period dependence inferred for the 13 observed pulsars with known pulsewidths.

2.4.2 Discussion of GO.

There are some criticisms that can be levelled against the work of Gunn and Ostriker, some of which benefit from hindsight and subsequent research. The most important of these are summarised below:

1) Lack of appreciation of selection effects

The initial assumption that the period distribution was largely unbiased was clearly wrong. We now know from Proszynski and Przybcien(1984) that the luminosity dependence of the observed sample on P and $\dot{P}$ is far removed from that used in GO, and it is hard to reconcile these even with severely biased data sets. This implies the observed period distribution will not, in general, follow the same form as that for the intrinsic population. There is also good evidence that 'fast' pulsars are more difficult to detect in surveys than intermediate period pulsars.

2) Lack of statistical rigour

Nowhere in GO is there any statistical test of how good any of the 'fits' are, or what significance can be attached to these results. Although it is not very meaningful to construct a histogram for a distribution of only 14 objects, which have a large spread in $\dot{P}$ values, and obtain firm conclusions, on several occasions the claim is made that the 'fit is acceptable' or that 'the match in distributions is satisfactory'. These are statistically meaningless when the appropriate tests have not been performed, and levels of significance assessed. In fairness, the shortage of available data in 1970 made this impossible for GO, but subsequent tests have shown their model to be relevant (see Chapter 5).

3) The 'fitting' of the data

GO fit the P_t distribution first (apparently an 'eyeball' fit) and infer quantities from that before they fit the period distribution. Since that distribution is model-independent, it should have been fitted first and parameters estimated from that, rather than the combinations inherent in $P_t = \text{con}.P\dot{P}$ and $\tau_{char} = P/2\dot{P}$ which involve both P and $\dot{P}$, and are model dependent quantities. In some sense the $\dot{P}$ information is being used in the fitting of the period distribution, which is not the correct way to proceed especially if P and $\dot{P}$ are not distributed independently. Viewed another way, it is possible to fit the $P\dot{P}$ and $P/\dot{P}$ distributions separately and yet not be able to fit the joint $P,\dot{P}$ distribution.

4) A misleading argument

They also plot B vs τ_c (that is $P\dot{P}$ vs $P/\dot{P}$) and claim evidence for decay of B but this is a flawed argument, as pointed out subsequently by Flowers and Ruderman(1977) and Lyne et al(1975). The result can be reproduced by assigning each pulsar the $\dot{P}$ value of its nearest neighbour in the catalogue, showing it to be spurious to the question of field decay. A further drawback is that if the 'deathline' on the $P,\dot{P}$ plane is transformed onto the B vs τ_c plane, it may act to constrain data to lie in the observed portion (see Appendix A5) independent of any field decay. This depends on the exact form taken for the deathline. For example, the deathline $\dot{P} \gtrsim A.P^3$ transforms to $B \lesssim A^{-1}\tau_c^{-2}$, which clearly constrains the data to the lower left corner of the B vs τ_c plane, would give the impression of a time-dependent B.

5) In their analysis of pulsewidths, GO concludes that there is a relation between period and beaming factor, but claim this is insignificant for their earlier conclusions, but without repeating the analysis. This claim is therefore unsubstantiated, and later work by Narayan in particular (Narayan(1987), Vivekanand and Narayan(1982)) has shown that such an effect can have serious consequences for pulsar evolution.

Overall, this paper is difficult to follow, through some obscure and misleading notation, and is guilty of a lack of rigour in the very areas where these are most required. It is not strictly correct to claim success for the field decay model on the basis of this work alone, and since this model has had a major influence on future analyses based on the GO work it is important to remember its inadequacies when interpreting other later contributions.

2.5 THE WORK OF LYNE, MANCHESTER AND TAYLOR

2.5.1 Review of paper.

This paper (Lyne, Manchester and Taylor(1985), hereafter LMT) is recognised as a major contribution to the field of pulsar evolution. Essentially it is a reworking of GO using the more abundant data of 1985, with a total of 316 pulsars used. The same distributions derived by GO are used in LMT, but it is a much more convincing and comprehensive treatment and includes more detail than the earlier paper. The main conclusions reached are very similar;

1) the galactic population is 70,000 pulsars with luminosities above 0.3 mJykpc^2, with a birthrate of 1/(30-120) years.

2) the field decays on a timescale of 9 Myrs, and L ~ B^2 for magnetic field B distributed initially as a log-normal with mean value 7.5x10^{11} Gauss.

3) The distribution in the galaxy is similar to that of OB stars and supernova remnants, but with a larger scale height.

4) The pulsars distribution in P and $\dot{P}$ can be qualitatively understood without invoking a cutoff in pulse production or luminosity, that is no 'deathline' is required.

By 1985, several major surveys had been conducted, which were subject to fairly well-understood selection effects. The data sample comprised 316 pulsars, from which LMT deals with a flux-limited sample of 265 pulsars. They also were able to establish a more reliable distance scale for the pulsars, using work on the interstellar electron distribution, thus reducing one source of systematic error. LMT derive the intrinsic spatial and luminosity distributions for the galactic population by an iterative method developed originally in Large(1971) and Manchester and Taylor(1977). This uses the observed distributions

in cylindrical coordinates r, z and luminosity L, includes known selection effects, and allows the galactic population to be found by integrating over all three variables. This gives 70,000 pulsars in the galaxy.

Next, LMT derive the equations governing the evolution of pulsars, in a manner equivalent to GO, and fit the distribution in τ_c (characteristic age) to give the magnetic field decay timescale t_b, in the LMT notation. Next, a least squares fit to the P_t distribution gives both the mean field at birth and the variance in the (assumed) ln-normal distribution in initial field strength. The resulting period distributions are then compared, although no formal goodness-of-fit criteria are found. A final check is carried out using the distribution in z, the theoretical function derived from an assumption of Maxwellian velocities that the pulsars acquire at birth.

The LMT birthrate is found in a different fashion from the GO paper. Using the assumption of stationarity, and the histogram in luminosity, a lower limit is obtained by insisting that in the most populous luminosity bin, the pulsars must 'traverse' the bin into the adjacent lower bin in a given time dependent on the decay timescale of the magnetic field. This gives an eventual birthrate of 1 pulsar/30-120 years, when an estimated beaming factor is accounted for. This is claimed by LMT to be comfortably compatible with the supernova rate.

2.5.2 Discussion of LMT.

We shall discuss several features of LMT. Firstly, the shortcomings inherent in GO are to an extent eliminated in LMT, which treats a much larger data sample. However, although they statistically fit theoretical distributions to data, this in still done in the wrong order, and the fit to the period distribution occurs last, not first. They also

do not fit the $P,\dot{P}$ distribution, but show a Monte-Carlo simulation of the $P,\dot{P}$ diagram without deriving an analytic expression for the joint distribution.

LMT does not give any formal indication of goodness-of-fit of the theoretical distributions to the observed equivalents. Purely on the basis of the 'fits' in the paper, some would appear to be approximate matches with those observations they are intended to explain.

The iterative scheme used in LMT may be subject to systematic errors. By adopting a separable distribution of r, z and L [cylindrical coordinates r and z, and luminosity L] for the intrinsic population, no correlation is assumed to be present between z and L. An explicit feature of their model is in fact that pulsars at high z have (by hypothesis) migrated from the plane, therefore are older objects and can safely be expected to have lower-than-average fields and luminosities (on the basis of the LMT model). The luminosity is assumed to depend on the square of the field strength, so some bias will be introduced. This effect is possibly counterbalanced by the observed correlation between magnetic field and transverse velocity discused in Section 1.6.7. In general, the distribution at higher z values will be dependent on the distribution in the plane at earlier times, and the problem is not at all trivial.

A related criticism is the distribution in luminosity that is used. A form for the intrinsic luminosity density comes from the iteration scheme. Later, the luminosity law $L \propto B^2$ is adopted. This immediately implies that the intrinsic distribution in luminosity could be derived once the distribution in initial field strength is assumed. However, two different luminosity distributions are used, and thus a possible inconsistency between the two parts of the analysis is apparent. This

is extremely important since the birthrate derivation is made on the basis of the luminosity histogram, but the error that this gives rise to is probably small.

The significance of the derived birthrate is questionable. Essentially it is the ratio of local surface density to a luminosity decay timescale. Since the latter is highly model dependent, and the former obtained in a model independent way, it is difficult to assess its importance, remembering that the iterative scheme is at odds with the decay of pulsar magnetic fields and luminosities. There is also the question of this estimate's independence of the binning scheme chosen- a different birthrate may well arise if a different histogram for luminosity had been chosen. Since this answer is then essentially multiplied by a large factor to give a total galactic birthrate, small discrepancies will be augmented. It is more desirable to use the P and $\dot{P}$ data since they are more reliable observable quantities.

The 'checks' using the z (galactic height parameter) distribution are not quantified.

To conclude this discussion, we note that the work in LMT is a major contribution to the solution of many problems of pulsar evolution, but is subject to some minor failings. There is a possible inconsistency between the two halves of the paper, thus the conclusions may be systematically biased to an extent that cannot be gauged until further work is devoted to this important question. The method for deriving the birthrate is not completely convincing, and suffers from a second inconsistency regarding the form of the luminosity distribution, which firstly, is not identical with the model luminosity law that is used, and secondly the role of the minimum luminosity referred to in LMT is not clear. A final criticism is the ordering of the fitting procedure, and

the reservation that despite the quality of the model fitting that is carried out, we have no guarantee that the LMT model actually fits the $P,\dot{P}$ distribution at any assigned level of significance. Putting the priority on the fitting of the marginal distributions is certainly suspect. These limitations should be dealt with before the field decay model can be properly tested.

2.6 THE ALIGNMENT MODELS OF CANDY AND BLAIR

2.6.1 Review of papers.

In a series of papers, (Candy and Blair(1983), Candy and Blair(1985), Candy and Blair(1986) and Blair(1987)) Candy and Blair developed a pulsar model based on the pulsewidth data and used it to predict a pulsar birthrate. No previous significant correlations of pulsewidth with other pulsar observables had been reported but Candy and Blair concluded from their work that the pulsewidth against characteristic age diagram (Fig. 6.6) showed a distinct minimum at ages around 10^7 years. They then proceeded to explain such behaviour via a combination of alignment of magnetic and rotation axes and a narrowing of the emission cone which they claimed best explained the observed data. The consequent beaming fraction was thus age dependent, and an estimate of the resultant birthrate in Blair(1987) was as high as 1psr/(4 ±1)yrs. The implications of such a high pulsar birthrate are clearly very important.

2.6.2 Discussion of the Candy and Blair models.

However, there is much that can be criticised in this work. Krishnamohan(1985) pointed out a flaw in the original argument, that the mean pulsewidth was not a good parameter to use, since it was sensitive to the presence of pulsars with large pulsewidths in any age bin. There is a large 'tail' in the pulsewidth data with the effect of

these large pulsewidths dominating in any particular bin. Krishnamohan showed that removal of only a few pulsars could also remove the 'minimum' that Candy and Blair found compellingly important. He demonstrated that the median pulsewidth showed no dependence with age and was a better, more stable parameter to use, being less sensitive to the presence of unusually large pulsewidths than the mean. This called into question the validity of the Candy and Blair work. A subsequent paper (Candy and Blair(1985)) reasserted their conclusions but with a more detailed statistical analysis. There is an obvious large scatter in the pulsewidth vs characteristic age diagram, [see Figure 6.6] making any conclusion as to a general trend difficult. Certainly, binning the data as Candy and Blair did is a dangerous procedure under these conditions.

There are some grave criticisms which cast doubt on this work, namely, the complete neglect of luminosity selection effects: they essentially assume that all pulsars are equally bright. Also, their derivation of the mean pulsewidth distribution is only approximate; the work in Chapter 6 shows how this should be conducted, taking proper account of the geometry of the problem, and deriving formally a distribution of pulsewidths.

In their later work (CB1986) the fit between data and model is improved by allowing the alignment timescale to be distributed, introducing a new parameter, and claim this is further evidence for the model. This is wrong, since the distribution is not included in the calculation from the start, as it should be, and again ignores selection effects. Their derivation of the static pulsewidth distribution (i.e. that from an ensemble of non-evolving pulsars) is not given, but if it is based on that of Henry and Paik(1969) it is wrong, since that work

ignores the spherical geometry inherent in the definition of the pulsewidth.

The birthrate estimate of Blair(1987) uses the value of Lyne et al (1985) for the galactic pulsar population, which was reached on the basis of a completely different evolutionary model, inconsistent with that of Blair(1987), who again ignores selection effects due to luminosity. No mention is made of interpulse pulsars, the proportion of which is a direct check on the theory. In short, there are many flaws in this work, and we present a more rigorous and realistic alignment model in the following pages.

2.7 THE INJECTION MODELS

2.7.1 Review of injection model papers.

In a series of papers [Narayan and Vivekanand(1981), Vivekanand and Narayan(1981), Narayan and Vivekanand(1983), Narayan(1987)] these authors introduced the idea of pulsar 'injection'. This basically invoked the 'turning-on' of pulsars at intermediate periods ($\triangleq$0.5 secs), not at pre-Crab-type values of 10 msec, say. In a model-independent argument (their expression) they showed how the so-called pulsar 'current', or flow of pulsars at any period to higher periods reached a maximum only at intermediate periods, and this related directly to the birthrate in these regions. They concluded that it was a genuine effect and from it estimated a birthrate of pulsars which was $\triangleq$ 1/50 years in the galaxy. Other authors in later work (Chevalier and Emmering (1986) and Stollmann(1987b) reached broadly similar conclusions regarding the birth-periods of pulsars.

The late 'turn-on' of pulsars may be related to the mechanism of Blandford et al(1983) where the pulsar magnetic fields are generated by the rotation of the star, on typical timescales of 10^4 years for

intermediate periods.

2.7.2 Criticism of injection models.

However, the model-independence of this approach is not entirely clear. The pulsar current is defined without reference to any model of spin-down, but almost certainly is biased by selection. This is realised by the above authors, but to correct for selection demands a knowledge of the luminosity law which is a component of any model. What is not always realised is the inevitability of injection in order to get round the problem of a luminosity dependence on period of the type $L \propto P^{-1}$ which renders young, fast pulsars highly luminous and thus making it difficult to explain their absence from the observed sample. Such luminous objects ought to be visible over large regions of the galaxy, yet few are seen. A way out is to postulate that the majority of pulsars only enter the scene once their periods reach intermediate values, or are created at these longer periods. This is difficult to reconcile with the observed young pulsars which clearly were born at periods of the order of 10 msec, and are amongst the most luminous pulsars. This was realised by Lyne et al(1985) as a problem, though they had no need for injection.

It is possible to simulate 'injection' even when the pulsars are born at P=10 msec, say. Using a simple model for evolution and a power law with indices α and β (equation 1.8) for luminosity the peak in the resulting pulsar current can be shown to be positioned according to the values of α and β, i.e. is subject to selection effects. See Appendix A6 for details. Drawing a conclusion therefore, from the observed current is fraught with likely misinterpretations.

2.8 MECHANISMS AND DISTRIBUTONS.

That a distribution in neutron star properties is not only likely, but

important in attempting to explain the $P,\dot{P}$ diagram or luminosity laws, should be emphasised. Since most models, in particular GO and LMT, use distributions in magnetic field as an essential ingredient but then attribute the 'success' of their approach to their model of spindown, whereas the two contributions from, in this case, field decay and a Gaussian in $\ln_e(B)$ are both important but to separate out their individual role is not easy mathematically. This is a feature which will prevail throughout all the models we shall study- it is impossible to get any 'fit' to the $P,\dot{P}$ diagram without a range of magnetic field values.

The error estimates on the distance scale are of crucial importance in all analyses of the pulsar population. Uncertainties in distance transmit themselves to determinations of the surface density and luminosities, with increased error bounds on these quantities. This question was investigated by Arnett and Lerche(1981) who concluded that such was our ignorance of several key facts that our resulting birthrate estimates could be out by as much as a factor of x20. They demonstrated that the fitting of pulsar distributions to given forms of electron density led to the parameters of these fitted distibutions so found being coupled in a highly non-linear manner. They also pointed out that uncertainty over the ageing rates of pulsars and the true ages meant that the timescale inherent to the determination of a birthrate was also in doubt to a considerable degree, thus contributing to the error in the birthrate estimate.

CHAPTER 3

TIME DEPENDENT TREATMENT OF PULSAR EVOLUTION

3.1 INTRODUCTION

We shall develop a method for studying pulsar evolution which is based on solving the time-dependent continuity equation in the pulsar distribution function. This will be presented later in this Chapter. This approach differs from all previous work known to the author by the inclusion of the time-dependent term in the continuity equation. The time-independent continuity equation has been used for pulsar studies by Harding(1984), Beskin(1983) and Phinney and Blandford(1981) but the full expression has not been investigated. This is usually justified by stating that pulsar lifetimes are much less than the age of the galaxy, so the assumption that the pulsar population is stationary follows. The subsequent solution of the equation is also simplified. No treatments of the time-dependent case are known, and it is of interest and importance to investigate the consequences of abandoning the steady-state assumption, with the expectation that in the appropriate limits, the results may reduce to those of the time-independent analysis.

3.2 STATIONARITY

Since the lifetime of a pulsar is in fact a model dependent quantity, the 'steady-state' assumption cannot go unchallenged. We do not know, a priori, the pulsar lifetimes, and it would be wrong to assume they will be short compared to the length of time over which they have been formed, which is another unknown quantity. The so-called kinematic ages of pulsars estimated from proper motion observations represent a small, highly biased sample of objects, from a small,biased sample of observable pulsars (see below). As emphasised by Phinney

and Blandford(1981), it would be wrong to base conclusions for the entire pulsar population on this small sample.

The characteristic ages of pulsars can be interpreted in a model-independent way as 'typical times over which the period changes significantly', and the observed distribution spans the range 10^3 yrs to 10^9 yrs. Although these would be considered less than the age of the galaxy, we should recognise that a continuous creation scenario may not be the only possibility, and that a time dependence in birthrate cannot be discounted. One other motivation for the time-dependent method is the ability to deal with scenarios other than those of continuous, uniform birthrates. In particular, the 'starburst' phenomenon could be modelled through a source term including a delta function in time, or the creation rate could be allowed to decay, for example. Such an approach could be motivated by studies of supernova rates in external galaxies (Richter and Rosa(1989) and references therein) which show that there may be 'starburst' galaxies with substantially higher supernova counts than others, suggesting periods of supernovae/star formation on short timescales compare to the galactic age, and not uniform creation.

3.3 SUPERNOVA AND PULSAR BIRTH RATES

Since it is generally accepted that pulsars are created in Type II supernova explosions, and the rate of these is observationally determined, then the pulsar birthrate may not exceed the supernova rate, especially as the end products of supernovae may be black holes, neutron stars or simply debris. Steady state models often find an uncomfortably high birthrate for pulsars in close proximity to the supernova rate which leads to the need for alternative birth scenarios for pulsars, such as accretion-induced collapse of a white dwarf

[Taam and Van den Heuvel(1986)] or 'quiet' death events to replace supernovae being invoked, [Blair(1989)] both of which are ad hoc and less than compelling. It is unsatisfactory to invoke that the collapse of a stellar core to neutron star densities will occur without the emission of neutrinos, shock waves and the expulsion of hot outer shell matter and result in a 'quiet supernova' event. Remembering the 90% of supernova remnants (SNRs) with no visible signs of pulsar activity compared with the 4 pulsars seen in SNRs emphasises the magnitude of this problem. Many supernovae may simply not produce pulsars, unless, somehow they 'turn on' after an implausible 10^{4-5} years (injection). This may be due to the generation of magnetic fields by the Blandford et al(1983) mechanism, but this is far from accepted as an established effect. Injection is in contradiction with the observations of the youngest pulsars which can be dated fairly reliably through the age of the SNR, and are seen to be highly energetic objects, directly influencing the evolution of the shells of gas in which they are embedded through their output of fast particles, magnetic fields and intense radiation.

Supernovae are the synthesis machines for heavy element production and to satisfy the observed abundances in the galaxy through production in supernovae requires fairly stringent limitations on the types and nature of progenitor stars which can pose problems for high pulsar birthrates unless one can produce pulsars and synthesise heavy elements in the one event. The mass range available for neutron star formation can be constrained by the requirement of production of the correct abundances of iron-peak elements (Ostriker et al(1974)) and it may not be possible to produce both a remnant neutron star and a significant yield of heavy elements unless substantial mixing has

occured before the supernova explosion, as one expects the heavy elements to be produced primarily in the core of the star.[Bethe and Brown(1989)]. Although these conclusions are tempered by the later work of Shipman and Green(1980) who, by using a more realistic stellar birthrate function, showed that the limits on the mass range of neutron star progenitors were less demanding than those suggested by Ostriker et al(1974), thus partially obviating the problem. However, they do not consider the question of iron abundance and heavy element production, and introduce the further difficulty created by the additional necessity to produce the required white dwarf numbers, which constrains neutron star production through the lower mass bound. Their conclusion, however, is of interest, in that they recognise a solution is possible to the various problems if the adopted pulsar birthrate is as low as observations allow- this shows that a high pulsar birthrate creates problems in many areas, and it is wise to look carefully at any birthrate which is sufficiently high to infringe on other established areas of knowledge. We also note the work of Hills(1978) who calculated an upper limit to neutron star production in the galaxy through the constraint of the galactic luminosity, and reached an extreme upper limit of $1/(27 \pm 10)$ years. This should alert us to question any birthrate which approaches near this bound. For compatiblility with the supernova rate estimates of Van den Bergh(1987), Van den Bergh(1988), bearing in mind this discussion, we would consider any pulsar birthrate of this size as uncomfortably high.

3.4 PULSAR KINEMATIC VELOCITIES

The 'short pulsar lifetimes' argument was apparently vindicated following the measurement of proper motions of a small sample of

pulsars by various groups (Lyne et al(1982), Helfand and Tademaru(1977), Anderson and Lyne(1983), Cordes(1986), Cordes(1987)) which suggested that pulsars are unusually high velocity objects. By measuring the separation from the galactic plane, z and its rate of change $\dot{z}$ a kinematic age could be defined $\tau_k = z/\dot{z}$ which suggested typical ages of $\sim 10^6$ yrs. for the sample. This appeared to justify the stationarity assumption but also to back up models where field decay takes place on a similar timescale, thus causing the pulsar to cease pulsation and hence 'die off'.

There are, however, several questionable features of this approach-

a) The true space velocities are unknown, since only transverse motion can be detected- thus the true direction of pulsar motion is unknown as is the birthplace.

b) Velocities measured by different techniques do not agree/correlate very well, casting some doubt on at least one set of observations

c) Only a small sample has been studied, 26 pulsars in Lyne et al(1982) and 71 pulsars in the Cordes sample [Phinney and Blandford(1981)]

d) Potental associations with nearby supernova remnants failed for all of the Lyne et al(1982) sample.

e) A correlation between transverse velocity and $B = (P\dot{P})^{1/2}$ was deduced from both samples, and taken to be a causal relationship. Some authors [Stollmann and Van den Heuvel(1987) and Phinney and Blandford(1981)] have argued that this could be due to selection effects since the sample may be highly biased, thus making it unsuitable as a basis for assumptions which crucially influence the rest of the approach to pulsar evolution.

f) The status of the interstellar scintillation measurements of pulsar

transverse velocities has been questioned by the work of Lee and Jokipii(1976) who argued that the typical speeds of plasma disturbances in the interstellar medium is of similar magnitude (100km/sec) or greater than the transverse velocities of the pulsars, thus making the assumption that the scintillation observations are due to the pulsar motion questionable. This has also been pointed out by Arnett and Lerche(1981). Lee and Jokipii(1976) actually use the scintillations to estimate the typical speed of interstellar disturbances.

g) In addition, some of the sample appear to be heading towards the galactic plane, contrary to the assumption of birth at z=0 and making age estimates impossible. The Crab pulsar, in many ways the best studied and canonically regarded pulsar, in fact has a large discrepancy between its (well-known) true age and the inferred kinematic age by a factor of 10^3. The Crab can be reliably dated by Chinese records of the 1054A.D. supernova which produced the pulsar.

The work of Hanson [Hanson(1979a) and Hanson (1979b)] on proper motion distributions in fact raises the kinematic ages deduced from proper motions thus partly reducing the discrepancy between these and the characteristic ages found from period derivatives. Hanson's estimate of the velocity dispersion (Hanson 1979b) appropriate to a Maxwellian velocity distribution is considerably smaller than that obtained directly from the calculated individual transverse velocities. This illustrates the

To the author's knowledge, this analysis has not been repeated with the more complete sample of Cordes(1986). It would be of great interest to test the conclusions of Hanson against the larger observed data sample.

It is probable that the apparent correlation between B (magnetic field strength) and V_t (transverse velocity) is due to selection effects, in this case the Malmquist Bias and the observational discrimination against slow-moving objects. To observe pulsars at large distances they have to be luminous and to observe a proper motion they must be moving at a substantial speed, both quantities in general above the 'average' expected for the population as a whole. It is quite possible that this gives rise to the correlation, especially if the luminosity of the pulsar depends e.g. on the magnetic field [GO take $L \sim B^2$ as do LMT] . It is difficult to see that such an 'unlikely' relation could be causal. However an attempt by Stollmann and Van den Heuvel(1986) to reproduce this from a simulation did not achieve more than partial success. They did point out that the degree of correlation was more dependent on what pulsars were included in their sample than the selection effects that they included. It is possible that given more extensive study, the correlation may turn out to be entirely spurious. Stollmann and Van Den Heuvel only treated one particular model of evolution, namely field decay, and it is possible other models would give substantially different conclusions.

The novel pulsar model of Cheng(1985) explains such a relationship using a model based on the capture of interstellar grains to generate pulsations in the magnetosphere, such that faster pulsars capture more grains, spin down more efficiently and hence have apparently higher magnetic fields. However it can be safely asserted that the energetics of the system are powered by the rotation of the neutron star not the motion of it through the sky, and even pulsars with low velocities can be highly luminous, independent of their space velocities.

3.5 CONSEQUENCES OF TIME INDEPENDENCE

We shall start by looking at the steady-state assumption as it has been used by other authors [GO,LMT, Chevalier and Emmering(1986), Emmering and Chevalier(1989)]. Firstly, it should be noted that the age of the galaxy is a little-publicised parameter in the steady-state models. This is to ensure there is only a finite number of pulsars in the intrinsic population, a total that is of some interest, and that the intrinsic distribution is normalisable. Secondly, the role played by the 'deathline' can be important. If the deathline marks a genuine cutoff in the pulsar emission process then pulsars do 'die' as they cross it, and drop out of the calculations. If it is the result of a luminosity selection effect, such as a power law in P and $\dot{P}$ then pulsars below the deathline are merely too faint to be detected, but are present in the intrinsic distribution function. This latter option would mean that stationarity of the pulsar population is determined by selection effects and the model of evolution that is being studied. This is a rather critical point. For example, in the field decay models, the dominant parameter τ virtually forces a steady-state since with exponential decay the age of the Galaxy t_0 is supressed by the terms including $\exp(-t_0/\tau)$. However, this does not necessarily happen for all combinations of luminosity laws and evolutionary mechanisms. The model of Gunn and Ostriker (GO) happens to be the best example of this effect.

We aim to show in this chapter, for simplified analytic models, that a steady state need not arise: hence the assumption of steady state with an incompatible model will have serious effects on for example, the birthrate determination. In their paper, Chevalier and Emmering(1986) attempted to generalise the models of GO and LMT by including an

arbitrary luminosity law of the form $L = \Delta P^{\alpha}\dot{P}^{\beta}$ for constants α , β and Δ. They failed to indicate that their approach would fail due to being un-normalisable for certain combinations of α and β. This applies to the age distribution that is derived.

We will solve the time-dependent continuity equation for two simplified models, 1 and 2, with and without field decay respectively. We show that $N_{obs}(t_o)$, the number of pulsars observable after galactic age t_o will not necessarily reach a fixed value. Hence the determination of the birthrate is uncertain if a steady state is assumed to have been reached. Also it will be shown that the birthrate cannot always be determined uniquely, but only in combination with other model parameters. This is a feature of other work that has not been stressed. For the field decay model (2) a steady state can be reached for some ranges of parameter space but in model 1 it cannot be reached except as a special case. These simplified models are not designed to explain or be compatible with the observed distribution of both period and period derivative, but instead to emphasise the importance of selection effects and show the application of our method. This will be developed in future chapters to create detailed models that can be fitted and tested against the observations. It will be found that some of the features inherent in the simple models will be present in the sophisticated treatments, even down to the determination of birthrates. This is why GO and LMT have different methods of determining birthrates. Despite using the theory of GO, LMT recognises the unsatisfactory nature of the earlier birthrate estimate and proceed with an entirely new method. As pointed out in Chapter 2, this may not be an ideal replacement. We shall only treat the case of constant, uniform creation here to maintain compatibility

with other studies and the case of time-dependent birthrates shall be considered later in Chapter 7.

3.6 TIME DEPENDENT CONTINUITY EQUATION METHOD

3.6.1 The time dependent continuity equation.

The implicit assumption of most analyses of pulsar statistics (and all treatments known to the author) is that the population is time-independent. Evidently, the solution of the time dependent case should be expected to contain the steady state solution as a special case. We shall formulate the problem in its most general terms and then apply the theory to particularly simple models in the remainder of this chapter, and again in more detail in later chapters.

A pulsar is described by the values of a number of variables, the obvious ones being the period P, period derivative $\dot{P}$ and luminosity L. The pulsar model specifies the dynamics of the pulsar's evolution. In general terms we denote the variables necessary to describe a pulsar by $x_1,x_2,\ldots x_n$ and assume the model specifies the dynamical laws $\dot{x}_j = f_j(x_1,x_2,\ldots x_n)$. When considered in the context of a population of pulsars, $x_1,x_2,\ldots x_n$ become statistical variables. Denoting the number density of pulsars in this coordinate space by $n(x_1,x_2, \ldots x_n)$, in the sense that the number of pulsars in the coordinate volume $dV = dx_1dx_2\ldots dx_n$ is given by $n(x_1,x_2,\ldots x_n)dV$, the number created per unit volume of coordinate space per second by $C(x_1,x_2,\ldots x_n)$. It then follows that $n(x_1,x_2,\ldots x_n)$ satisfies

$$\frac{\partial n}{\partial t} + \frac{\partial (n.\dot{x}_1)}{\partial x_1} + \frac{\partial (n.\dot{x}_2)}{\partial x_2} + \ldots = C(x_1, x_2, \ldots ;t) \quad ..(3.1)$$

3.6.2 Solution of the time-dependent continuity equation.

The general solution to this continuity equation may be written

$$n(x_{1o}, x_{2o}, \ldots; t_o) = n(x_{1I}, x_{2I}, \ldots; t_I) \cdot \frac{\partial(x_{1I}, x_{2I}, \ldots)}{\partial(x_{1o}, x_{2o}, \ldots)} + \int_{t_I}^{t_o} \frac{\partial(x_1, x_2, \ldots)}{\partial(x_{1o}, x_{2o}, \ldots)} C(x_1, x_2, \ldots; t)\, dt \qquad (3.2)$$

where the suffix 0 refers to the time of observation and the suffix I to the initial time. Thus equation (3.2) gives the number density at the present epoch as a sum of two terms. The first term represents the initial number density multiplied by a factor that simply amounts to the ratio of dV_I/dV_0, i.e. the Jacobian. In absence of creation, all pulsars initially in dV_I at t_I will be "advected" into dV_0 at time t_0. The second term is the integral along the pulsar trajectory on which $x_{10}, x_{20}, \ldots x_{n0}, t_0$ lies of the number of pulsars created per unit time per unit volume of coordinate space again multiplied by the dilatation factor dV_I / dV_0. It is thus simply the integrated contribution to the present number density of pulsars created between times t_I and t_0. We shall now prove this result. For simplicity, we look at the case of one variable, x, so the continuity equation will be:

$$\frac{\partial n(x;t)}{\partial t} + \frac{\partial}{\partial x}(\dot{x}.n(x,t)) = C(x;t) \qquad (3.3)$$

Referring to Figure 3.1, we see how pulsars from points A and B flow (evolve) to C and D as time passes. To find the number density at C, which is the point (t_o, x_o), we must integrate over all contributions from pulsars created between an initial time t_I (the onset of pulsar creation) and a present time t_o. A model will be specified by the

form for $\dot{x}$ as a function of x and t. We solve this, to give formally;

$$x = f\ (t,x_*,t_*) \qquad (3.4)$$

where each trajectory is specified by one reference point (x_*,t_*), and a parameter, in this case t. We could equivalently have allowed x to be the parameter. Let points A, B and C have coordinates (t,x_1), $(t,x_1+\Delta x_1)$ and (t_o,x_o).

The number of pulsars created in the range AB will be $C(x_1;t)\Delta x_1$.

From (3.4) we see that $x_1 = f(t;x_o;t_o)$ (3.5)

Similarly, we get an expression giving the coordinates of point B as follows:

$$x_1+\Delta x_1 = f(t;x_o+\Delta x_o;t_o) \approx f(t;x_o;t_o) + \frac{\partial\ f(t;x_o;t_o)}{\partial\ x_o}.\Delta x_o \qquad (3.6)$$

Thus the number density contribution at (t_o,x_o) from those pulsars created at time t is $dn(x_o;t_o)\Delta x_o = C(x,t).\Delta x_1$

$$\text{Thus } dn(x_o;t_o) = C(x,t).\frac{\Delta x_1}{\Delta x_o} \qquad (3.7)$$

So the integrated contribution will be:

$$n(x_o;t_o) = \int_{t_I}^{t_o} \left|\frac{\partial x}{\partial x_o}\right| C(x;t)\ dt \qquad (3.8)$$

The second contribution is from pulsars already present before the creation onset at t_I, possibly from a previous burst of pulsar creation. Normally, this will be ignored, in a steady creation model.

$$\text{This will be simply } n(x_I;t_I).\frac{\Delta x_I}{\Delta x_o} \qquad (3.9)$$

i.e. the Jacobian factor times the original number density.

Hence, by applying this argument to several variables, we get the result of equation (3.2)

3.6.3 Predicting the observed distribution.

So far we have not related the number density n to the number of observed pulsars with generalised coordinates in a certain range. In principle it is possible to consider the positional coordinates of the pulsars as included in these generalised coordinates. For simplicity we shall assume that the number density is homogeneous within the galactic disc. Since the pulsars are concentrated in the plane of the disc we shall refer to a surface density.

The total number of pulsars per unit area is

$$n_0(t) = \int\int...\int n(x_1,x_2,....x_n;t)dx_1dx_2...dx_n \qquad (3.10)$$

The joint density for x_1 and x_2, say, is similarly

$$n_{12}(x_1,x_2\ ;t) = \int\int..\int n(x_1,x_2,..x_n;t)dx_3dx_4...dx_n \qquad (3.11)$$

As we have already indicated, n_0 and the joint densities discussed above refer to the intrinsic population of pulsars. The observable distributions will depend on the selection effects, the most important of which we take to be the flux-limitation of the pulsars surveys and the beaming of the pulsar radiation. We also note the period-dependent selection inherent to the detection process, as outlined in LMT, whereby fast pulsars are less likely to be detected.

Under the assumption that the number densities of pulsars are spatially homogeneous within the galactic disc, the observable number density becomes

$$n_{obs}(x_1,x_2,...x_n\ ;t) = \int_0^R n(x_1,x_2,...x_n\ ;t)B(x_1,...x_n) \times H(L-4\pi r^2F_{min})2\pi rdr \qquad (3.12)$$

where $B(x_1,x_2,..x_n)$ is the beaming selection fraction, which can in general depend on the x_j and gives the fraction of all pulsars that are visible to us by virtue of favourable orientation; R is the galactic radius, F_{min} the flux threshold at which a pulsar is observable and H

a Heaviside step-function.

The beaming fraction B has been discussed by a number of authors [Proszynski(1979), Candy and Blair(1983), Candy and Blair(1986), Narayan(1987), Narayan and Vivekanand(1983) and Lyne and Manchester(1988)] and evidently depends on the particular model for the pulsar beam. If we accept the polar cap model for the emission and the idealised geometry of a conical beam(see Proszynski(1979)) then the factor B will be constant when the alignment angle (defined here as the angle between magnetic and rotation axes) does not change as the pulsar evolves. In alignment models for pulsar evolution the B factor will become a variable dependent on period, introducing a more complicated selection effect. Equation (3.12) relates the observed number density to the intrinsic number density. The marginal distribution of any variable may be found by integrating out over all the others.

3.7 APPLICATION OF METHOD TO SIMPLE MODELS

3.7.1 MODEL 1 : No field decay.

For pure magnetic dipole radiation we know that the spindown law can be written $\dot{P} = k/P$, for constant k. This can be generalised by the introduction of the braking index n, defined by the new spin-down law

$$\dot{P} = k\, P^{2-n} \qquad (3.13)$$

The case $n = 3$ corresponds to pure dipole radiation. If there are substantial magnetic moments higher than dipole present then n may be greater than 3 [Phinney and Blandford(1981)], but inertial effects tend to reduce n [Roberts and Sturrock(1972)]. Observations of the Crab pulsar indicate $n \simeq 2.5$ [Groth(1975a,1975b)], though the values are uncertain for other pulsars through the errors in measuring $\ddot{P}$ [Kundt(1988)]. The solution of (3.13) gives us the pulsar trajectory:

$$P^{n-1} - (n-1)kt = P_o^{n-1} - (n-1)k_o t_o \quad ..(3.14)$$

$$k = k_o \quad ..(3.15)$$

So the Jacobian required in (3.2) is

$$\frac{\partial(P,k)}{\partial(P_o,k_o)} = \frac{P_o^{n-2}}{P^{n-2}} \quad ..(3.16)$$

so that from (3.2) and (3.16) it follows that:

$$n(P_o,k_o;t_o) = \frac{P_o^{n-1}}{P^{n-1}} n(P_I,k_o;t_I) + \int_{t_I}^{t_o} \frac{C(P,k;t)P_o^{n-2}}{P^{n-2}}\, dt \quad ..(3.17)$$

By choosing t_I to be the start of the pulsar-forming epoch, we can set $n(P_I,k_o;t_I) = 0$. We take the source term to be the following:

$$C(P,k;t) = c_o\, \delta(P-Q)\, H(t)\, K(k) \quad ..(3.18)$$

so that all pulsars are created with initial period Q, but with a distribution in k of K(k), and the Heaviside step-function H(t) allows only $t \geq 0$. This gives:

$$n(P_o,k_o;t_o) = c\, P_o^{n-2} \int_0^{t_o} \frac{\delta(P-Q)\, K(k)\, H(t)}{P^{n-2}}\, dt \quad ..(3.19)$$

Changing the variable of integration to P, equation (3.19) becomes:

$$n_{obs}(P_o,k_o;t_o) = c\, P_o^{n-2} k_o^{-1} K(k)\, H(Q^{n-1} + (n-1)k_o t - P_o^{n-1}) H(t)\Big|_{P=Q} \quad (3.20)$$

so applying the luminosity and beaming selection effects to obtain the observed distribution :

$$n(P_o,k_o;t_o) = \frac{Bc_o\Delta}{4F_{min}} P_o^{n-2+\alpha-\beta} k_o^{\beta-1} K(k_o) H_1 H(t)\Big|_{P=Q} \quad (3.21)$$

where H_1 is the first of the two step-functions above. Now we split the work into two cases 1a and 1b. In 1a we treat the simpler case of K(k) being a delta function i.e. $K(k) = \delta(k-k_o)$ and in 1b k is distributed as

$$K(k) = k a^{-2} \exp(-k/a) \quad ..(3.22)$$

where a is the modal value of k.

First we treat case 1a. By integrating over k in equation (3.21) with $K(k) = \delta(k-k_0)$, we get the observed period distribution

$$n_{obs}(P_o;t_o) = c_o B \Delta (4F_{min})^{-1} P_o^{\epsilon-1} k_o^{\beta-1} H(t)\Big|_{P=Q}^{H(P-Q)} \quad ...(3.23)$$

where $\epsilon = n+\alpha-1-\beta$ ....(3.24)

This takes the form of a power law in P_o. This is not of course similar to the observed period distribution but that is not the primary objective of this part of the work. We can see that both the braking index n and the parameter $\alpha-\beta$ (one parameter only due to our assumption of $K(k) = \delta(k-k_0)$) will determine the form of this distribution. A further integration over P_o will give the total number of observable pulsars, which, when normalised to the observed total of 250 above F_{min} = 10 mJy will determine the combination that appears in equation (3.23) ,namely $Bc_o\Delta k^{\beta-1}/4F_{min} = \lambda$, say. Here the beaming fraction B can be taken as 0.2, a typical figure [Proszynski(1979) and Lyne and Manchester(1988)] but now we notice that to find c_o explicitly it is necessary to know both Δ and k_o i.e. that it depends on both the 'mean' magnetic field and the luminosity law that is being used. Thus, to find the total number of pulsars observed after galactic age t_o, $N_{obs}(t_o)$, there are three cases that can be discriminated:

We define $\epsilon = n-1+\alpha-\beta$, so that the three cases correspond to $\epsilon > 0$, $\epsilon = 0$ and $\epsilon < 0$ respectively. We note that the above results hold for $n > 1$ so a condition can be made on the combination $\alpha-\beta$. We can write:

$$N_{obs}(t_o) = B (4F_{min})^{-1} c_o \Delta k^{\beta-1} \int_Q^{P_{max}} P^{\epsilon-1} dP \qquad (3.25)$$

where $P_{max} = (Q^{n-1} + (n-1)kt_o)^{n-1}$ (3.26)

and Q is the period at birth.

So we get the following:

$$\epsilon > 0 \quad : N_{obs}(t_o) \triangleq \lambda \epsilon^{-1} [(n-1)k_o t_o]^{\epsilon/(n-1)} \qquad (3.27)$$

$$\epsilon = 0 \quad : N_{obs}(t_o) \triangleq \lambda \ln [1 + (n-1)k_o t_o Q^{n+1}]^{1/(n-1)} \qquad (3.28)$$

$$\epsilon < 0 \quad : N_{obs}(t_o) \triangleq \lambda Q^{\epsilon} | \epsilon |^{-1} \qquad (3.29$$

It is immediately clear that the ageing of the Galaxy does not necessarily result in a constant number of pulsars being observed. Only in the case $\epsilon < 0$ does a steady-state result. In the other cases, the observed number of pulsars will increase with increasing galactic age. The above approximations have assumed $Q \ll P$ to simplify the expressions. There is a minimum period pulsars can be created with, since stability of the star demands a rotation period of approximately 1 msec or more [See Friedman(1983), Friedman et al(1986)]. From the expression for the constant λ we see that when an attempt is made to determine c_o by equating N_{obs} to 250 pulsars, the combination of parameters is actually determined, not the birthrate uniquely. If the parameters n, Δ, α and β are assumed known, along with k_o then we can find $c_o B$. A further estimate of B allows c_o to be found. But since none of these quantities can be observed or deduced without an evolutionary model, the real value of the birthrate remains unknown.

Clearly, this model does not fit in comfortably with conventional stationarity assumptions. We can show the estimated birthrates for various luminosity laws and how the mean field strength and birthrate are inextricably linked. For convenience, we choose $n=3$ as the

birthrate estimates are more strongly linked to our knowledge of the luminosity law than the braking index, which is almost certainly in the approximate range 2-4, although direct observation cannot help identify a reliable value.

The birthrates are tabulated in Table 1a, for various values of n, k_o and t_o and for five different luminosity law pairings of α and β. Before these are discussed, we move on to derive the corresponding expressions for Case 1b.

Case 1b of Model 1.

Now $K(k) = ka^{-2}\exp(-k/a)$ ...(3.30)

K is distributed according to the above expression, a gamma-type distribution. Here a is the modal period, referring to the intrinsic, not the observed distribution. Integration over equation (3.21) now gives an observed period distribution of :

$$n_{obs}(P_o;t_o) = \int_{k_{min}}^{\infty} n_{obs}(P_o,k_o;t_o)dk \qquad (3.31)$$

where the existence of k_{min} is a consequence of time-dependence. If the galaxy is an age t_o then to have reached a period P_o in that time a pulsar must have had at least a minimum field strength to have spun-down as far as P_o. In fact k_{min} is :

$$k_{min} = \frac{P^{n-1} - Q^{n-1}}{(n-1)t_o} \qquad (3.32)$$

so this gives for the period distribution:

$$n_{obs}(P_o;t_o) = c_o B \Delta \frac{P^{n-2+\alpha+\beta(2-n)}}{4F_{min}} a^{\beta-1}\Gamma\left[\beta+1, \frac{P^{n-1}-Q^{n-1}}{(n-1)at_o}\right] \qquad (3.33)$$

where $\Gamma(\ ,\ )$ is an incomplete Gamma function defined in the sense of Press et al(1986) such that $\Gamma(a,0) = G(a)$, $\Gamma(a,\infty)=0$. (Here G(a) is a conventional (complete) gamma function). A further

integration of (3.33) allows $n_{obs}(t_o)$ to be found and tabulated for various n, a and pairs of α and β.

Next we derive expressions for Model 2.

3.7.2 MODEL 2 : FIELD DECAY

The following equations govern the pulsar's spindown:

$$\dot{P} = k\, P^{-1} \qquad \ldots(3.34)$$

and $k = k_o \exp(-(t-t_o)/\tau)$ $\ldots(3.35)$

We have assumed $n = 3$ for convenience. Now τ is the e-folding time for the magnetic torque k. The pulsar trajectory, on integration, is:

$$P^2 + 2k\tau = P_o^2 + 2k_o\tau \qquad ..(3.36)$$

It follows that the Jacobian is

$$\frac{\partial(P,k)}{\partial(P_o,k_o)} = \frac{P_o k}{P\, k_o} \qquad (3.37)$$

Adopting the same source term as before, (3.18)

$C(P,k,t) = c_o \delta(P-Q)K(k)H(t)$, we solve (3.2) to get

$$n(P_o,k_o;t_o) = c_o P_o k_o^{-1} \int_o^{t_o} \delta(P-Q)K(k)kP^{-1}H(t)dt \qquad (3.38)$$

$$\text{so } n(P_o,k_o;t_o) = c_o P_o k_o^{-1} K(k_o+(P_o^2-Q^2)/2\tau)H_1H_3 \qquad (3.39)$$

$$\text{where } H_3 = H(Q^2 + 2\tau k_o[\exp(t/\tau)-1]-P_o^2) \qquad (3.40)$$

and H_1 is as before, $H_1 = \delta(P-Q)$.

Include the selection effects as before to get the observed distribution

$$n_{obs}(P_o,k_o;t_o) = \frac{c_o \Delta\, B\, k_o^{\beta-1}\, P_o^{1+\alpha-\beta} K\{k_o+(P_o^2-Q^2)\}H_1H_3}{4F_{min}\qquad\qquad 2\tau} \qquad (3.41)$$

For the case where $K(k) = \delta(k-k_*)$ (from now on Case 2a)

the marginal density in period is:

$$n_{obs}(P_o;t_o) = \frac{c_o \Delta B P_o^{1+\alpha-\beta}\{k_* + (P_o^2 - Q^2)\}^{\beta-1} H_1 H_3}{4F_{min}} \qquad (3.42)$$

and integration over P_o gives the observed total number of observable pulsars in terms of c_o, τ, Δ, F_{min}, k_* and B. These results are displayed in Table 2a. The last case is thus that featuring the same distribution of initial magnetic torques as in 1b, so we complete this section by deriving the results for Case 2b.

Case 2b. Integration of equation (3.41) with K(k) as given in (3.30) leads to the following expression for the observed period distribution:

$$n_{obs}(P_o,t_o) = c_o B \Delta P_o^{1+\alpha-\beta} a^{\beta-1} \exp-\left[\frac{P^2-Q^2}{2a\tau}\right] G(\beta)\{X\} \quad ...(3.43)$$

where $\{X\} = a^{\beta} Q'\left(\beta+1, \frac{k_{min}}{a}\right) + \frac{(P_o^2-Q^2)}{2\tau} Q'\left(\beta, \frac{k_{min}}{a}\right)$ ...(3.44)

and $G(\beta)$ is a normal single-argument proper gamma function, whereas $Q'(a,x)$ is an incomplete gamma function, in the notation of Press et al(1986). Thus we integrate over (3.44) to find $n_{obs}(t_o)$ in the usual way. Now we look at the luminosity laws to be used.

3.8 LUMINOSITY LAWS

Several laws have been discussed in the literature: we look at five pairs of α and β that span the range believed to be relevant.

The five laws of interest are:

(1) $\alpha = -1$, $\beta = 0.33$ This is the law proposed by Proszynski and Przybcien (1984) on the basis of a regression fit to the observed data.

(2) $\alpha = 1$, $\beta = 1$. This is the law used by GO and LMT. It is equivalent to setting $L \propto B^2$ and is clearly different from (1).

(3) $\alpha = 0$, $\beta = 1$ This law was briefly considered by LMT, but retains an implicit P-dependence through $\dot{P}$ although $\alpha = 0$.

(4) $\alpha = -1.5$,$\beta = 0.5$ Stollmann(1987a,b) suggested this law on the basis of his model for pulsar evolution.

(5) $\alpha = -1$, $\beta = 1$ This allows $L \propto \tau_c^{-1}$ where τ_c is the characteristic age of the pulsar.

For each of these laws we shall determine the inferred birthrates. First we must find a value for the parameter Δ. Although not a realistic approximation, we shall assume all pulsars have the same Δ. Using the Crab and Vela pulsar data for P and $\dot{P}$, Δ is calculated for each. These two values, found for each law, will be used in the birthrate evaluations.

For models 1a and 1b we choose two values each of braking index n, galactic age t_0 and mean magnetic torque k_0, so that for each luminosity law, 16 different birthrates are found.

For models 2a and 2b, n is fixed at 3, but we use two values of decay timescale τ, again giving 16 birthrates for each (α,β) pairing, and 80 altogether, for each model.

3.9 RESULTS AND DISCUSSION

3.9.1 Models 1a,1b

We can see immediately the influence on the pulsar birthrate of different luminosity laws. Looking at Tables 1a, 1b, 2a and 2b we see a large range of derived creation rates, and a variety of different dependencies on the model parameters. Perhaps the most important point to note is that, for model 1, no steady state is reached except for the particular case of $n=2$, $\alpha=-1.5$ and $\beta=0.5$. The other luminosity laws produce a birthrate that depends on the age of the galaxy explicitly. This proves that not all models of pulsar evolution are consistent with the steady-state hypothesis

The braking index influences the birthrate too (Tables 1a and 1b). No

overall conclusion is readily apparent, but $n = 3$ generally gives a higher birthrate, except for some cases with $\beta=1$. The effect of increasing parameter k_0 is similarly difficult to summarise. In some cases birthrate is independent of k_0 (law 5, Table 1a, $n = 2$), in others the birthrate rises/falls as k increases.

The introduction of a distribution in k tends to alter the birthrate. This is a consequence of luminosity selection: since $\beta > 0$ for all our laws, it is pulsars with higher k values that will be more luminous. Since there is a distribution of k-values, one particular range of k will be favoured through selection, depending on the value of α as well, since high k implies faster spindown as well. Thus the higher the modal value a, the fraction of all pulsars that will be visible may rise or fall, thus demanding a change in the birthrate to maintain the fixed total of observed pulsars. There is a very considerable gap between the extremal values of birthrate found:

Highest birthrate in model 1: 1 pulsar /0.67 years

Lowest birthrate in Model 1: 1 pulsar /10^4 years.

3.9.2 Models 2a,2b.

Now we see the influence of field decay in creating a steady-state, provided t_0 is sufficiently large compared to τ, the decay timescale. For larger τ, it simply takes longer for a steady-state to arise. The effect of raising the initial torque a can lower or raise the birthrate depending on the luminosity law. Introducing a distribution in initial field strengths also tends to raise the birthrate, in the field decay case. Again, a wide range of birthrates is calculated:

Highest birthrate in model 2: 2.4 pulsars/ year

Lowest birthrate in model 2: 7 pulsars/10^3 years.

These models are not intended to reproduce the observed properties

of the pulsar population. They demonstrate instead the difficulty in finding the true pulsar birthrate when the sample is subject to selection effects, whose mathematical form is not precisely known, and the interdependence of the birthrate and the model parameters in some cases.

Of crucial importance is the role of the time-dependence. Although model 1 is not necessarily realistic in terms of explaining the $P,\dot{P}$ diagram, for example, it is not possible to study the effects of it without including time-dependence: we cannot always assume stationarity. For models with field decay, stationarity holds for galactic ages of more than a few times the decay timescale. However, both of these are parameters that we may wish to estimate on the basis of our studies of the pulsar population, so it is dangerous to assume a prior relation between them. The time-dependent continuity equation approach avoids all these pitfalls and is easy to apply.

We now proceed to develop more detailed models for pulsar evolution and to test them against the observed data to attempt to discriminate between competing evolutionary hypotheses.

3.10 INVERSE PROBLEMS

It can be seen from equation 3.21, for example, that the expression for the observed period distribution involves an integration over the intrinsic distribution in k. This suggests the solution for an unknown K(k) by using the observed period distribution on the left-hand side of the equation and proceeding to solve an inverse problem. This aspect of the time-dependent method is discussed more fully in Appendix A7, for a variety of different problems. This is a novel and potentially useful means of broadening our insight into the problems of pulsar evolution. We return to this question in Chapter 7.

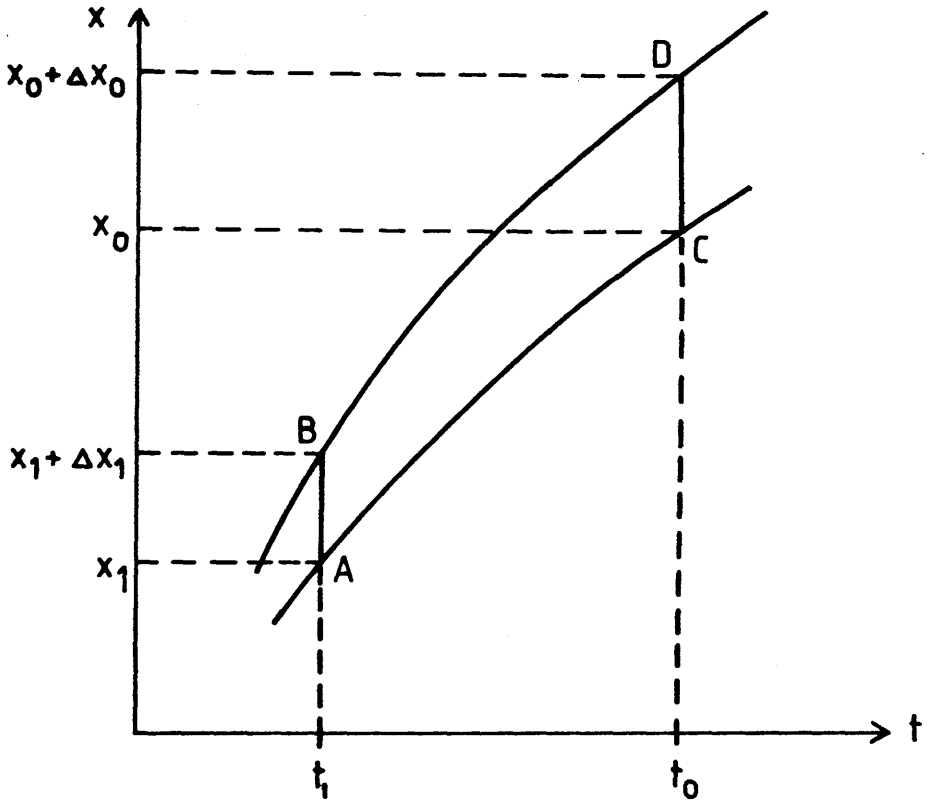

FIGURE 3.1

Diagram to illustrate the 'flow' of pulsars as described by the continuity equation. All the pulsars initially in the segment AB at time t_1 will be in the region CD at time t_0. The Jacobian relates the relative 'volumes' of these regions. When only one variable is involved, this becomes the ratio of the lengths of the line segments AB and CD.

TABLE 1A

PULSAR BIRTHRATES FOR MODEL 1A

				AGE = 1.E16 s		AGE = 1.E17 s	
ALPHA	BETA	DELTA	MEAN-K	C2.0	C3.0	C2.0	C3.0
			x1.E-16 s/s	x1.E-2 psrs/yr		x1.E-2 psrs/yr	
-1.00	0.33	0.14E+07	10.0	0.808	3.682	0.762	1.703
-1.00	0.33	0.22E+07	10.0	0.514	2.343	0.485	1.084
-1.00	0.33	0.14E+07	1.0	0.198	1.703	0.173	0.787
-1.00	0.33	0.22E+07	1.0	0.126	1.084	0.110	0.501
1.00	1.00	0.23E+18	10.0	0.069	0.034	0.007	0.003
1.00	1.00	0.11E+18	10.0	0.143	0.072	0.014	0.007
1.00	1.00	0.23E+18	1.0	0.686	0.343	0.069	0.034
1.00	1.00	0.11E+18	1.0	1.435	0.717	0.143	0.072
0.00	1.00	0.76E+16	10.0	3.005	4.643	2.254	1.468
0.00	1.00	0.10E+17	10.0	2.284	3.529	1.713	1.116
0.00	1.00	0.76E+16	1.0	4.499	14.682	3.005	4.643
0.00	1.00	0.10E+17	1.0	3.419	11.158	2.284	3.529
-1.50	0.50	0.30E+08	10.0	1.665	27.255	1.664	22.929
-1.50	0.50	0.94E+08	10.0	0.531	8.698	0.531	7.318
-1.50	0.50	0.30E+08	1.0	0.531	10.622	0.527	8.619
-1.50	0.50	0.94E+08	1.0	0.170	3.390	0.168	2.751
-1.00	1.00	0.25E+15	10.0	6.318	103.424	6.313	87.010
-1.00	1.00	0.89E+15	10.0	1.775	29.052	1.773	24.441
-1.00	1.00	0.25E+15	1.0	6.375	127.470	6.318	103.424
-1.00	1.00	0.89E+15	1.0	1.791	35.806	1.775	29.052

TABLE 1A

Table of pulsar birthrates calculated for model 1a of Chapter 3, for a uniform planar galaxy of surface area 1000kpc^2. The birthrates are shown in units of number of pulsars/100 years in the final four columns. The headings 'C2.0' and 'C3.0' refer to braking index $n = 2$ and $n = 3$ respectively. 'MEAN-K' gives the value of mean magnetic torque in units of 10^{-16}, and columns ALPHA, BETA and DELTA give the values of the luminosity law parameters α, β and Δ for each of 5 (α,β) pairings discussed in the text and two values of Δ, found from the Crab and Vela pulsars. 'AGE = 'refers to t_0,the assumed age of the galaxy, the two cases $t_0 = 10^{16}$ and $t_0 = 10^{17}$ years being considered.

TABLE 1B

PULSAR BIRTHRATES FOR MODEL 1B

				AGE = 1.E16 s		AGE = 1.E17 s	
ALPHA	BETA	DELTA	MEAN-K	C2.0	C3.0	C2.0	C3.0
			x1.E-16 s/s	x1.E-2 psrs/yr		x1.E-2 psrs/yr	
-1.00	0.33	0.14E+07	10.0	1.653	2.914	1.2218	1.2974
-1.00	0.33	0.22E+07	10.0	1.052	1.854	0.7775	0.8256
-1.00	0.33	0.14E+07	1.0	0.697	1.546	0.3533	0.6229
-1.00	0.33	0.22E+07	1.0	0.444	0.984	0.2248	0.3964
1.00	1.00	0.23E+18	10.0	0.014	0.069	0.0001	0.0069
1.00	1.00	0.11E+18	10.0	0.029	0.145	0.0003	0.0144
1.00	1.00	0.23E+18	1.0	1.506	0.751	0.0137	0.0694
1.00	1.00	0.11E+18	1.0	3.149	1.571	0.0287	0.1451
0.00	1.00	0.76E+16	10.0	2.081	4.688	0.2077	1.4704
0.00	1.00	0.10E+17	10.0	1.581	3.563	0.1578	1.1175
0.00	1.00	0.76E+16	1.0	23.014	15.724	2.0809	4.6882
0.00	1.00	0.10E+17	1.0	17.491	11.951	1.5815	3.5631
-1.50	0.50	0.30E+08	10.0	9.769	31.002	9.4818	25.9056
-1.50	0.50	0.94E+08	10.0	3.118	9.894	3.0261	8.2677
-1.50	0.50	0.30E+08	1.0	4.103	12.581	3.0894	9.8038
-1.50	0.50	0.94E+08	1.0	1.309	4.015	0.9860	3.1289
-1.00	1.00	0.25E+15	10.0	91.484	103.616	68.5331	87.0246
-1.00	1.00	0.89E+15	10.0	25.698	29.106	19.2509	24.4451
-1.00	1.00	0.25E+15	1.0	150.402	129.895	91.4840	103.6163
-1.00	1.00	0.89E+15	1.0	42.248	36.487	25.6978	29.1057

TABLE 1B

Table of pulsar birthrates calculated for model 1b, for a uniform, planar galaxy of surface area 1000kpc^2. The birthrates are in units of number of pulsars /100 years in the final four columns. The 'MEAN-K' now refers to the parameter a in the text, the modal value of magnetic torque. The other headings are as explained in Table 1a.

TABLE 2A

PULSAR BIRTHRATES FOR MODEL 2A

				AGE= 1.E15 s		AGE= 1.E16 s	
ALPHA	BETA	DELTA	MEAN-K	C14	C15	C14	C15
			x1.E-16 s/s	x 1.E-2 pulsars/year			
-1.00	0.33	0.14E+07	10.0	6.8	5.6	6.8	3.1
-1.00	0.33	0.22E+07	10.0	4.3	3.5	4.3	2.0
-1.00	0.33	0.14E+07	1.0	3.4	2.7	3.3	1.5
-1.00	0.33	0.22E+07	1.0	2.2	1.7	2.1	0.9
1.00	1.00	0.23E+18	10.0	6.9	1.1	6.9	0.7
1.00	1.00	0.11E+18	10.0	14.3	2.3	14.3	1.4
1.00	1.00	0.23E+18	1.0	68.6	10.9	68.6	6.9
1.00	1.00	0.11E+18	1.0	143.5	22.7	143.5	14.3
0.00	1.00	0.76E+16	10.0	47.5	18.6	47.5	14.8
0.00	1.00	0.10E+17	10.0	36.1	14.2	36.1	11.2
0.00	1.00	0.76E+16	1.0	157.6	60.1	157.6	47.5
0.00	1.00	0.10E+17	1.0	119.8	45.6	119.8	36.1
-1.50	0.50	0.30E+08	10.0	37.1	33.7	37.0	29.5
-1.50	0.50	0.94E+08	10.0	11.8	10.7	11.8	9.4
-1.50	0.50	0.30E+08	1.0	15.8	13.9	15.8	11.7
-1.50	0.50	0.94E+08	1.0	5.0	4.4	5.0	3.7
-1.00	1.00	0.25E+15	10.0	166.1	133.7	166.1	127.5
-1.00	1.00	0.89E+15	10.0	46.7	37.5	46.7	35.8
-1.00	1.00	0.25E+15	1.0	238.0	176.7	238.0	166.1
-1.00	1.00	0.89E+15	1.0	66.9	49.6	66.9	46.7

TABLE 2A

Table of pulsar birthrates calculated for model 2a, for a uniform, planar galaxy of surface area 1000 kpc^2. Now 'C14' and 'C15' refer to the birthrate calculated for field-decay times of 10^{14} and 10^{15} secs respectively, and are shown in units of number of births/100 years in the final four columns. Other notation is explained in Table 1a.

TABLE 2B

PULSAR BIRTHRATES FOR MODEL 2B

				AGE= 1.E15 s		AGE= 1.E16 s	
ALPHA	BETA	DELTA	MEAN-K	C14	C15	C14	C15
			x1.E-16 s/s	X 1.E-2 pulsars/year			
-1.00	0.33	0.14E+07	10.0	11.1	7.4	11.0	5.0
-1.00	0.33	0.22E+07	10.0	7.1	4.7	7.0	3.2
-1.00	0.33	0.14E+07	1.0	5.6	3.6	5.5	2.4
-1.00	0.33	0.22E+07	1.0	3.6	2.3	3.5	1.5
1.00	1.00	0.23E+18	10.0	7.7	1.2	7.7	0.8
1.00	1.00	0.11E+18	10.0	16.0	2.5	16.0	1.6
1.00	1.00	0.23E+18	1.0	76.5	12.1	76.5	7.7
1.00	1.00	0.11E+18	1.0	160.0	25.3	160.0	16.0
0.00	1.00	0.76E+16	10.0	50.8	19.9	50.8	15.8
0.00	1.00	0.10E+17	10.0	38.6	15.1	38.6	12.0
0.00	1.00	0.76E+16	1.0	169.1	64.3	169.1	50.8
0.00	1.00	0.10E+17	1.0	128.5	48.8	128.5	38.6
-1.50	0.50	0.30E+08	10.0	46.6	40.0	46.5	36.2
-1.50	0.50	0.94E+08	10.0	14.9	12.8	14.9	11.6
-1.50	0.50	0.30E+08	1.0	20.7	16.7	20.6	14.7
-1.50	0.50	0.94E+08	1.0	6.6	5.3	6.6	4.7
-1.00	1.00	0.25E+15	10.0	169.7	136.0	169.7	129.6
-1.00	1.00	0.89E+15	10.0	47.7	38.2	47.7	36.4
-1.00	1.00	0.25E+15	1.0	245.6	180.9	245.6	169.7
-1.00	1.00	0.89E+15	1.0	69.0	50.8	69.0	47.7

TABLE 2B

Table of pulsar birthrates calculated for model 2b, for a uniform, planar galaxy of surface area 1000 kpc^2. 'MEAN-K' gives the modal value of magnetic torque in units of 10^{-16}, (the quantity a in the text). Other notation is identical to that of Table 2A.

CHAPTER 4

ANALYIS OF THE SIMPLE MODEL

4.1 INTRODUCTION

It is the aim of this work to rigorously compare several models of pulsar evolution against the observed data. The primary means of doing this will be to obtain theoretical distributions in P and $\dot{P}$ and to statistically compare these using the chi-squared test against the distribution found in the observed $P,\dot{P}$ diagram. The best fits for each model are found by minimising the χ^2 statistic, thus obtaining best-fit values for the model parameters. Models can then be compared with each other. This will indicate which, if any, of the models can claim to represent the observed distribution. A similar approach has been made by Cheng(1989), but he uses Monte-Carlo simulations rather than analytic forms for distributions, and does not try to identify the 'best-fit' values of the parameters. It is important to utilise the information in the $P,\dot{P}$ diagram since these parameters are two most reliable "pure observables" that can be measured for every pulsar, given time to conduct the observations. The uncertainties inherent in the determination of luminosity and its rather arbitrary definition for pulsars means we do not attempt to fit the joint distribution of $P,\dot{P}$ and L. As noted earlier, the observed sample would make for a rather sparse distribution in any realistic three dimensional grid of boxes that could be devised, unsuitable for the requirements of the chi-squared test.

4.2 MODEL 1 : THE SIMPLE MODEL

4.2.1 The derivation of the intrinsic distribution.

The first detailed model to be considered for pulsar evolution is what we term the simple model, which features no field decay or alignment.

This has been generally dismissed in the past as being incompatible with the observations yet we contend that as yet no rigorous analysis has conclusively ruled it out. This is because the correct methods for establishing such a claim have not been used. The 'lack' of long period pulsars which is often invoked as an indicator that field decay is necessary effectively uses only the information in the period distribution, which, we hope to show, is compatible with a number of evolutionary scenarios.

The simple model has the following spin-down law:

$$\dot{P} = k.P^{2-n} \quad ....(4.1)$$

where the braking index n takes the value 3 for pure dipole radiation, and

$$\dot{k} = 0. \quad ....(4.2)$$

The luminosity law is

$$L = \Delta.P^{\alpha}.\dot{P}^{\beta} \quad ...(4.3)$$

where

$$\dot{\Delta} = 0. \quad ...(4.4)$$

Since k and Δ are constant, and since dealing with logarithmic quantities is more convenient, we take the variables describing a pulsar to be:

$$x_1 = \ln(P) \; ; \; x_2 = \ln(k) \; ; \text{ and } x_3 = \ln(\Delta) \quad (4.5)$$

Also we define

$$y_1 = \ln(P) = x_1 \; ; y_2 = \ln(\dot{P}) \text{ and } y_3 = \ln(L) \quad (4.6)$$

So we get $y_2 = x_2 + (2-n).x_1$ .....(4.7)

and $\dot{x}_1 = e^{x_2} e^{x_1(1-n)}$ ....(4.8)

The solution of this gives the trajectory equation for $x_1(t)$;

$$e^{x_1(n-1)} = e^{x_{10}(n-1)} + (n-1).e^{x_2}.(t-t_0) \quad (4.9)$$

and $x_2 = x_{20}$; $x_3 = x_{30}$ ....(4.10).

So we get $\frac{\partial x_1}{\partial x_{10}} = \frac{e^{x_{10}(n-1)}}{e^{x_1(n-1)}}$ ....(4.11)

The source function to be taken is

$$C(x_1,x_2,x_3,t) = c_0\delta(x_1-\ln(Q))X(x_2,x_3)H(t)..(4.12)$$

where $X(x_2,x_3)$ is a bivariate normal distribution in x_2 and x_3, [See Appendix A3], δ is a delta function which restricts all pulsars to be born with periods P=Q, and H(t) is a Heaviside step function, restricting t to be ≥ 0, such that t = 0 marks the onset of pulsar formation. The bivariate form of X allows the magnetic torque k to have a marginal intrinsic distribution that is ln-normal, as was assumed both in GO and LMT, but also allows the parameter Δ to be correlated with k, in addition to giving some intrinsic scatter in the values of Δ. The c_0 term is effectively the creation rate, expressed as the number of pulsars born per unit time per unit square kiloparsec: For simplicity it has been assumed that the pulsars are uniformly distributed in a planar disc round the observer. So, by equation (3.2), applying the method developed in Section 3.6 of Chapter 3, we get

$$n(x_{10},x_{20},x_{30};t_0) = c_0X(x_2,x_3)e^{x_{10}(n-1)-x_{20}}\,H(t)\,\Big|_{x_{10}=\ln(Q)} \quad (4.13)$$

where step function H(t) introduces the constraint

$$e^{x_{20}} \leqslant \frac{e^{x_{10}(n-1)} - Q^{n-1}}{(n-1)\,t_0} \quad (4.14)$$

via equation (4.9). Note that H(t) applies to the value of t which is found from the solution of (4.9).

Now we switch coordinates to y_1 , y_2, and y_3.

So $n(y_1,y_2,y_3,t_0) = n(x_{10}, x_{20},x_{30},t_0) \left| \frac{\partial(x_{10},x_{20},x_{30})}{\partial(y_1,y_2,y_3)} \right|$ (4.15)

The Jacobian term can be shown to be equal to unity, by (4.5,4.6) Therefore, the new distribution is;

$$n(y_1,y_2,y_3,t_0) = c_0.e^{y_1-y_2}.X(x_{20}(),x_{30}())\ H(t)\big|_{y_1=\ln(Q)} \qquad (4.16)$$

where x_{20} and x_{30} are regarded as functions of y_1,y_2 and y_3, through equations (4.5) and (4.6).

This is the intrinsic distribution in ln(P), ln($\dot{P}$) and ln(L).

4.2.2 Inclusion of selection effects.

To obtain the observed distribution we now apply the selection effects described in the earlier chapter. These three effects are:

(1) the pulsar must be above the flux threshold F_{min};

(2) the pulsar must be beaming in our direction and;

(3) the period-dependence of detection probability which can be incorporated as a factor $f(y_1)$ in the density of y_1 and y_2.

We shall assume a uniform spatial dependence, such that the pulsars are distributed equally in the galactic plane. Thus only the radial distribution need be considered, as the azimuthal symmetry is assumed. Effect (1) means that when integrating out over this radial coordinate r, we can define an r_{max} as a function of luminosity, i.e.

$$r_{max}^2 = \exp(y_3)/4\pi F_{min}. \qquad (4.17)$$

The second selection effect (2) can be dealt with in this case by the introduction of the 'beaming fraction', B_0, which is assumed constant in this model since no alignment is taking place. Thus we choose B_0 = 1/5, a typical estimate. [GO, Lyne and Manchester(1988)]. Including effect (3), we can take account of the period-sensitivity of pulsar surveys through $f(y_1)$ where the form of $f(y_1)$ is that taken by LMT, so that fast pulsars are discriminated against:

$$f(y_1) = (1+0.25\exp(-2y_1))^{-0.25} \quad \text{.....(4.18)}$$

So the combined effect of (1), (2) and (3) is multiplication of the intrinsic distribution function by a factor $B_0.f(y_1)$ and integration over distance only out to r_{max}, from (4.17). So we now integrate out over the spatial dependence, using (4.16) and (4.17):

$$n_{obs}(y_1,y_2,y_3;t\ ) = \int_0^{\infty} n(y_1,y_2,y_3;t)\ B_0 f(y_1) H(r_{max}-r) 2\pi r.dr \qquad (4.19)$$

$$= c_0 B_0 f(y_1\ )\ \frac{e^{y_1-y_2+y_3}}{4F_{min}}\ X(x_2\ (),x_3\ ())H(t\ )\Big|_{y_1=\ln(Q)} \qquad (4.20)$$

Now X is a bivariate normal with arguments

$$x_2 = y_2 + (n-2)y_1\ ;\ x_3 = y_3 - \alpha y_1 - \beta y_2. \qquad (4.21)$$

By the properties of the bivariate normal distribution, (see e.g. Mood and Graybill (1963)) ,X can be expressed in form

$$X(x,y) = D.\exp(-R) \qquad (4.22)$$

where $D^{-1} = 2\pi\sigma_x\sigma_y\sqrt{(1-\rho^2)}$ (4.23a)

and $R = (1/2(1-\rho^2)\{(x-\mu)^2/2\sigma_x^2+(y-\nu)^2/2\sigma_y^2-2\rho(x-\mu)(y-\nu)/\sigma_x/\sigma_y\}$ (4.23b)

a quadratic form in x and y. Here μ and ν are identified as the means of the marginal distributions of x any y respectively, σ_x^2 and σ_y^2 as the respective variances and the correlation between the two variates is denoted by ρ. D is chosen to normalise the distribution to unity, in the sense that:

$$\int_{-\infty}^{\infty}\int_{-\infty}^{\infty} D.\ \exp(-R).dx.dy\ = 1 \qquad (4.24)$$

Now x_2 and x_3 are related to y_1, y_2 and y_3 as above so the form of R is altered to give a new quadratic form R' such that

$$X\ = D'\ \exp(-R') \qquad (4.25)$$

where R' is now a function of y_1, y_2 and y_3. We also introduce σ_2 and σ_3 as the standard deviations in ln k and ln Δ respectively which

appear in the quadratic form R'. Thus :

$$n_{obs}(y_1,y_2,y_3;t) = \frac{c_o B_o f(y_1) e^{y_1-y_2} e^{-R'} H(t)\big|_{y_1=\ln(Q)}}{4F_{min} 2\pi\sigma_2\sigma_3\sqrt{(1-\rho^2)}} \quad (4.26))$$

Using the result of Theorem 2 in Appendix A3, we can integrate out over y_3 to get the observed distribution in y_1 and y_2, that is:

$$n_{obs}(y_1,y_2;t_o) =$$

$$= \lambda f(y_1) e^{\frac{-\rho^2\sigma_3^2}{2}} \frac{e^{y_1-y_2+\alpha y_1+\beta y_2-\frac{A^2}{2}+\rho A\sigma_3} H(t)\big|_{y_1=\ln(Q)}}{\sqrt{(2\pi)}\sigma_2} \quad (4.27)$$

where $A = (y_2-\bar{\mu}_2)/\sigma_2$; $\gamma = 2(1-\rho^2)$; $\bar{\mu}_2 = \mu_2 - (n-2)y_1$. (4.28a)

and $$\lambda = c_o B_o \exp(\mu_3+\sigma_3^2/2)/4F_{min} \quad (4.28b)$$

and $$\exp(y_2) \geq \frac{e^{(n-1)y_1} - Q^{n-1}}{(n-1)t_o e^{(n-2)y_1}} = \Phi_3(y_1) \quad (4.28c)$$

This is the distribution that we shall use to compare the predicted and actual densities of pulsars on the $P,\dot{P}$ plane and provide evidence for whether this model can explain the evolution of pulsars.

4.2.3 The deathline in the simple model.

It is important to note the effect of the final term which acts as a cutoff and when plotted on the $P,\dot{P}$ diagram produces a 'deathline' (equation 4.28c) below which no pulsars can appear simply because the galaxy is not old enough for them to have reached that region. We have not assumed anything about the nature of the pulsed emission and this 'deathline' is independent of the magnetic field distribution, depends only weakly on braking index and for small Q ($Q \ll 1$sec) is approximately independent of Q. This is also unrelated to any of the selection effects we have introduced, but is a fundamental constraint

on the location of pulsars on the $P,\dot{P}$ plane due to the finite length of time over which pulsars have been created. This is a unique feature of the time-dependent approach in that it 'naturally' explains the deathline without any need for pulse-production thresholds or even selection effects. The lowest value of t_o , the galactic age which is compatible with all the observed pulsars turns out to be t_o = $1.17X10^{17}$secs =$3.707X10^9$ years, when Q = 1msec. See diagram (4.1), which shows the deathline and the sample of observed pulsars.

4.2.4 Distribution of related quantities.

It is also possible to look at the joint distributions of quantities which are functions of P and $\dot{P}$. In general, if u and v are new variables dependent on P and $\dot{P}$, which are distributed as $f(P,\dot{P})$, then the distribution of u and v can be found from

$$\tilde{f}\,(u, v) = \left| \frac{\partial(P, \dot{P})}{\partial(u, v)} \right| f\,(P, \dot{P}) \qquad (4.29a)$$

Of interest is the distribution of $P\dot{P}$ and $P/\dot{P}$, which are usually taken as measures of magnetic field strength and characteristic age respectively. It can be shown, that although in the simple model the field does not decay, the influence of the deathline and braking index can formally make the expectation value of field at fixed age vary with age, i.e. $E_{obs}(P\dot{P}|P/\dot{P})$ may vary with $P/\dot{P}$. This is because the resulting distribution is not strictly separable because of the presence of the deathline cutoff. The effect only becomes significant as $\tau=P/\dot{P}$ becomes large but if the braking index is greater or less than 3 then the inferred expectation value $E_{obs}(P\dot{P} \mid P/\dot{P})$ can both rise and fall with increasing τ if n = 3 is assumed. This is shown in Figure 4.3. This demonstrates the possibility of inferring spurious results from what are essentially model-dependent arguments, that is assuming $P\dot{P}$

does give the true value of B^2, for field strength B.

4.2.5 The marginal period distribution.

Firstly we can derive the observed period distribution by integrating equation (4.27) over y_2. The limits of integration are from the 'deathline' to $+\infty$.

Thus we get

$$n_{obs}(y_1;t) = \frac{\lambda' f(y_1)\, e^{y_1(1+\alpha+(\beta-1)(2-\eta))}}{8F_{min}} \operatorname{erfc}\left[\frac{\Phi_3(y_1)-\bar{\mu}_2}{\sqrt{2}\,\sigma_2}\right] \qquad (4.29b)$$

after some algebra, where erfc represents the usual complementary error function [erfc(0) = 1], $\Phi_3(y_1)$ is the deathline as defined in equation (4.28c) and λ' is the constant which ensures our total observed sample equals the observed number of pulsars, and includes the creation rate c_0, which is, from (4.28b)

$$\lambda' = \lambda.\exp[\ (\beta-1).(\mu_2 + \rho\sigma_2\sigma_3 + (\beta-1)\sigma_2^2/2\ ] \qquad (4.30a)$$

and $$\bar{\mu}_2 = \bar{\mu}_2 + \sigma_2^2\ (\beta-1+\rho\sigma_3/\sigma_2\ ) \qquad (4.30b)$$

Now the entire normalisation constant is

$$\lambda' = \Gamma_0 c_0 \exp(\mu_3+\sigma_3^2+(\beta-1)(\mu_2+\rho\sigma_2\sigma_3+(\beta-1)\sigma_2^2/2)/4F_{min}. \qquad (4.31)$$

It will be noticed from the form of (4.27), (4.28a) and (4.28b) that the parameters that determine the model appear in combinations in such a way that they cannot be individually determined. This feature was already noticed in the simpler models discussed earlier in Chapter 3, i.e. that the determination of the birthrate could not be made, only the combination of the birthrate and the mean magnetic field. This aspect

carries over into these more detailed treatments.

4.3 MODEL FITTING PROCEDURE.

4.3.1 The chi-squared statistical test.

This test is used to compare two samples of data and to determine if they follow the same distribution. We are interested in the version where one sample is taken as fixed (the observed pulsar $P,\dot{P}$ distribution) and the second is generated by our evolutionary model. This approach has been adopted by Cheng (1989) but with a Monte-Carlo method. To quantify the observed pulsar distribution in the $P,\dot{P}$ plane, a grid is set up with 26 boxes such that all 240 pulsars in the flux-limited sample (F_{min}=10mJy) are approximately evenly split up into the boxes. This is shown in Figure 4.1. This grid covers the entire $P,\dot{P}$ plane from P=1ms to 5s and from the deathline up to $\dot{P} = 10^{-10}ss^{-1}$. A computer program then evaluates the numbers of pulsars predicted to occupy these same boxes by integrating over the joint distribution function in equation (4.26) and then a χ^2 statistic is found as follows:

$$\chi^2 = \Sigma_{i=1}^{26} \frac{(m^i_{obs} - m^i_{pre})^2}{m^i_{pre}} \qquad ....(4.32)$$

where m^i with the appropriate subscript refers to observed and predicted occupancies in the i^{th} box of the grid.[See Appendix A2]. One also must compute $p(\chi^2|\nu)$, the significance level of the result, for ν degrees of freedom. Here the number of degrees of freedom is

ν = (number of grid boxes -1 - the number of free model parameters)

4.3.2 Significance levels and target χ^2.

A predetermined level of significance must be achieved in order to be

able to say that a particular model does sufficiently resemble the observed distribution. If we adopt the same criterion used by Cheng(1989), that is that for 31 degrees of freedom, that a value of χ^2 less than 58 (approximately) is acceptable, then a significance of $\geqslant$0.2% is required.

This means that for a given number of degrees of freedom, a 'target' χ^2 is defined as that which must be obtained so that the model cannot be rejected at the 5% level of significance. Roughly, for ν degrees of freedom, a $\chi^2 \triangleq \nu$ is required as a target. It is customary, and in this case more stringent, to use the 5% level of significance. This implies that for Cheng's work, the 'target' chi-squared should have been 44.98, which is much more restrictive. For the simple model, with 21 degrees of freedom, we find that the 5% target is 32.76.

4.3.3 Optimisation of the χ^2 fit.

Regarded as a function of the model parameters (mean magnetic field, luminosity law parameters, etc.) χ^2 is a multidimensional function. We wish to minimise this function and hence obtain the best-fit parameter values. This cannot be done analytically so a numerical treatment is required. Several methods can be used to minimise a multidimensional function. The 'downhill Simplex' method of Nelder and Mead(1965) as outlined in Press et al(1986) was used, as well as various routines from the standard Numerical Algorithm libraries to corroborate the results that were obtained. It is possible to look at a χ^2 fit for both the joint $P,\dot{P}$ data and the marginal P data, where now χ^2 is defined on the histogram values rather than the bin occupancies in the $P,\dot{P}$ plane. This can similarly be optimised with respect to the model parameters. The parameters in the simple model are as follows :

* The intrinsic mean magnetic torque strength μ_2

* The luminosity law parameters α and β

* The braking index n from equation (4.1)

* The correlation and variances ρ, σ_2^2 and σ_3^2 for the bivariate distribution in x_2 and x_3

* The intrinsic mean value of $\Delta = \mu_3$

The values of Q and t_0 are considered to be fixed.

It should be noted that in the simple model, the above parameters appear in combinations and that these combinations are the effective 'parameters' of the distribution that will be determined from any minimisation procedure. These combinations are

$$: u_1 = 1 + \alpha - (\beta-1)(n-2) \qquad (4.33a)$$

$$: u_2 = \mu_2 + (\beta-1)\sigma_2^2 + (\rho\sigma_3)\sigma_2 \qquad (4.33b)$$

$$: u_3 = \sigma_2 \qquad (4.33c)$$

$$: u_4 = n \qquad (4.33d)$$

$$: u_5 = \lambda \text{ from (4.28b)} \qquad (4.33e)$$

Of these, u_5 is essentially a normalisation constant to ensure our predicted sample contains the same number of pulsars as the observed data set. So there are 4 free parameters now, giving 21 degrees of freedom for the chi-squared test. It is these combinations that are to be regarded as free when the fitting of the model is carried out. This is not a feature unique to the simple model, however, and later models will show similar "degeneracy". Notice that the special case of $\beta=1$ causes considerable simplification in the above expressions and this will carry forward to other models. In general, however, the parameters of direct physical interest cannot be isolated without assuming some further relations between them and the determinable $u_1,\ldots u_5$ or inputting some supplementary knowledge from a different analysis. This is of importance when we attempt to find the birthrate

c_0 which appears as a factor in the normalisation constant λ.

4.3.4 Determination of the birthrate c_0.

To get a realistic estimate of c_0 entails estimating separately the other factors that appear with in λ from some independent source. This will only prove to be necessary if the fit obtained by minimising χ^2 is found to be significant at the prescribed level. Then the inferred birthrate becomes a quantity of interest. An attractive option would be to utilise the luminosity data (further integration to give marginal densities will only preserve some of the combinations inherent in the joint density, and thus will be unhelpful). In fact, Emmering and Chevalier(1989) demand that their simulated pulsar populations satisfy the regression law found by Proszynski and Przybcien(1984) such that the inferred α and β agree with those detemined from that work. This is a rather stringent criterion, given the large scatter present in the data. When this is looked at analytically for the simple model, it is found that unfortunately the new relations that are obtained involve the same combinations already identified, so the system of equations, taken as a whole, contains more unknowns than there are equations and the problem is ill-posed. This may be repeated for future models, so the other option is to simply determine the birthrate for a variety of 'realistic' values of other parameters. This redundancy is a feature, virtually unmentioned, of other work, and is probably the reason why other authors use a variety of methods for determining the birthrate and in some cases omit the calculation altogether (Chevalier and Emmering(1986)). The advantage of fitting the joint distribution of $P,\dot{P}$ and L would be to remove this degeneracy from the problem.

4.4 IMPACT OF TIME DEPENDENCE

A further point to be noted is the impact of time-dependence on this. We saw in Chapter 3 how the time-dependent continuity equation method does not guarantee a steady-state solution, this being dependent on which model is being studied. This means that the total number of pulsars may not be constant in time, so that the normalisation of the distribution will depend on the age of the pulsar-formation epoch, t_0 in our notation. This age can be the age of the galaxy or the time since star formation started and can be got from either external (e.g. cosmological) arguments or from the fitting of the 'deathline' to the observed $P,\dot{P}$ diagram. Thus in general, the fitting of our distibutions should include the 'age of the Galaxy' parameter, in the time-dependent formulation. That it is also a latent feature of the steady state models is not always appreciated. A finite galactic age is required to normalise the intrinsic pulsar distribution and this can be disregarded only if a decay timescale τ is a lot less than the galactic age - this is usually satisfied for exponential field decay models, as $\exp(-t_0/\tau) \triangleq 0$, i.e. whenever t_0 is greater than a few decay times.

4.5 MARGINAL AND JOINT DISTRIBUTIONS

4.5.1 Priority of fitting.

It is of extreme importance to recognise the correct priorities in fitting our models to the pulsar data, as discussed in Chapter 2. A model will predict the observed distribution in P and $\dot{P}$, which we will test using the χ^2 test. The observed data is binned such that a given bin consists of bounds for both P and $\dot{P}$ and each bin contains > 5 pulsars. A total of 26 bins are used. It is this fit which should be regarded as the most important test of our models, not the fitting of

the marginal distribution of P, for example. This can be illustrated in the following idealistic case.

4.5.2 Example of misleading fitting.

Consider a bivariate normal distribution N(x,y). (See Appendix A3 or any statistics text for properties of multivariate distributions). The variates x and y are governed by this distribution which has as a parameter ρ, the correlation between x and y. ρ can take any value n the range $-1 < \rho < +1$. If we look at the marginal density for x alone, it is a univariate normal, independent of ρ, with a similar result for y. Thus the marginal distribution tells us nothing of the correlation, and any one of an infinite set of parent bivariate normal distributions could produce one given marginal distribution. Even given both marginals for x and y, we cannot infer the true form of the joint distribution in x and y without further information or assumptions. This shows the erroneous nature of conclusions drawn from consideration of the restricted information present in any marginal density when the full joint density is available. Thus we shall regard the fitting of the $P,\dot{P}$ data as paramount in importance, and the fitting of period data alone of little relevance unless a previous fit has been made to the $P,\dot{P}$ diagram.

An alternative way of looking at this is that if one of the two marginal distributions associated with a given joint distribution cannot be fitted with the parameters found by fitting the other marginal, then clearly it will not be possible to fit the joint distribution.

4.6 χ^2 FITS TO THE SIMPLE MODEL

4.6.1 The joint $(P,\dot{P})$ distribution.

Treating χ^2 as a function of u_1,u_2,u_3 and u_4 as defined in relations (4.33a-e) we minimise χ^2 to find the best-fit solution. Since there are

26 boxes in the grid, the number of degrees of freedom is ν=21 (4 free parameters and 1 from normalisation). The target χ^2 defined in Section 4.3.2 is 32.67, with the significance level of 5%. The best fit obtained was:

χ^2 = 233.4 , $p(\chi^2|\nu) \triangleq 0$ at the following point:

u_1 = 0.019

u_2 = -33.76

u_3 = 1.817

u_4 = 1.603

This is a very poor fit, as the $p(\chi^2|\nu) \triangleq 0$. Although this may not be regarded as a surprising result, we claim that this is the first definite indication of the inadequacy of the simple model, with no field decay. Previous authors have dismissed this model because of the lack of long-period pulsars or simply because the field decay model was seen to be successful. We shall show in the following pages how the period distribution can be fitted to an acceptable level using the simple model, with no deficit of pulsars at any period. This then illustrates the fallacy of making deductions based solely on the marginal distribution when the joint data is available and simultaneously questions the motivation for field decay solely on this information.

4.6.2 The marginal period distribution.

Using the same pulsar sample, we construct a histogram for pulsar period data and integrate equation (4.29b) to give the predicted contributions to these bins. Then a similar χ^2 optimisation is carried out and the best-fit found is:

χ^2 = 7.31 ; v = 12 (16 bins-1 (normalisation) -3 free parameters) and $p(\chi^2|\nu)$ = 86% at the point

u_1 = 6.4

$v_1 = -4.86$

$v_2 = 0.9775$

where u_1 is as defined in (4.33a), and v_2,v_1 are defined as:

$v_2 = (n - 1)/\sqrt{2}\sigma_2$ and $v_1 = (u_2 + \ln(2t_0))/\sqrt{2}\sigma_2$. (4.34)

This gives a satisfactory fit, well within the levels that were assigned beforehand. This proves that completely erroneous conclusions may be drawn from the fitting of a marginal distribution unless the corresponding joint density has already been tackled. On the basis of this fit alone, one would conclude that the simple model was a possible scenario for pulsar evolution whereas we know from our failure to match the joint density that it is not. To correctly identify or rule out candidate models, fitting the joint distribution is the correct approach. That this fit to the period data is not an artefact of the binning scheme can be shown using the Kolmogorov-Smirnov test on the cumulative distribution of periods (see Appendix A1). This uses the parameter d, the maximum departure of the theoretical and observed cumulative curves from each other and is independent of the binning scheme introduced above. This gives, for the above best-fit values, d = 0.02 with a corresponding probability of 98%, which can only be interpreted as an excellent correspondence. This is sufficiently good that we can reliably say that our fit is genuine and independent of the grouping of the data. This is shown in Figure 4.2b, with an offset between the curves for the purposes of clarity only.

4.7 REJECTION OF THE SIMPLE MODEL

We can reject the simple model as it is defined in this Chapter with assurance, since it fails to account for the observed distribution of pulsar periods and period derivatives. Despite its ability to produce the observed period distribution alone, it can safely be dismissed, and

now we can proceed to develop and test other models using these methods. As a final remark, we note that we have only treated one particular form of distribution in the parameters k and Δ. It is conceivably possible that other forms of source function in these quantities would allow a better fit to be made. This has not been attempted, on the grounds that since most other realistic functional forms can be well-approximated by normal distributions with appropriate means and variances, and we have minimised over the parameter set which includes those parameters of the bivariate normal (introduced in equation 4.12) no substantial improvement in fitting is expected over that already achieved.

4.8 DIAGRAMS FOR CHAPTER 4.

FOOTNOTE: The chi-squared test

There is a limitation in the chi-squared test because of its inability to incorporate regions where there are few or no observed or expected pulsars. This is relevant information for fitting a trial distribution on the $P,\dot{P}$ plane. The inclusion of sparse or empty bins will give a large contribution in the chi-squared summation. However strictly speaking the quantity defined in equation 4.32 will not be chi-squared distributed. It gives none-the-less an approximation to the goodnesss of fit. The use of other test statistics could help to get round this problem.

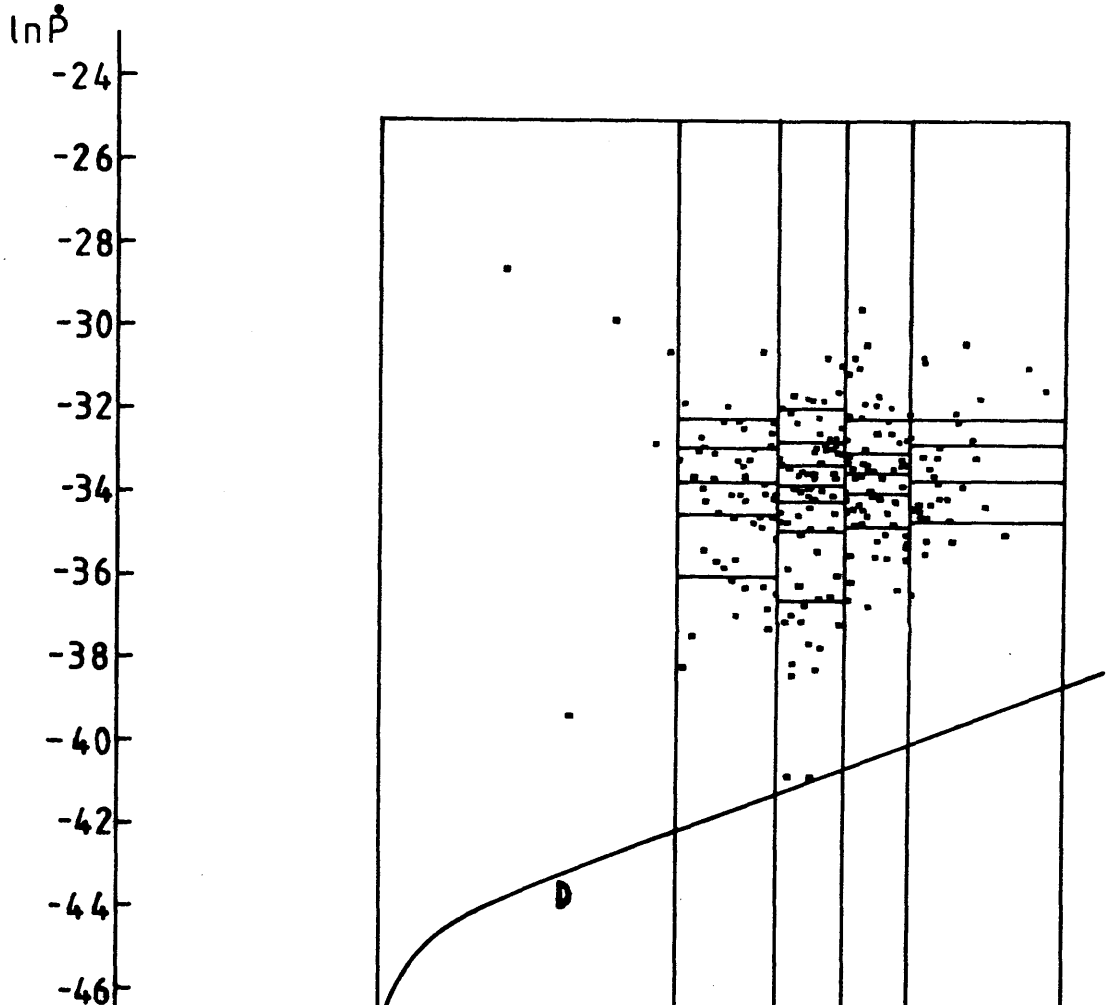

FIGURE 4.1

The bins in the P,$\dot{P}$ plane adopted for the chi-squared fitting of the models. There are 26 bins in total, chosen such that at least 5 observed pulsars are found in each bin, from the sample of 240 pulsars with fluxes greater than 10 mJy. Also shown is the deathline (D), predicted by all time-dependent models, which has been drawn for the simple model here, corresponding to a galactic age of $t_o = 1.5 \times 10^{17}$ secs = 4.8×10^9 years.

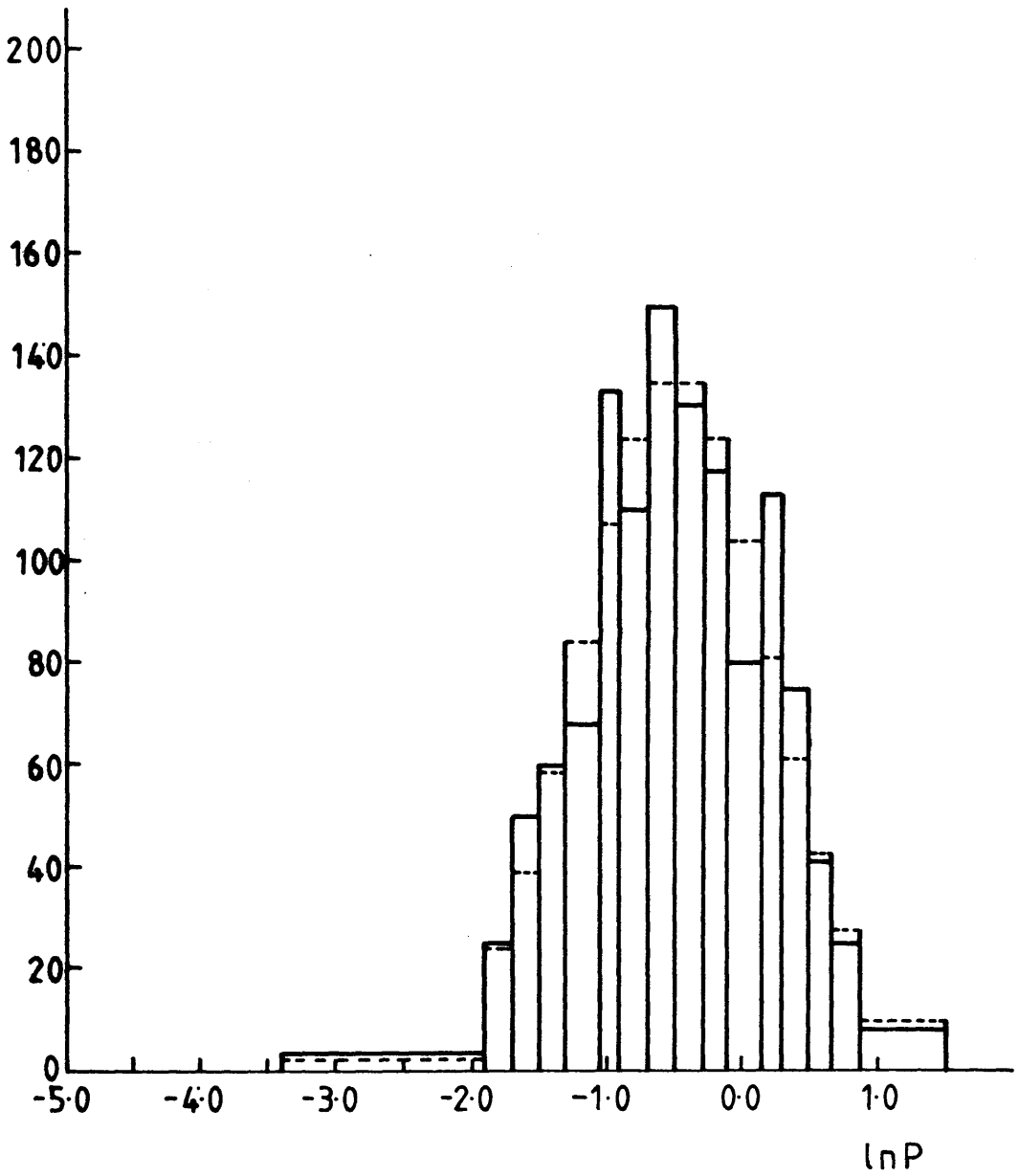

FIGURE 4.2A

The marginal period histogram for the observed data is shown by the solid line and that predicted by the simple model as a best fit to it by the dashed line. This fit has a χ^2 of 7.3, which with 12 degrees of freedom gives a $p(\chi^2|\nu)$ = 83% (See Appendix A2). The parameters of the simple model for this fit are those given in Section 4.6.2.

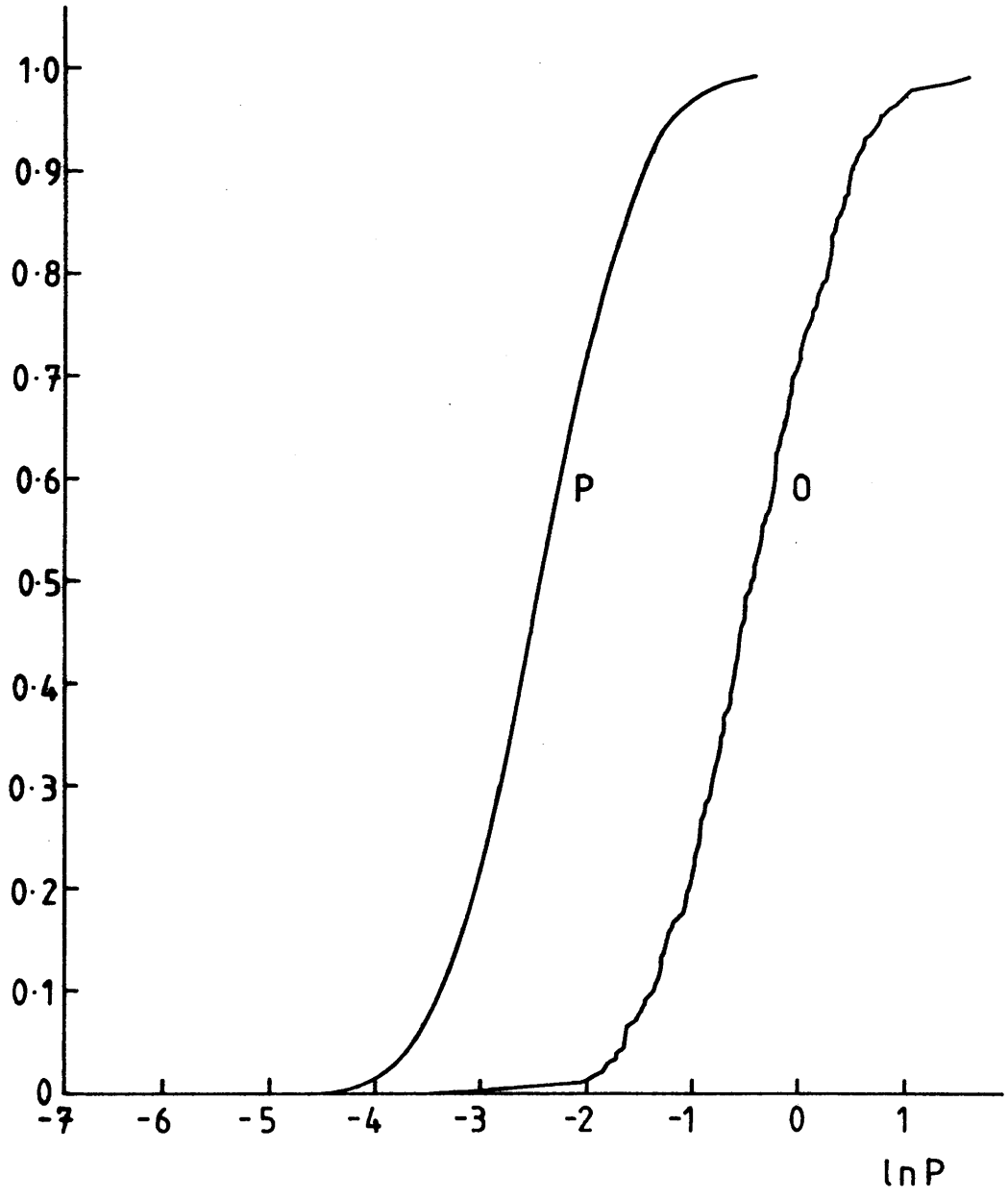

FIGURE 4.2B

The cumulative distribution of periods observed (O curve) and predicted (P curve) by the simple model. The two curves are drawn with a constant offset of ln(P) = 0.2 to give clarity. The Kolmogorov-Smirnov test produces a statistic d = 0.02, the maximum departure of the curves from each other. The parameters of the fit are the same as those obtained in Section 4.6.2.

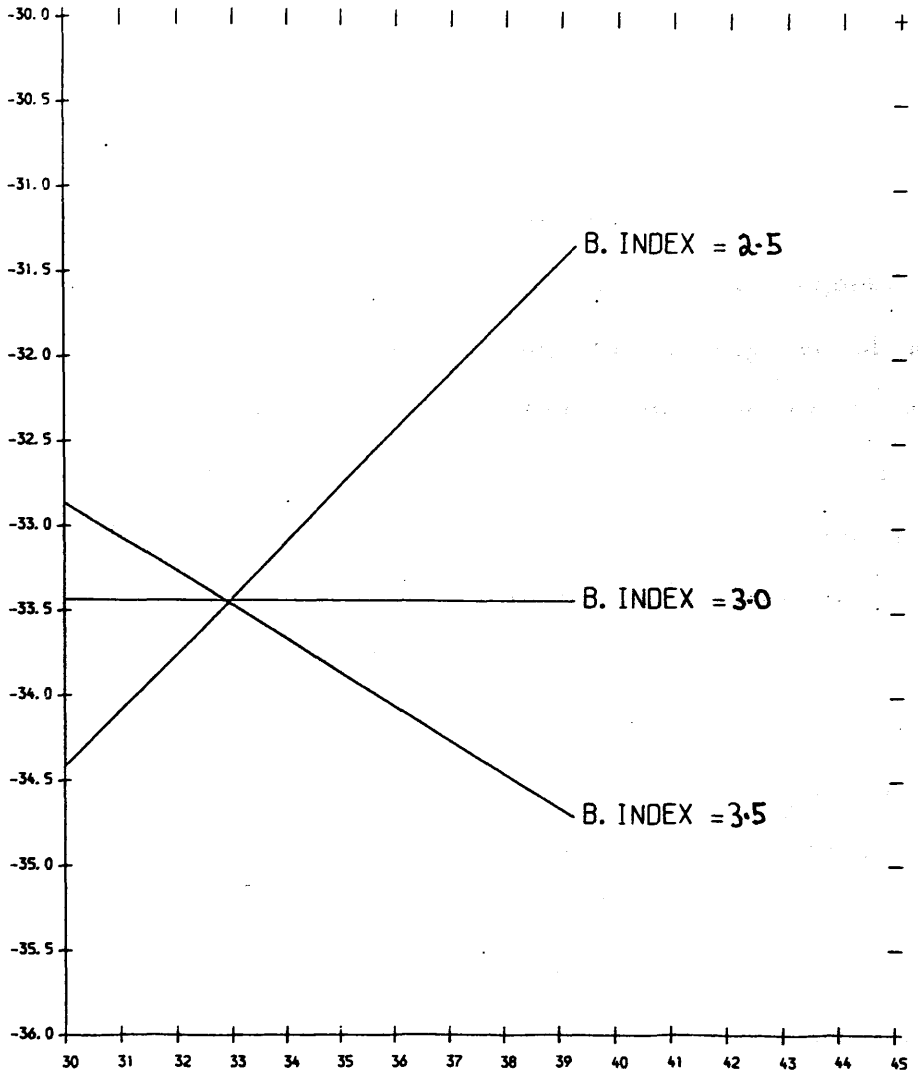

FIGURE 4.3

Plot of $E_{obs}(y|x)$ for the simple model, for three different braking indices n as shown, where $x = \ln(P/\dot{P}) = \ln(\text{characteristic age})$ and $y = \ln(P\dot{P})$. P is in seconds and $\dot{P}$ is in ss^{-1}. $n = 3$ is pure magnetic dipole radiation.

CHAPTER 5

ANALYSIS OF THE FIELD DECAY MODEL

5.1 INTRODUCTION

The next model to be studied can reasonably be called the 'standard' model of pulsar evolution, that is where the magnetic field of the pulsar decays with time, usually in an exponential manner. This feature is the essential ingredient of the work of Gunn and Ostriker(1969),GO, Lyne et al(1985), LMT, Chevalier and Emmering(1986), henceforth CE, and others. The need for torque decay (which is a more general statement than that for purely field decay) is variously taken to be the lack of long-period pulsars ($P \gtrsim 2$secs), the shape of the observed $P,\dot{P}$ distribution, the kinematic age argument and at first even the study of the conductive properties of neutron star material. We have already discussed some aspects of field decay in Chapter 3. Our model is more general than that of GO, LMT and CE in that it includes both the braking index and luminosity law indices amongst the free parameters. CE allowed α and β to be different from the $\alpha = \beta = 1$ of GO and LMT but we intend to vary them to find the best-fit values.

A key feature of field-decay is the existence of the 'terminal period' which is dependent on the product of decay timescale and initial magnetic field strength. Pulsars nearing this period have $\dot{P}$'s which tend to zero. The lack of observed pulsars at long periods is then explained through luminosity decay and/or the existence of some 'deathline' in the $P,\dot{P}$ plane.

We intend to look at the model of LMT as a special case of field decay, this will be done in Section 5.4.

5.2 MODEL 2 : FIELD DECAY MODEL

5.2.1 Derivation of the intrinsic distribution.

The key equations of field decay are thus:

$$\dot{P} = k.P^{2-n} \qquad ...(5.1)$$

and $$k = k_0 \exp(-(t-t_0)/\tau) \qquad ...(5.2)$$

which allows for exponential decay of the magnetic torque k, on timescale τ. Here $k = k_0$ at time $t = t_0$. We adopt logarithmic variables as before, such that:

$$x_1 = \ln(P) \; ; \; x_2 = \ln(k) \text{ and } x_3 = \ln(\Delta) \ldots . (5.3)$$

and $$y_1 = \ln(P) \; ; \; y_2 = \ln(\dot{P}) \text{ and } y_3 = \ln(L) \ldots . (5.4)$$

so from (5.1) and (5.2) we get the equation

$$e^{(n-1)x_1} = e^{(n-1)x_{10}+(n-1).\tau.e^{x_{20}}\{ 1- e^{-(t-t_0)/\tau}\}} \qquad ..(5.5)$$

and $$x_2 = x_{20} - (t-t_0)/\tau \qquad ....(5.6)$$

We choose the same source function as before in (3.18) i.e.

$$C (x_1,x_2,x_3;t) = c_0 \delta(x_1-\ln(Q))X(x_2,x_3)H(t) \ldots . (5.7)$$

where the symbols have the same interpretation as before.

We solve the continuity equation (3.1) in the familiar way to get:

$$N(x_{10},x_{20},x_{30};t) = \int \frac{e^{(n-1)x_{10}} c_0 \; \delta(x_1-\ln(Q))X(x_2,x_3)H(t)dt}{e^{(n-1)x_1}} \; ..(5.8)$$

$$= c_0 \; e^{2x_{10}-x_2} X(x_2,x_3)H(t)\Big|_{x_1=\ln(Q)} \qquad ..(5.9)$$

Applying the constraint H(t) at $x_1=\ln(Q)$ via equation (5.5) gives the condition

$$e^{(n-1)x_{10}} \leq Q^{n-1} + (n-1)\tau \, \xi \, e^{x_{20}} \qquad ..(5.10)$$

where $$\xi = \exp(t_0/\tau)-1 \qquad (5.11)$$

and $$x_2 = x_{20} + \ln(1+\lambda^2) \qquad (5.12)$$

where $\lambda^2 = \dfrac{e^{(n-1)x_{10}}\, Q^{n-1}}{(n-1)\tau e^{x_{20}}}$ (5.13)

Now we change the variables from x_j to y_j where

$y_1 = x_1$; $y_2 = x_2 + (2-n)x_1$ and $y_3 = x_3 + \alpha x_1 + \beta x_2$ (5.14)

with a Jacobian of J=1 for this transformation. Therefore the new distribution in the y_js is

$$n(y_{10},y_{20},y_{30};t_0) = \frac{c_0 e^{(n-1)y_{10}} X(x_2(),x_3()) H(y_1-\ln(Q)) H(t)}{e^{y_{20}+(n-2)y_{10}}(1+\lambda^2)} \Bigg|_{y_1=\ln(Q)} \quad ..(5.15)$$

5.2.2 The observed distribution.

Again, we integrate out over the spatial dependence, which has thus far been suppressed, and is assumed to be that of a uniform disc population as before in Chapter 3. This gives a maximum radius

r_{max} as $r_{max}^2 = \exp(y_3)/4\pi F_{min}$ ...(5.16) , so that

$$n_{obs}(y_{10},y_{20},y_{30};t_0) = B_0 f(y_{10}) e^{y_{30}} n(y_{10},y_{20},y_{30};t_0)/4F_{min} \quad ..(5.17)$$

We now define the following quantities:

$$\nu_2 = \mu_2 - (n-2)y_{10} \quad ...(5.18)$$

$$\nu_3 = \mu_3 + \alpha y_{10} + \beta y_{20} \quad ...(5.19)$$

$$A = (y_2 - \nu_2 + \ln(1+\lambda^2))/\sigma_2 \quad ....(5.20)$$

$$\bar{\nu}_3 = \nu_3 + \rho A\sigma_3 + \gamma\sigma_3^2/2 \quad ...(5.21)$$

and X has form $\exp(-R)/\sigma_2\sigma_3 \sqrt{(2\pi(1-\rho^2))}$ ...(5.22)

where R is a quadratic form in x_2 and x_3 regarded as functions of y_1, y_2 and y_3. In a way similar to the analysis in Chapter 4 we can write $\exp(y_3).X(x_2(),x_3())$ as the following:

$$Xe^{y_3} = \frac{\exp(-A^2/2 + \bar{\nu}_3 + \rho A\sigma_3 + \gamma\sigma_3^2).\exp\{-(y_3-\bar{\nu}_3)^2/\gamma\sigma_3^2\}}{\sqrt{(2\pi(1-\rho^2))}\sigma_2\sigma_3} \quad ...(5.23)$$

So now integrate out over y_3

$$n_{obs}(y_{10},y_{20};t_0)=\lambda f(y_{10})\frac{e^{y_{10}-y_{20}-A^2/2+\bar{\nu}_3}H(y_{10}-\ln(Q))H(t)}{\sqrt{(2\pi)}\sigma_k\ (1+\lambda^2)}\Big|_{y_1=\ln(Q)} \quad (5.24a)$$

where $\lambda = c_0B_0\exp(\mu_3+\sigma_3^2)/4F_{min}$. ...(5.24b)

which is the observed joint distribution in ln(P) and ln($\dot{P}$) for the full field decay model.

5.2.3 The deathline in the field decay model.

Note the 'deathline' term is now given by:

$$e^{y_2} \geq \frac{e^{(n-1)y_1} - Q^{n-1}}{(n-1)t_0\xi\ e^{(n-2)y_1}} = \Phi_4(y_1) \quad ....(5.25)$$

[where ξ is defined in (5.11)], which is independent (approximately) of Q for periods that satisfy the inequality $\ln(Q) << y_1$. The functional dependence on y_1 is the same as for Model 1 but now much smaller galactic ages are required to fit the observed deathline for typically quoted decay times τ (in range 10^5-10^7 years). As t approaches reasonable galactic ages, the deathline 'disappears' in the sense that lower and lower $\dot{P}$ values become accessible at any P. The lower τ values are those found from more model-independent approaches of Fujimara and Kennel(1980) and Phinney and Blandford(1981), whereas the upper range is favoured by the more recent determinations of LMT, Chevalier and Emmering(1986), Emmering and Chevalier(1989) and Narayan and Ostriker(1990). Clearly there is a big discrepancy between these values, possibly due to the power of selection effects which were treated differently or given less weighting in the different approaches. These used essentially the same observational data and reached radically different conclusions, with

the treatment of luminosity evolution probably accounting largely for the differences.

5.2.4 Impact of time dependence.

A key point emerges here regarding stationarity and the consequences of field decay. Since the timescale is (for convenience) taken to be a universal constant for all pulsars, and most luminosity laws discussed have the luminosity falling off as the pulsar ages, the typical pulsar has an observed lifetime on the $P,\dot{P}$ plane of the same order as τ and the steady-state assumption clearly appears to hold, in that these lifetimes are considerably less than reasonable galactic ages which are $>10^9$ years. Thus the stationarity of previous analyses [GO, LMT, Phinney and Blandford(1981), Narayan(1987), Chevalier and Emmering(1986), etc.] can be retrospectively justified. But it must be remembered that these lifetimes are model-dependent and, *a priori,* no lifetimes are known as these cannot be inferred independently of an evolutionary model. The existence of such a 'dominant' constant as τ virtually forces a steady-state to arise as all timescales can be compared to it. A distribution in τ can be included, but complicates matters considerably, since trajectories can cross in the $P,\dot{P}$ plane for different initial values of k. However the continuity equation method is well suited to such increased complexity.

The work of Ewart et al(1975) indicates that different masses of neutron star will necessarily have different timescales for decay of their magnetic fields. However, for expediency a single τ value will be retained in this work, which is therefore compatible with all other major analyses that include field decay.

5.3 DISCUSSION OF THE BASIS OF FIELD DECAY

The original paper by Gunn and Ostriker(1969), GO, quoted Canuto's

(1970) work on neutron star conductivity and timescale for field decay of $\triangleq$ a few Myrs. This was found to be consistent with their value deduced from pulsar evolution. Since then, as pointed out by Ewart et al(1975), these timescales have had to be lengthened as calculations of superconductivity in neutron star matter have improved. In general, the calculated timescales are much longer than those inferred as necessary from pulsar studies. There is also some doubt as to whether exponential decay is an appropriate description for the problem of a neutron star with a crust surrounding a superconducting interior. The work of Ewart et al(1975) concluded that negligible decay in 10^7 yrs was likely, for masses of neutron star $\triangleq$1.4 solar masses, unless either a) neutron star were much hotter than expected on the basis of cooling theory

or b) the crusts are exceedingly impure or are composed of an extremely fine mosaic of crystallites

and the field could only decay in the extreme outermost portions of the crust. Similar conclusions were reached by Sang and Chanmugam(1987), Brecher and Chanmugam(1983) who estimated that even on a Hubble-timescale, a decay factor of $<$ 100 in field strength was the most that could be expected, and that no significant decay would take place on typical pulsar 'lifetimes'. They also favoured a more gradual decay in preference to exponential decline.

From the analysis of pulsar statistics, some supporting evidence for steady magnetic fields has been found by Brecher and Chanmugam(1983), Nowakowski(1987) and Kundt(1981,1988). Nowakowski discovered that the timescale for decay τ could in principle be inferred from observation of $\ddot{P}$ for suitable pulsars, but that due to flaws in the fitting of timing data both $|\ddot{P}|$ and the proper motion

could be overestimated. This would have serious consequences for the kinematic age estimates of the pulsars which are a cornerstone of the 'stationarity' argument.

Kundt(1988) was led to the view that since field decay and alignment could not be distinguished easily, there was a good case for no field decay. Indeed the alignment model of Candy and Blair(1983,1986) claimed to explain some of the pulsewidth data which field decay could not. Thus the question of whether field decay is required for pulsar evolution is still open- we hope to be able to help answer this question by our approach to pulsar evolution in this thesis.

5.4 FITTING THE FIELD DECAY MODEL

5.4.1 The LMT model.

We wish to look at the model of LMT as a particular case of the more general field decay model outlined above. This can be retrieved by repeating the above analysis without a spread in Δ, and fixing the parameters $n = 3$, $\alpha = 1$, $\beta = 1$. Then we let the age of the galaxy (t_0) tend to infinity, so the deathline disappears. This produces the LMT predicted distribution for P and $\dot{P}$, which is:

$$N_{obs}(P,\dot{P}) = \frac{c_0 B_0 \Delta P \exp-\left[\left[\ln(P\mu_k^{-1}(\dot{P} + P/2\tau)\right]^2/2\sigma_k^2\right]}{2F_{min}\sqrt{(2\pi)}\sigma_k (2\tau\dot{P} + P)} \qquad (5.26)$$

where the usual notation applies.

5.4.2 Fitting the LMT model.

Using the same grid in the $P,\dot{P}$ plane, (Figure 4.1), we minimise the chi-squared statistic in the same way as for the simple model. The LMT model has three parameters, since n, α and β are fixed in value. Thus we have 22 degrees of freedom: adopting the 5% level of significance gives a target χ^2 value of 33.92. The free parameters are μ_2 , σ_2 and τ : respectively the mean and standard deviation in the

distribution of initial torque, and the decay timescale.

The best fit found was: $\chi^2 = 58.12$, with $p(\chi^2|\nu) = 4.2\text{x}10^{-5}$, at the point $\mu_2 = -35.43$

$\sigma_2 = 1.45$

$\tau = 1.4\text{x}10^{14}$ seconds = 4.4Myrs.

These are very similar to the values found by LMT from a different method. Note that our timescale is for the decay of k which is $\propto B^2$, so τ is about half of the LMT value. However, this fit is not significant at our chosen level. In Cheng(1989) a better fit is obtained for this model, but using a different grid. Cheng's fit is not acceptable at the 5% level since his degrees of freedom are not accounted for properly, as he neglects the fact that the LMT values for the parameters are already best-fit values, so degrees of freedom are lost.

There is no easy way to assess the influence of the chosen bin scheme on this, without simply running several trials over different bin arrangements. The Kolmogorov-Smirnov test cannot be applied to the two-dimensional case in the manner that was useful for the marginal fitting. Since time did not permit a more comprehensive approach, no greatly improved fits could be found using slightly altered bin boundaries. Thus the LMT model fails to meet our required criteria for acceptance, and should be rejected. We note, however, the work of Cheng(1989), Emmering and Chevalier(1989) and Narayan and Ostriker(1990) concludes that the LMT/GO field decay model does provide a good explanation for pulsar evolution. This work in Chapter 5 finds that the LMT model cannot fit the observed $P,\dot{P}$ distribution at the 5% level of significance.

5.4.3 Fitting the full field decay model.

Now we use the full form of equation (5.24). The parameters are now

μ_2, σ_2, ρ, τ, n, α and β, for the usual notation. No apparent combination of parameter effects could be identified since unlike the simple model, further analytic integration could not be done over the full field decay $P,\dot{P}$ distribution (equation 5.24a). Any degeneracy present in the field decay model will be apparent if identical fits are found at separate points in parameter space as part of the χ^2 minimisation. If there is any degeneracy present, we will be able to achieve the optimum fit with less than 7 parameters. We start with 7 free parameters, giving 18 degrees of freedom. This makes our target χ^2 at the 5% level 28.87. So we minimise χ^2 as usual, and the best fit found is

FIT 1 : $\chi^2 = 27.75$, and $p(\chi^2|\nu) = 6.5\%$ at the point

$\mu_2 = -35.04$

$\sigma_2 = 1.56$

$\alpha = 1.66$

$\beta = 0.65$

$\rho = -0.14$

$\tau = 4.2 \times 10^{13}$ secs = 1.33 Myrs

$n = 3.25$.

A simulation of this fit to the $P,\dot{P}$ diagram is shown in Figure 5.1a. This is achieved by randomly generating points appropriately in the bins used for the χ^2 test. This gives a qualitative idea of the goodness-of-fit of this model. Clearly, since we can fit the joint distribution of P and $\dot{P}$ it will be easy to fit the marginal distributions of P or $\dot{P}$ to the desired accuracy. The reverse, as we have seen in Chapter 4, is not true.

We can test roughly for redundancy in the parameter set by fixing the values of, say, ρ and n, and minimising χ^2 again over the

remainder, giving 20 degrees of freedom, and a target χ^2 of 31.14. Thus we achieve another fit:

FIT 2 : χ^2 = 27.8 , $p(\chi^2|\nu)$ = 11.4% at the point

μ_2 = -34.9

σ_2 = 1.39

α = 1.59

β = 0.63

τ = 4.1×10^{13} secs = 1.3 Myrs, with fixed values ρ = 0 and η = 3.0

This is an almost identical χ^2, but with greater significance owing to the 2 extra degrees of freedom. This suggests that a possible degeneracy may exist, but since the values are very similar for the 5 free parameters, it could be that we are close to a 'shallow' minimum which only slowly depends on β and ρ. This fit is simulated in Figure 5.1b, which shows it to be similar to the previous fit.

Next, a further minimisation is done, but this time fixing the luminosity law to the GO/LMT law, by holding α = 1 and β = 1. This produces a best-fit of :

FIT 3 : χ^2 = 42.4, $p(\chi^2|\nu)$ = 9.7×10^{-4} at the point

μ_2 = -35.9

σ_2 = 2.12

ρ = -0.35

τ = 1.5×10^{14} secs = 4.7Myrs

η = 3.93.

This fit is not significant at the 5% level. Thus any degeneracy in the parameter set leaves only one of α and β as a free parameter, in the same way that the simple model does. This is similar to the work of Chapter 3, where α-β appeared as a parameter, rather than both α and β.

The two acceptable fits both have a τ of $\triangleq$ 1.3 Myrs, which is slightly shorter than the normally quoted figures, but well within the range that is found from a variety of methods. We note that when $\alpha = \beta = 1$ is fixed, the best τ is larger than this by a factor of about 4. This merely serves to emphasise the interdependence of our parameter estimations.

5.4.4 The birthrate in the field decay model.

The normalisation parameter λ for the above fit is 0.11, to two significant figures. This is, from (5.24b), a combination of c_0, B_0, σ_3 and μ_3. Since B_0 is chosen to be fixed at 0.2, it remains to estimate the parameter $\mu_3 + \sigma_3^2$, which cannot be found from the χ^2 fitting. The $\rho = 0$ case corresponds to dropping the σ_3^2 term, i.e. ignoring the spread in the parameter Δ. A simple and demonstrative solution is simply to use the Crab pulsar data and the inferred α and β to give a value of $\Delta = \exp(\mu_3)$, as we did in Chapter 3. This gives a birthrate of $c_0 = 3\text{x}10^{-1}$ pulsars /year in the galaxy. This of course depends on the Δ chosen, and is to an extent arbitrary. A lower value of Δ will raise the birthrate. So no firm conclusion can be reached on the birthrate c_0 without more exact knowledge of the value of Δ.

5.5 CONCLUSIONS

We have seen that field decay does provide a satisfactory fit to the $P,\dot{P}$ diagram, and even in the case where braking index and correlation parameter are fixed. This means that no distribution in the parameter Δ is required to fit the $P,\dot{P}$ data, (although evidently to explain spread in L one does need a spread in Δ) and magnetic dipole braking is perfectly adequate as a spin-down mechanism in this model. Of greater interest, however, is the incompatibility of the two standard luminosity laws with this optimum χ^2 solution, that is both the (α,β) pairs

(-1,0.33) and (1,1) are far removed from the 'best' solution, (although the fit with $\beta = 1$ fixed is as good as the β-varying case). We note from our discussion in Chapter 1 that we do not expect the Proszynski-Przybcien law to be the intrinsic luminosity law governing the population so this is perhaps not a surprising observation. In fact, it is not possible from this work alone to say precisely which pairings of α and β are compatible with the field decay model due to the interdependence of the parameters we have used in the optimised fitting. It is clear that positive values of α and β are necessary for the field decay model to match the observations, which is difficult to reconcile with the conclusions of Proszynski and Przybcien(1984). Further work is necessary to establish if these different intrinsic and apparent luminosity laws can in fact be consistent.

It is also found that the model of GO and LMT is not an acceptable fit at the 5% level of significance, although the dependence of this conclusion on the binning scheme chosen is not easy to assess conclusively.

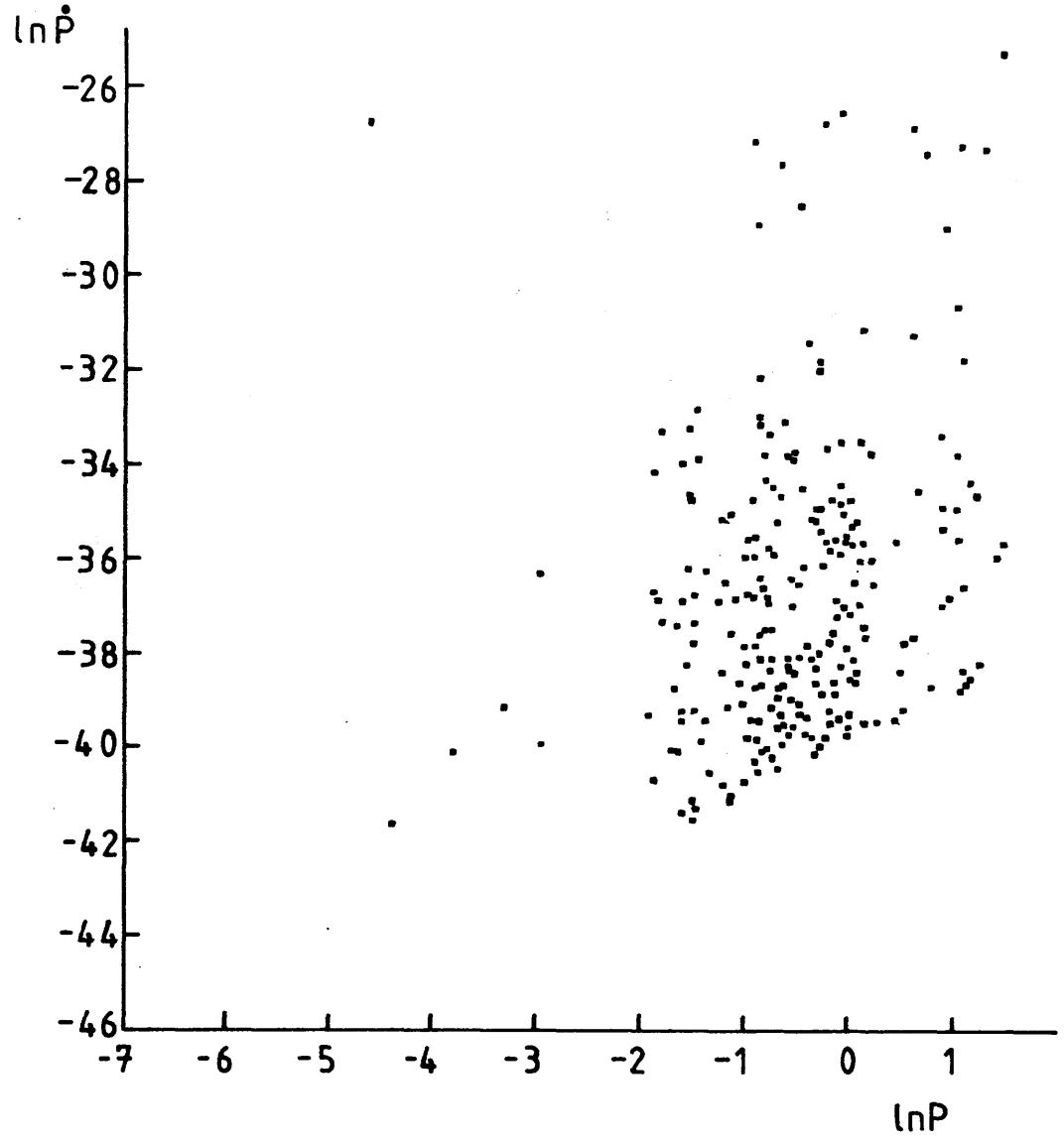

FIGURE 5.1A

A simulation of the P,$\dot{P}$ diagram for FIT 1 of the field decay model, for the best-fit parameters obtained in the χ^2 fitting in Section 5.4.3 In each bin of figure 4.1, the predicted number of pulsars is found, and rounded to the nearest integer. These pulsars are randomly assigned periods and period derivatives within the bin and then plotted. This simulation corresponds to the fit with the 18 degrees of freedom.

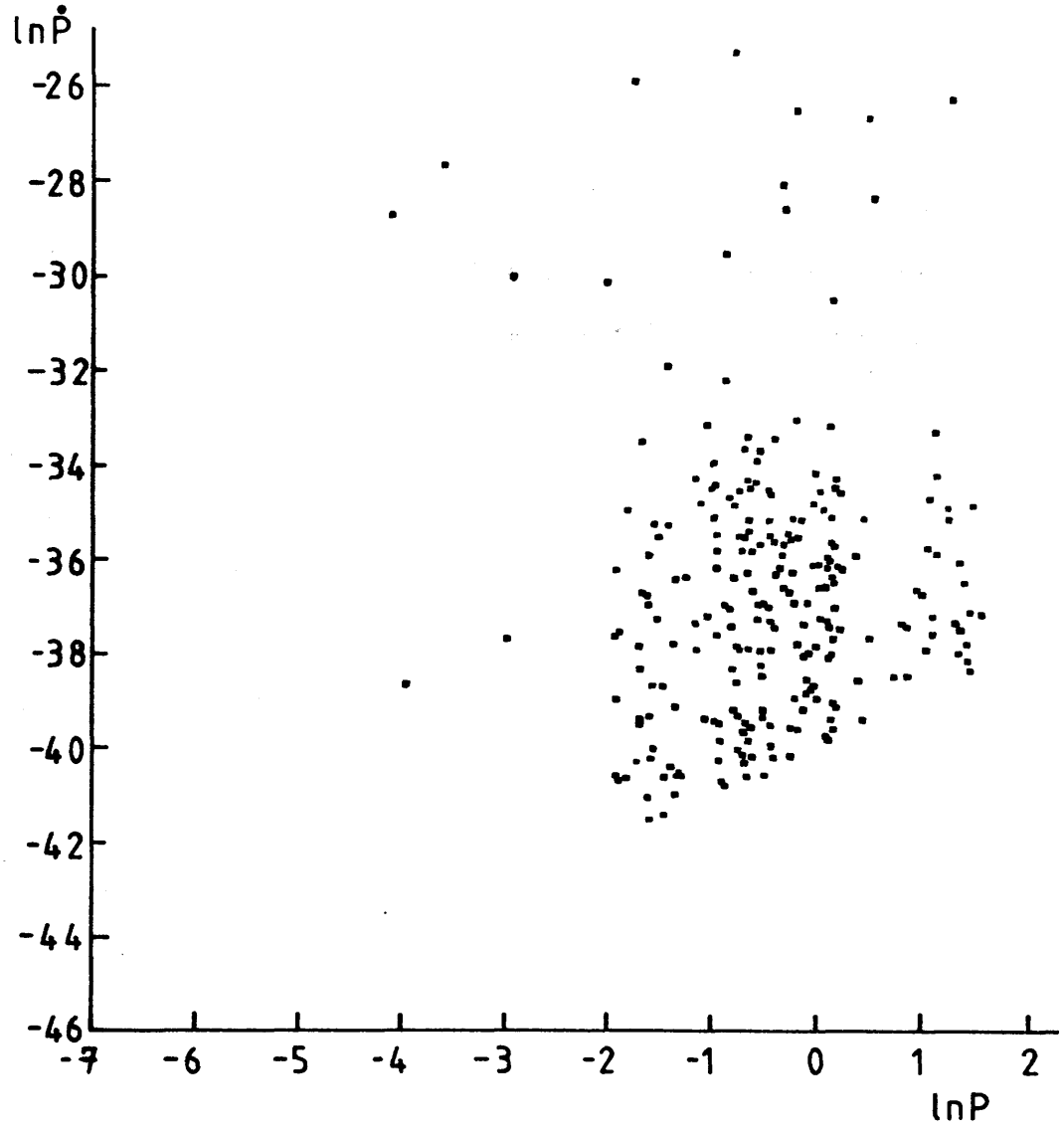

FIGURE 5.1B

A simulation of the P,$\dot{P}$ diagram for FIT 2 of the field decay model, with 20 degrees of freedom, the parameters being those of Section 5.4.3. This is for the full field decay model of Chapter 5.

CHAPTER 6

MODEL 3: THE ALIGNMENT MODEL

6.1 INTRODUCTION

In this chapter we will develop Model 3, which is an alignment model for pulsar evolution. Alignment occurs when the (alignment) angle between rotation and magnetic axes tend to zero as time passes. We firstly develop the complete alignment model in Section 6.2, using our method. The derived $P,\dot{P}$ distribution is obtained in Section 6.2 and compared in the usual way against the observations, to obtain best-fit parameter values. (Section 6.3). A comparison and discussion of the results of the field decay and alignment models is held in Section 6.4. The importance of pulsewidths is discussed in Section 6.5, and it is argued that it may be possible to use the pulsewidth data to further test evolutionary models. To show how this can be done, the distribution of pulsewidths expected from a non-evolving model is obtained in Section 6.6, to show the geometry involved in this approach which will be needed for the derivation of the pulsewidth distribution associated with the complete alignment model. A non-evolving model is one where the orientation of the pulsar axes does not change as it spins down. Next, in Section 6.7, the distribution of pulsewidths expected for an alignment model is derived, followed in Section 6.8 by the derivation of the expectation of pulsewidth conditional on characteristic age, as discussed by Candy and Blair(1983). A further avenue of approach is shown in Section 6.9, where the effective beaming fractions for the alignment model are analysed. The discussion and conclusions are found in Section 6.10.

6.2 ALIGNMENT MODEL FOR PULSAR EVOLUTION

It is convenient to deal in this case with the quantities P,k,Δ directly

instead of their logarithmic counterparts. We also use θ to represent the alignment angle between the pulsar axes and Φ to denote the angle between the polar direction and the line of sight of the observer. This is the same notation as in the section below on pulsewidths.

Pulsar spindown is therefore governed by the following equations:

$$\dot{P} = \frac{k \sin^2(\theta)}{P} \qquad (6.1)$$

and $$\sin(\theta) = \sin(\theta_0) \exp(-(t-t_0)/\tau) \qquad (6.2)$$

where τ is the alignment timescale (analogous to the decay timescale in the field decay model). The solution of these gives:

$$P^2 = P_0^2 + \tau k \sin^2(\theta_0)(1-\exp(-2(t-t_0)/\tau) \qquad (6.3)$$

or, $$P^2 + \tau k \sin^2(\theta) = P_0^2 + \tau k \sin^2(\theta_0) = \text{constant} \qquad (6.4)$$

We choose the source function to be :

$$C(P,k,\Delta,\theta,\Phi;t) = c_0 \delta(P-Q) K(k,\Delta) \sin\theta \sin\Phi H(t) H(1-\sin\theta) H(\sin\theta) \qquad (6.5)$$

such that pulsars are born only at P=Q, with a bivariate log-normal distribution in k and Δ and a uniform distribution of orientations of magnetic to rotation axis.

Only after t=0 can pulsars be created. Next we find the Jacobian J which is, from equations (6.2) and (6.3)

$$J = \partial(P,\theta)/\partial(P_0,\theta_0) = P_0 \cot(\theta)/P\cot(\theta_0) \qquad (6.6)$$

Thus from (3.2) we can write the formal solution for the intrinsic density $n(P,k,\Delta,\theta,\Phi;t)$ as:

$$n(P_0,k_0,\Delta_0,\theta_0,\Phi_0;t_0) = \frac{c_0 P_0 \cot(\theta_0)\sin(\Phi_0) K(k_0,\Delta_0) H(t)}{k_0 \sqrt{(1-\sin^2(\theta_0)+\lambda^2)}}\Big|_{P=Q} \qquad (6.7)$$

where $$\lambda^2 = \frac{P_0^2 - Q^2}{\tau k_0} \qquad (6.8)$$

and t is found from equation (6.3), solved when P = Q.

Now we transform to the variables $P,\dot{P},L,\theta$ and Φ by the following relations: $L = \Delta\, P^{\alpha}\, \dot{P}^{\beta}$ and $\dot{P} = k \sin^2(\theta)/P$ as above.

This has the transformation Jacobian of:

$$\frac{\partial(\dot{P},L)}{\partial(k,\Delta)} = \sin^2(\theta) P^{\alpha-1}\, \dot{P}^{\beta} \qquad (6.9)$$

So $n(P_o,\dot{P}_o,L_o,\theta_o,\Phi_o;t_o) =$

$$\frac{c_o P_o^{1-\alpha} \dot{P}_o^{-\beta-1} K(P_o\dot{P}_o \mathrm{cosec}^2(\theta_o), L_o P_o^{-\alpha}\, \dot{P}_o^{-\beta}) H(t)}{(1 - \sin^2(\theta_o)/\epsilon^2)^{1/2}} \Big| \cot(\theta_o)\sin(\Phi_o) \quad (6.10a)$$

$P=Q$

where $\epsilon^{-2} = 1 + \dfrac{P_o^2 - Q^2}{\tau P_o \dot{P}_o}$ (6.10b)

Now include the flux limitation effect and the survey sensitivity to the period as before: this entails multiplying the above by the factor $Lf(P_o)/4F_{min}$ to give the observed distribution in $P,\dot{P}$,etc. To get the desired observed joint $P,\dot{P}$ distribution it is necessary to integrate over the geometrical variables θ and Φ and over L, the luminosity. By referring to Figure 6.4 the required region in the θ,Φ plane is shown: observable pulsars all lie in the box, with interpulse pulsars in the upper right-corner triangle. We integrate over L as follows. The L-dependence is contained in both a factor of L and inside the bivariate ln-normal distribution. Define

$$I(P_o\dot{P}_o \mathrm{cosec}^2\theta_o) = \int_0^{\infty} L_o K(P_o\dot{P}_o \mathrm{cosec}^2\theta_o, L_o P_o^{\alpha}\, \dot{P}_o^{\beta}) dL \qquad (6.11)$$

To perform the integral, change the variables to the following:

$a=P_o\dot{P}_o \mathrm{cosec}^2\theta_o$ and $z=\ln(L_o)$, so that $dL = e^z dz$. Using Theorem 2 in Appendix A3, it can be shown that:

$$I(a) = \frac{\exp(-a - A^2/2 + \rho A\sigma_3 + \gamma\sigma_3^2/4 + \mu_3)}{\sqrt{(2.\pi.\sigma_k^2)}} \qquad (6.12)$$

where $A = \frac{\hat{\quad}}{\sigma_k} = c_0 f(P_0) e^{\mu_3+\gamma\sigma_3^2/4} P_0^{\alpha}\, \dot{P}_0^{\beta-2} 2\sin\beta_0\, \cos\theta_0 \sin^2\theta_0 e^{-A^2/2+\rho A\sigma}$

and $\gamma = 2(1-\rho^2)$, and σ_3, ρ, etc. are the usual parameters of the bivariate normal distribution in k and Δ that have been used in earlier Chapters. Thus we obtain:

$$n_{obs}(P_0, \dot{P}_0, \theta_0, \phi_0, t_0) =$$

$$\frac{c c_0 f(P_0) P_0^{\alpha}\, \dot{P}_0^{\beta-2} \sin^2\theta_0 \cot\theta_0 e^{\mu_3+\gamma\sigma_3^2/4} e^{-A^2/2+\rho A\sigma_k} \sin\phi_0 H(t)}{4\, F_{min}\sqrt{(2\pi\sigma_k^2)}\sqrt{(1-\sin^2(\theta)/\epsilon^2)}}\Bigg|_{P=Q} \qquad (6.14)$$

Now, the angle ϕ does not change in time, so we can integrate over ϕ with purely geometrical constraints. Noticing that for negative values of ϕ, the function is symmetrical through the θ axis, we can split the range of integration into two regions. For the moment we shall neglect the interpulse region of Figure 6.4. We get:

$$\text{Region a}: \int_{\theta_0-\beta_0}^{\theta_0+\beta_0} \sin\phi\, d\phi = 2\sin\beta_0 \sin\theta \qquad (6.15)$$

$$\text{Region b}: \int_{\theta_0-\beta_0}^{\pi/2} \sin\phi\, d\phi = \cos(\theta_0)\cos(\beta_0) + \sin(\theta_0)\sin(\beta_0) \qquad (6.16)$$

where the 'upper' region has different limits so that the interpulse zone is included. So now our functional dependence takes two forms:

$$n_{obs}(P_0, \dot{P}_0, \theta_0; t_0) =$$

$$= \frac{c_0 f(P_0) e^{\mu_3+\gamma\sigma_3^2/4} P_0^{\alpha}\, \dot{P}_0^{\beta-2} 2\sin\beta_0\, \cos\theta_0 \sin^2\theta_0 e^{-A^2/2+\rho A\sigma} H(t)}{4\, F_{min}\sqrt{(2\pi\sigma_k^2)}.\sqrt{(1-\sin^2(\theta)/\epsilon^2)}}\Bigg|_{P_0=Q} \qquad (6.17)$$

when the inequality $\cos(\beta_0) \geq \epsilon$ is satisfied, and when it is

reversed, the θ-dependent terms only are different, giving

$$\frac{\sin^2\theta_0\cot\theta_0(\cos(\theta_0)\cos(\beta_0)+\sin(\theta_0)\sin(\beta_0))\exp(-A^2/2+\rho A\sigma_3)}{\sqrt{(\,1-\sin^2(\theta_0)/\epsilon^2)}} \quad (6.18)$$

Now the limits for integration over θ are also dependent on which is being considered. $\theta = \sin^{-1}(\epsilon)$ is an upper limit, but as this may be in either region, depending on P and $\dot{P}$, care must be taken. When $\sin^{-1}(\epsilon)$ is an upper limit, the integrand is undefined at this limit. Therefore a change of variables is required. It is convenient to choose x as the new variable, where $\sin(\theta) = \epsilon\cos(x)$. Thus we get, finally, for the distribution in period and period derivative for the alignment model the following expressions, with the corresponding regions of validity.

$$n_{obs}(P_0,\ \dot{P}_0;\ t_0) = \frac{c_0 f(P_0) e^{\mu_3+\gamma\sigma_3^2/4}\ P_0^{\alpha}\ \dot{P}_0^{\beta-2}\ I\ (P_0,\dot{P}_0,\epsilon,\beta_0)}{4F_{min}\sqrt{(2\pi)}\sigma_k} \quad (6.19)$$

where the factor $I\ (P_0,\dot{P}_0,\epsilon,\beta_0)$ takes the following form:

When $\epsilon \leqslant \cos(\beta_0)$;

$$I = 2\ \sin(\beta_0)\ \epsilon^3 \cdot \int_0^{\pi/2}\cos^2 x\ \exp(-A^2/2 + \rho A\sigma_3)\ dx \quad (6.20)$$

When $\epsilon > \cos(\beta_0)$;

$$I = 2\ \sin(\beta_0)\ \epsilon^3 \cdot \int_a^{\pi/2}\cos^2 x\ \exp(-A^2/2 + \rho A\sigma_3)\ dx$$

$$+\quad \cos(\beta_0)\ \epsilon^2 \cdot \int_0^{a}\ \cos x\ \sqrt{(1-\epsilon^2\cos^2 x)}\cdot\exp(-A^2/2 + \rho A\sigma_3)dx$$

$$+\quad \sin(\beta_0)\ \epsilon^3 \cdot \int_0^{a}\ \cos^2 x\ \exp(-A^2/2 + \rho A\sigma_3)\ dx \quad (6.21)$$

where $a = \cos^{-1}(\cos\beta_0/\epsilon)$ and $A = \dfrac{\ln(P_0\dot{P}_0\sec^2 x/\epsilon^2\mu_k)}{\sigma_k}$ (6.22)

These are the expressions that will give us the $P,\dot{P}$ distribution

predicted by the alignment model.

6.3 FITTING THE ALIGNMENT MODEL.

6.3.1 The chi-squared test.

Since the above expressions involve a triple integration to obtain the numbers of pulsars in boxes, the combinations of parameters that created a problem earlier in Chapters 3 and 4 are less easy to identify now. Since braking index has not been included, for simplicity, this will lead to a lessening of the 'interdependence' of the parameters that was encountered earlier. When minimising χ^2 over the parameter space, care must be taken to check that the redundancy problem will arise and not be recognised. There are the following model parameters:

* α and β from the luminosity law;
* μ_2 and σ_2, the mean and variance of the magnetic torque
* μ_3 and σ_3, the mean and variance of the Δ parameter
* ρ and τ, the correlation ρ from the bivariate source term in k and Δ, and τ the alignment timescale.

The same two combinations can be seen again:

$\mu_3 + \sigma_3^2$ and $\rho\sigma_3^2$ both appear as before.

We vary over 5 parameters to begin with, μ_2, σ_2, α, β and τ, with fixed $\beta_0 = 0.175$ and $\rho = 0$. This means we have a fixed cone angle ($\beta_0 = 10^{\circ}$) and ignore any correlation between the parameters Δ and k, as was done for the full version of the field decay model.

This gives $\nu = 20$ degress of freedom, so the 5% targets for chi-squared are 10.85 and 31.41. The best fit found is :

$\chi^2 = 28.29$, $p(\chi^2|\nu) = 10.3\%$, at the point

$\mu_2 = -32.7$

$\sigma_2 = 1.33$

α = 0.74

β = -0.37

τ = 7.7×10^{13} secs = 2.44 $\times 10^{6}$ years.

This is a significant fit at the 5% level. No better values of χ^2 could be found even by varying all 7 possible parameters, suggesting strongly that redundancy within the parameter set again limits the fitting procedure. The most unexpected feature is the negative value of β, the power of the period derivative in the luminosity law. This will be of some importance when we discuss the pulsewidth distribution associated with the alignment model, and this fit in particular.

Thus the alignment model does give an acceptable fit to the period and period derivative distribution, at the assigned level of significance. The field decay model gives a fit which has an almost identical chi-squared statistic. This, broadly speaking, means the two are indistinguishable purely on the basis of the period and period derivative distributions that they predict to be observed.

6.3.2 The birthrate in the alignment model.

Again we adopt the Crab value of Δ to establish the value of c_0. This gives a birthrate of c_0 = 4.5 psrs/100 years in the galaxy, which is comparable with other estimates of the pulsar birthrate. This of course is only an illustrative example, as we have pointed out the difficulty in inferring the true birthrate for these models.

6.3.3 The impact of time-dependence in the alignment model.

The deathline for alignment is identical in form to the field decay deathline (5.28c). We again find the parameter τ (now the alignment rather than field decay timescale) dominates, there is a terminal period for each pulsar, and a steady state is reached for galactic ages t_0

greater than a few times τ. Letting $t_0 \to \infty$ creates the steady state, as before.

6.4 ALIGNMENT VERSUS FIELD DECAY

There are of course other strategies that can be utilised to try and decide if one model is a better fit than the other. One possibility is to include the luminosity in the way suggested by Emmering and Chevalier(1989), that is, demand a Proszynski/Przybcien type law for luminosity with parameters α' and β' within a determined tolerance of those deduced from the regression on the data.

The other avenue, which is original by virtue of not having been properly used or appreciated by previous authors, is that of the pulsewidth information, which is entirely separate from the period and period derivative information. We have shown below how the non-evolving pulsewidth distribution could be derived, this being relevant to models where the alignment angle does not feature in the spin-down law for $\dot{P}$. A similar approach will give the distribution of pulsewidths in the alignment model, only we expect to have more complicated algebra to deal with. This can be simplified somewhat by the assumption of a) $t_0 \to \infty$ (allow the steady state)

b) $Q \to 0$ (vanishingly small initial periods)

c) $\rho = 0$ (ignore all variation in Δ)

d) Ignore f(P) factor (Set equal to 1)

Thus we can proceed to derive the pulsewidth distribution relevant to the alignment model.

6.5 ALIGNMENT AND PULSEWIDTHS.

A pulse of radiation is observed once per revolution of the star when a beam of unknown shape and dimensions sweeps across the Earth. The section through the beam that is observed allows the study of

pulse shapes and their dependence on other pulsar parameters and observing frequency. The most direct observable is the pulsewidth, defined usually at either 10% or 50% of the peak intensity. The duty cycle is defined as the width of the pulse (in seconds) to the total period, and typically is a few per cent. In some pulsars it is possible to identify an interpulse, lying between the main pulses. Most authors consider this to be due to radiation from the opposite pole of the star but some models have both pulses originating at the same pole. See, for example, Lyne and Manchester(1988) and references therein.

It is important to study the distribution of pulsewidths, and to compare it with the predictions of models. This gives an independent and useful check on the validity of the theory. The stability of the long-term pulse profile of a pulsar and the wide variety of phenomena associated with them make the study of pulsewidths not only of interest but important as a further means of shedding light on the pulsar phenomenon. Consideration of the available data on pulsewidths and their distribution and correlations with other important parameters is a potential means of diagnosing any general trends for pulsars to align or counteralign as they evolve, in the sense defined in Chapter 2. If we adopt the simple model of a circular beam, as in the work of Radhakrishnan and Cooke(1969), Henry and Paik(1969), and Candy and Blair(1983),(1986), it will be shown that for a cone angle of $2\beta_o$ pulsewidths from 0 to 2π are possible for certain relative orientations of observer and star. The geometrical arrangement is shown in Figures 6.1a and 6.1b, with the special cases of (a) observer always in the beam (Fig.6.2) and (b) interpulses, or two pulses per rotation (Fig.6.3) also shown. It will be clear that in an alignment model, older pulsars ought to have larger pulsewidths, in general, where in

counter-alignment the pulsewidths could be at most $2\beta_0$ for the oldest pulsars, which ought to show interpulses more frequently. Under either scenario, the beaming factor will become dependent on pulsar age. However, existing treatments have not, we contend, addressed or correctly tackled the analysis of the pulsewidth distribution and the beaming factor with the exceptions of Candy and Blair(1983 and 1986) and Lyne and Manchester(1988). In fact it is wrongly claimed by Proszynski(1979) that it is not possible to derive analytically an expression for the pulsewidth distribution but it is shown below how this can be done.

More complicated phenomena can cloud the picture somewhat. The beam shapes may not be exactly circular, they may change in shape as the pulsar evolves and there may well be variation in intensity across the beam. All of these effects give contributions to the beaming factor and can be modelled. However, we choose to concentrate on the steady, circular beam geometry so that definite conclusions can be identified. The work of Lyne and Manchester(1988) has shown that these effects can be treated, but they conclude that the elongation of pulsar beams is not as important as suggested by Narayan and Vivekanand(1983) and luminosity variation is not too important for typical pulsars.

The following diagrams (Figs.6.4 and Fig.6.5) show the idealised picture of the pulsar geometry, the areas of the θ, Φ plane that correspond to 0,1 and 2 pulses and the same information but in the more convenient rotated frame, as defined below.

6.6 NON-EVOLVING PULSEWIDTH DISTRIBUTION.

6.6.1 Preamble.

The simplest means of showing the importance of orientation effects is to deal firstly with a non-evolutionary model and deduce the

pulsewidth distribution corresponding to a random orientation of pulsars in space. This reveals how the observed pulsewidth can be seen as less than, equal to or greater than the intrinsic width of the emission cone, also how interpulses arise and that many pulsars are simply not seen at all. A single value of ρ_0 is adopted, the cone half-angle (see Figs. 6.1a and 6.1b). For simplicity, we assume that when pulsars are born, the direction of the magnetic field to rotation axis is randomly and uniformly distributed. Let θ and ϕ be the alignment and orientation angles respectively, with probability density function $f(\theta,\phi)d\theta d\phi$. For a uniform distribution

$$f(\theta,\phi) = \sin(\theta).\sin(\phi). \qquad .. (6.23)$$

The pulsewidth w is given by

$$w = 2\cos^{-1}((\cos\rho_0 - \cos\theta\cos\phi)/\sin\theta\sin\phi) \qquad ..(6.24)$$

As shown by Proszynski(1979) the rectangular box in Figure 6.4 covers the region where one pulse will be observed, the small triangle corresponds to 2 pulses per rotation and the rest of the plane to the case of the pulsar being unobserved. It is noted that the lower small triangle covers the cases where the observer is always in the beam, and sees only modulated (M) emission, hence no pulsewidth can be defined: we assume the object is not identifiable as a pulsar under these conditions, or cannot be detected. The probabilities of seeing 0,1 or 2 pulses and modulation (M) are :

$$Pr(1) = \iint_{box1} f(\theta,\phi)d\theta d\phi \qquad \text{over box "1" of Figure 6.4}$$

$$Pr(2) = \iint_{box2} f(\theta,\phi)d\theta d\phi \qquad \text{over the triangle "2"}$$

$$Pr(M) = \iint_{box3} f(\theta,\phi)d\theta d\phi \qquad \text{over the triangle "M"} \qquad ...(6.25)$$

$$Pr(0) = 1.0 - Pr(1) - Pr(2) - Pr(M)$$

These turn out to be, for the non-evolutionary model, for probability density function given by (6.23)

$$Pr(1)= (\pi/2 - \beta_0).\sin(\beta_0)$$

$$Pr(2)= 0.5\ \beta_0\ \sin(\beta_0)$$

$$Pr(M)= 1 - \cos(\beta_0) -0.5\beta_0\sin(\beta_0) \qquad ...(6.26)$$

$$Pr(0)= \cos(\beta_0) - (\pi/2-\beta_0)\sin(\beta_0)$$

Thus the effective beaming fraction in this case is Pr(1)+Pr(2). For a cone angle of $\beta_0 = 10^\circ$ it is found that

$$\Gamma_0 = Pr(1)+Pr(2) = 0.5(\pi-\beta_0)\sin(\beta_0) \triangleq 0.25 = 1/4 \qquad ...(6.27)$$

The derivation of theoretical pulsewidth distributions has not been carried out in this way for evolutionary models in the literature, to the author's knowledge. Proszynski(1979) claimed that such a distribution could not be derived. This is not so, and a stationary analysis was done by Henry and Paik(1969), Candy and Blair(1986), but not explained, and also below in Section 6.6. The Henry and Paik(1969) version ignores the spherical geometry of the problem.

This approach provides the basis of the correct way to tackle the interpretation of the pulsewidth vs age diagram used by Candy and Blair(1983,1986) and to fully utilise the information obtainable from pulsewidth observations. We are primarily interested purely in the pulsewidth data, not in the diversity of other phoenomena such as subpulses, drifting, nulling etc, as discussed in Rankin(1990). To show our method, the simplest course is to develop the distribution of pulsewidths for a non-evolving population of pulsars and subsequently proceed to apply the ideas to the more interesting alignment model, where the approach is most relevant.

6.6.2 The non-evolving pulsewidth distribution.

We shall derive the pulsewidth distribution as follows. We use a rotated frame to make use of the symmetry of the problem, with new angular variables x and y replacing θ and ϕ. We then use (6.2) to find

the joint distribution of x and C, where C = cos(w/2). Integration out over x produces the marginal distribution of pulsewidth C alone. Our starting point is the same as above: the diagram in Figure 6.4 shows the regions in θ,ϕ space that observed pulsars occupy. It is more convenient to consider the problem in rotated coordinates as follows:

Define $x = (\theta-\phi).\sqrt{2}$

and $y = (\theta+\phi).\sqrt{2}$ ..(6.28)

so that the region of diagram in Fig.6.4 transforms to that of the diagram in Fig.6.5 , which is symmetrical about the y-axis.

So x and y have a probability density function given by

$$f'(x,y) = f(\theta,\phi).\left|\frac{\partial(\theta,\phi)}{\partial(x,y)}\right| = f\left(\frac{(x+y)}{\sqrt{2}}, \frac{(y-x)}{\sqrt{2}}\right) \qquad (6.29)$$

$$x \leqslant \beta_0/\sqrt{2} \quad \text{and} \quad x \geqslant \beta_0/\sqrt{2}$$

$$\text{and} \quad y \geqslant \beta_0/\sqrt{2} \quad \text{and} \quad y \leqslant (\pi-\beta_0)/\sqrt{2} \qquad ...(6.30)$$

Define $C = \cos(w/2)$ (6.31a)

where w is the pulsewidth. By the definition of w (equation 6.2) we get

$$C = \frac{\cos(\beta_0) - \cos(x' + y')\cos(y'-x')}{\sin(x'+y')\sin(y'-x')} \qquad (6.31b)$$

where x' and y' indicate $x/\sqrt{2}$ and $y/\sqrt{2}$ respectively.

Now we can obtain the distribution in x and C from:

$$f(x,C) = f(x,y).\left|\frac{\partial y}{\partial C}\right| \qquad (6.31c)$$

(6.31a) can be rearranged to give

$$\cos^2(y')\,(1-C) = \cos(\beta_0) - C + \sin^2(x')(1+C) \qquad (6.32)$$

$$\text{so} \quad y = \sqrt{2}\,\cos^{-1}\sqrt{\left[\frac{\cos\beta_0 - C + \sin^2 x(1+C)}{1-C}\right]} \qquad (6.33)$$

Note the symmetry between positive and negative x. Treating C as a constant in this equation allows one to plot contours of constant pulsewidth in the x,y plane, as in Fig 6.5. We now need to find the intercepts of these contours with the line $y = (\pi-\beta_0)/\sqrt{2}$, to give the limits for the integration over x. From the above equation,

$$\frac{\cos^2(\pi-\beta_0)}{2} = \frac{\sin^2(x/\sqrt{2}) + \cos(\beta_0) - C\cos^2(x/\sqrt{2})}{1-C} \qquad (6.34)$$

Solving for x therefore, we get after rearranging;

$$\cos^2(x/\sqrt{2}) = \frac{\cos^2(\beta_0/2) + \cos(\beta_0) + C\sin^2(\beta_0/2)}{1 + C} \qquad (6.35)$$

$$\text{so} \quad x = \sqrt{2}\cos^{-1}\sqrt{\left[\frac{\cos^2(\beta_0/2) + \cos(\beta_0) + C\sin^2(\beta_0/2)}{1 + C}\right]} \qquad (6.36)$$

and this holds for all C satisfying the condition

$$C \geq \frac{3\cos^2(\beta_0/2) - 2}{\cos^2(\beta_0/2)} = 3 - 2\sec^2(\beta_0/2) = C_{crit} \quad \text{say.} \qquad (6.37)$$

Thus for integration over x, when $C \leq C_{crit}$ the whole range in x is allowed, but when $C > C_{crit}$ then integrate from $-\beta_0/\sqrt{2}$ to x_- where x_- is given by equation (6.36). By symmetry, this can be doubled to give the contribution from the upper 'branch' of the curve. From Figure 6.5 it can be seen that curve C_3 has $C > C_{crit}$ so the integration over x is only needed from $-\beta_0/\sqrt{2}$ to x_- and from x_+ to $\beta_0/\sqrt{2}$, these two giving identical contributions by symmetry. We now need to find the integral over x and C for the boxed region of Figure 6.5. This will give the probability of one pulse being seen, Pr(1), since the original distribution in θ and ϕ was normalised to give unity after integration

over all θ and ϕ. We now find Pr(1);

$$Pr(1) = \int_{-\beta_0}^{\beta_0}\int_{\beta_0}^{\pi-\beta_0} \sin(x'+y')\sin(y'-x')dydx \qquad (6.38)$$

$$Pr(1) = (\pi/2 - \beta_0)\sin(\beta_0) \qquad (6.39)$$ after the algebra.

Now we can carry out the transformation of variables from x,y

to x,C. We now calculate the Jacobian J which is $\partial C/\partial y$.

From equation (6.9a) we calculate

$$\frac{\partial C}{\partial y} = \frac{\sin(\sqrt{2}y).(\cos(\sqrt{2}x)-\cos(\beta_0))}{\sqrt{2}\,\sin^2((x+y)/\sqrt{2}).\sin^2((y-x)/\sqrt{2})} \qquad (6.40)$$

so from (6.18) and (6.9b) the distribution in C and x will be:

$$F(C,x) = \frac{\sin^3(x'+y')\,\sin^3(y'-x').\sqrt{2}}{|\sin(\sqrt{2}y)(\cos(\sqrt{2}x-\cos(\beta_0))|} \qquad (6.41)$$

and the pulsewidth distribution will be $F^*(C)$ where

$$F^*(C) = 2\int_{-\beta_0/\sqrt{2}}^{0} F(C,x)\,dx \quad \text{when } C < C_{crit} \qquad (6.42)$$

$$\text{and} \quad = 2\int_{-\beta_0/\sqrt{2}}^{x_-} F(C,x)\,dx \quad \text{when } C > C_{crit} \qquad (6.43)$$

where x_- is defined in equation 6.36.

It can be shown that the contours of constant C are in fact conic sections, with eccentricities depending on the 'pulsewidth' C. The only parameter of the resulting pulsewidth distribution is in fact the cone half-angle β_0. For β_0 equal 10^0 we show contours of constant C in Figure 6.5, the distribution of $w = 2\cos^{-1}(C)$ in Figure 6.7 and the observed distribution of pulsewidths in Figure 1.4.

This approach must be adapted to be included in all models where the pulsar geometry changes in time, thus giving a period-dependent beaming factor.

6.7 THE PULSEWIDTH DISTRIBUTION IN THE ALIGNMENT MODEL

6.7.1 Deriving the pulsewidth distribution.

It is of immediate interest to derive the pulsewidth distribution that arises in the alignment model. Clearly one expects a small number of interpulses in the younger objects, and that older pulsars will have larger pulsewidths, providing selection due to luminosity does not render them all invisible to us. The exact details can be derived, using a similar approach to that in Section 6.6, but with the other parameters such as period included also.

For simplicity, we shall assume a steady state here, in that the age of the galaxy shall be assumed to be infinite. This leads to some simplification in the analysis, which is quite involved.

We assume as before that the pulsars are born uniformly in $\sin\theta$ and $\sin\Phi$. The previous source function is again used, but we omit Δ as a variable for clarity, so Δ is regarded as a universal constant. So the entire expression is otherwise as in Section 6.2, namely:

$$C(p,k,\theta,\Phi) = c_0\, K(k)\, \delta(P-Q)\, \sin(\theta)\sin(\Phi)\, H(1-\sin\theta)H(\sin\theta) \qquad (6.44)$$

K(k) is now a ln-normal distribution in k. The analysis starts identically as before: we derive the intrinsic distribution in all quantities to get the equivalent of equation 6.7. For convenience we retain k as a variable in preference to $\dot{P}$. Thus we have:

$$N(P,k,\ \theta,\Phi) = \frac{c_0 P\, \cot(\theta)\, \sin(\Phi)\, K(k,\Delta)H(1-\sin(\theta)H(\theta)}{4\sqrt{(\ 1-\sin^2\theta\ -\lambda^2)}} \qquad (6.45)$$

where $\lambda^2 = (P^2-Q^2)/\tau k$. Now apply the same luminosity law as before, but in the new form of

$$L = \Delta\ P^{\alpha-\beta} k^{2\beta} \sin(\theta)^{2\beta} \qquad (6.46)$$

So the observed distribution in the same quantities is:

$$n_{obs}(P,k,\theta,\Phi) = \frac{c_0 \Delta P^{1+\alpha-\beta} k^{\beta-1} \cot(\theta) \sin(\theta)^{2\beta} \sin(\Phi)\ K(k)}{16\ F_{min}\ \sqrt{(1-\sin^2(\theta)\ -\lambda^2)}} \qquad (6.47)$$

Now transform to the rotated frame as before, Fig.6.5, with new angular variables x and y, related by:

$$\theta = \frac{x + y}{\sqrt{2}} \qquad \Phi = \frac{y - x}{\sqrt{2}} \qquad (6.48)$$

and transform immediately from x,y to x,C in the usual way, where

$$C = \frac{\cos(\beta_0) - \cos(x'+y')\cos(y'-x')}{\sin(x'+y')\sin(y'-x')} \qquad (6.49)$$

adopting the convention of x' representing $x/\sqrt{2}$. The resulting distribution in P,k,x and C is :

$$n_{obs}(P,k,x,C) = \frac{\sqrt{2} c_0 \Delta P^{1+\alpha-\beta} k^{\beta-1} K(k) \cot(+) \sin^3(-) \sin(+)^{2\beta+2}}{16 F_{min} \sin\sqrt{2}y (\cos(\sqrt{2}x) - \cos\beta_0) \sqrt{(1-\sin^2(+)-\lambda^2)}} \qquad (6.50)$$

using the shorthand notation (+) = x'+y' and (-) = y'-x'.

The integral over P will be done first: between the limits of Q (the birth period) and $P_{max} = \sqrt{(Q^2+\tau k \cos^2(x'+y'))}$ (6.51)

This maximum is the the largest period P attainable for a pulsar with given values of k and θ, with θ regarded as a function of x and C. In all these expressions, we consider y' to be the function of x and C given in equation 6.33.

$$\text{Define } J(Q,P_{max}) = \int_Q^{P_{max}} \frac{P^{1+\alpha-\beta}\, dp}{\sqrt{(1-\sin^2(+)-\lambda^2)}} \qquad (6.52)$$

$$= \int_Q^{P_{max}} \frac{P^{1+\alpha-\beta}\ \sqrt{(\tau k)}}{\sqrt{(\tau k \cos^2(+)\ -P^2\ )}} \qquad (6.53)$$

After some algebra this turns out to be:

$$J(Q,P_{max}) = \frac{\sqrt{(\tau k)}[Q^2+\tau k \cos^2(+)]^{\frac{1}{2}+\alpha-\beta}}{2} \{\ 1 - I_x(\ \frac{\alpha-\beta+2}{2}\ ,\ \frac{1}{2})\} \qquad (6.54)$$

where $x = Q^2/(Q^2+\tau k\cos^2(+))$ and $I_x(\ ,)$ an incomplete beta function. Now, since $Q \neq 0$, we can ignore this term, since $I_0 = 0$. Thus we can write : (equation (6.55):

$$n_{obs}(k,x,c) = \frac{c_0\sqrt{2}\Delta k^{\beta-1}K(k)\sin^{2\beta+2}(+)\cot(+)\sin^3(-).(\tau k)^{3/2+\alpha-\beta}\cos^{1+\alpha-\beta}(+)}{16F_{min}\sin(\sqrt{2}y)[\cos(\sqrt{2}x-\cos(\beta_0)].2}$$

Now we can integrate over k analytically. This would not have been possible without making the assumption of $Q \to 0$. Define the factor M as:

$$M = \int_0^\infty k^{\beta-2}\exp-\left[\frac{\ln(k)-\ln(\mu_k)}{\sigma_k}\right]^2 .\frac{k^{3/2+\alpha-\beta}}{\sqrt{(2\pi)}\sigma_k}\,dk \qquad (6.56)$$

introducing explicitly the dependence of the ln-normal distribution in k. By changing variable to $z=\ln(k)$, we can rearrange and after some algebra, it is found that:

$$M = \text{constant}.[\tau\cos^2(+)]^{(1+\alpha-\beta)/2} \int_{-\infty}^{\infty}\exp-\left(\frac{z-\bar{\mu}}{\sigma_k}\right)^2 dz \qquad (6.57)$$

so this can be integrated to give unity, and we are left with:

$$n_{obs}(x,C) = \frac{C_0.\cot(+)\sin^{2\beta+2}(+)\sin^3(-)\cos^{1+\alpha-\beta}(+)}{32F_{min}\sin(\sqrt{2}y)[\cos\sqrt{2}x)-\cos(\beta_0)]} \qquad (6.58)$$

where C_0 is a constant dependent on c_0 (the birthrate) and parameters μ_2, σ_2, α and β and τ. Thus to find $n_{obs}(C)$ we must integrate over x, with limits dependent on C. These limits will be the same as in the non-evolving case of the pulsewidth distribution, but the form of the density above (6.56) is significantly different. If the complete case including time dependence had been tackled, we would find in fact two different forms for this density, in two separate regions of the x,C plane. This leads to a less tractable solution and

obscures the main objective of the exercise. In fact, the calculation of the limits is then where the time dependence arises if the full treatment is attempted. The plot in Figure 6.9 shows the pulsewidth distribution predicted by this model, for the same parameters found in the chi-squared fit in Section 6.3. We can see immediately a long-tail of high-pulsewidth objects, these will be pulsars which are nearly aligned yet still visible. Comparison with the observed histogram in Figure 1.4 shows a number of objects with large pulsewidths, but not the same proportion that is predicted by this version of the alignment model.

6.7.2 Interpulse pulsars in the alignment model.

A quantitative check is to look at the proportion of interpulse pulsars that is predicted, given that there are 9 out of the present population of 500 or so with interpulses [Biggs(1990)]. By developing the above theory to give not the $P,\dot{P}$ distribution but the θ,Φ observed distribution we can calculate the proportion of interpulses expected for the model parameters of the chi-squared fit in Section 6.3. This turns out to be very small for these parameter values: the number of interpulse pulsars from a 500-strong sample is only 2.8×10^{-3}, which means our pulsars are aligning at a rate which makes it unlikely for many interpulses to be observed, or our assumption of random orientations at birth is inaccurate. However, if there is some redundancy in the parameters for the chi-squared fit, then this lack of agreement between model and observations may be less serious than appears at first.

6.8 THE PULSEWIDTH-AGE DISTRIBUTION.

6.8.1 Preamble.

Since the main evidence for the model of Candy and Blair comes from

the distribution of pulsewidth and characteristic age, we now seek to derive this for the alignment model. Then to examine how pulsewidth may be expected to depend on age, we look at the conditional distribution of pulsewidth for fixed age to discern any trends that would support the Candy and Blair hypothesis and to see the role of selection effects in this context.

Formally, the conditional distribution of pulsewidth on age can be written: $$n_{obs}(w|a) = \frac{n_{obs}(w,a)}{n_{obs}(w)} \qquad (6.59)$$

and the conditional expectation of pulsewidth w on age a is :

$$E_{obs}(w|a) = \int w\, n_{obs}(w|a)\, dw \qquad (6.60)$$

where the integral is over all pulsewidths from 0 to 2π. We shall now derive the distribution in characteristic age a and C, where C is the variable cos(w/2) which is more convenient for our purposes.

6.8.2 Derivation of $E_{obs}(C|a)$.

We start with the observed distribution in P, k, θ and ϕ, found in Section 6.4. First we transform from P to variable a, the so-called characteristic age, where a is defined by:

$$a = P^2.k^{-1}.\mathrm{cosec}^2(\theta)/2 \qquad (6.61)$$

So we get the observed distribution in a, k, θ and ϕ:

$$n_{obs}(a,k,\theta,\phi) = \frac{C_0.\ \sin(\theta)^{1+\alpha+\beta}\ \cos(\theta)\ a^{(\alpha-\beta)/2}\ H(\theta_{max}-\theta)}{\sqrt{(\ \cos^2\theta\ -\ 2a\tau^{-1}\sin^2\theta)}} \qquad (6.62)$$

where $\theta_{max} = \tan^{-1}(\tau/2a)$ (6.63)

is the maximum θ consistent with age a, and C_0 is a constant with all the k dependence included, and since it does not affect the end

result, we ignore it from now on. We get from (6.59) and (6.23) that:

$$E_{obs}(\ C(\theta,\phi)|\ a\ ) = \int\int C(\theta,\phi).n_{obs}(\theta,\phi|a)d\phi d\theta \qquad (6.64)$$

now we must consider the ranges of θ and ϕ, consistent with Fig. 6.4. It can be shown, that for $a < a_*$, θ can exceed $\pi/2-\beta_0$, but for

$a > a_*$, θ is in range $0 < \theta < \pi/2-\beta_0$,

where $a_* = \tau \tan^2(\beta_0)/2$ (6.65)

This means physically that older pulsars must have aligned by at least an angle β_0 during their lifetime. So for $a < a_*$, the different restrictions on θ needed in the two regions in Figure 6.4 are needed, but for $a > a_*$, $\theta < \pi/2 - \beta_0$ is considered. Therefore, after the algebra we get:

$$\text{For } a < a_* : E_{obs}(\ C(\theta,\phi)|a) = \int_0^{\pi/2-\beta_0} E_1.d\theta + \int_{\pi/2-\beta_0}^{\theta_*} E_2.d\theta \qquad (6.66)$$

$$\text{For } a > a_* : E_{obs}(\ C(\theta,\phi)|a) = \int_0^{\theta_*} E_1\ .d\theta \qquad (6.67)$$

where $\theta_* = \tan^{-1}(\sqrt{(\tau/2a)}) = \theta_{max}$ from (6.61) and

$$E_1 = \frac{\sin^{1+\alpha+\beta}\theta.\cos\theta.[\ 2\beta_0\cos\beta_0\operatorname{cosec}\theta - 2\sin\beta_0\cos\theta.\cot\theta]}{\sqrt{(\ \cos^2\theta - 2a\tau^{-1}\sin^2\theta)}} \qquad (6.68)$$

$$E_2 = \frac{\sin^{1+\alpha+\beta}.\cos\theta.[\cos\beta_0\operatorname{cosec}\theta.(\pi/2+\beta_0-\theta) - \cot\theta(1-\sin(\theta-\beta_0))]}{\sqrt{(\ \cos^2\theta - 2a\tau^{-1}\sin^2\theta)}} \qquad (6.69)$$

where the distribution has been normalised by dividing by $n_{obs}(a)$. This result is shown in Figure 6.10, for the parameters of the fit to the $P,\dot{P}$ distribution in Section 6.3.

6.8.3 Discussion of the pulsewidth-age result.

It is clear from this result plotted in Figure 6.10 that $C = \cos(w/2)$ falls monotonically as characteristic age rises. This is what we would anticipate in an alignment model, that the pulsewidth would rise for

older pulsars when the cone angle β_0 is constant. This method is the correct way to approach the analysis of the 'full' Candy and Blair model when β_0 is allowed to depend on period. From the form of equations (6.66) and (6.67), we see that α and β will influence the exact form of the conditional dependence of pulsewidth on age, so selection must be included in the Candy and Blair work to make any conclusion reliable.

6.9 OBSERVED DISTRIBUTION OF θ IN ALIGNMENT MODEL.

In the simple non-evolving model, we identified the regions of the θ,ϕ plane that corresponded to pulsars being observed with 0,1 or 2 pulses. This was seen in Sections 6.2 and 6.3. Now these ideas can be extended to the alignment model to give Pr(1), the probability of seeing a pulsar from the observed distribution with a single pulse. The starting point is the observed distribution in P,k,θ and ϕ that was derived above as equation 6.62. We again treat the 'steady-state' case for simplicity. The first step is to integrate out over both P and k, thus getting the observed distribution in θ and ϕ. This can be shown to be:

$$n_{obs}(\theta,\phi) = D.(\sin\theta)^{2\beta}(\cos\theta)^{2+\alpha-\beta}\sin\phi.\ H(\theta+\beta_0-\phi)H(\theta-\beta_0-\phi) \quad (6.70)$$

for constant D. Now we integrate over the region of the rectangle in Fig.6.4, firstly over ϕ. This gives two results, depending on θ.

$$\text{Case 1. } \theta < \pi/2 - \beta_0 : \int_{\theta-\beta_0}^{\theta+\beta_0} \sin(\phi)\, d\phi = 2\sin(\beta_0)\sin(\theta) \quad (6.71)$$

$$\text{Case 2. } \pi/2 - \beta_0 < \theta : \int_{\theta-\beta_0}^{\pi-\beta_0-\theta} \sin(\phi)\, d\phi = 2\cos(\beta_0)\cos(\theta) \quad (6.72)$$

So the observed distribution in θ is :

$$n_{obs}(\theta) = D.2\ \sin(\beta_0).\ \sin^{2\beta}(\theta)\ \cos^{2+\alpha-\beta}(\theta) \quad \text{for Case 1} \qquad (6.73)$$

and $$n_{obs}(\theta) = D.2.\cos(\beta_0).\ \sin^{2\beta-1}(\theta)\ \cos^{4+\alpha-\beta}(\theta) \text{ for Case 2.} \qquad (6.74)$$

For the complete expression of Pr(1) we need to normalise by integrating over θ and ϕ, but over the entire range from 0 to π in each case. This will give a normalisation constant A say, where

$$A = \int_0^{\pi} \int_0^{\pi} n_{obs}(\theta,\phi)\ d\theta\ d\phi = \int_0^{\pi} n_{obs}(\theta)\ d\theta \qquad (6.75)$$

after the ϕ integration is done trivially.

This approach may be used to find the proportion of interpulse pulsars, by integration over the upper triangle (2) in Figure 6.4. This gives the result discussed in Section 6.8.

6.10 DISCUSSION AND CONCLUSIONS

In this Chapter we have developed an alignment model which has been found to be compatible with the distribution of observed pulsars on the $P,\dot{P}$ plane, thus making it a rival to field decay as an explanation of pulsar evolution. In the course of this analysis, we have used the geometrical visualisation of Proszynski(1979), but extended this useful viewpoint to incorporate the pulsewidth data , by showing how to properly derive the distribution of pulsewidths both in the static (i.e. non-evolving) case and for the alignment model. This can thus be extended to any model of pulsar evolution. The importance of this is firstly, it is totally exact, and therefore improves on the approximate method of Candy and Blair(1983),(1986) and Henry and Paik(1969), and secondly provides a possible diagnostic tool for distinguishing between models. The pulsewidth distributions predicted

for field decay and alignment models are totally different, as we have seen, although their predicted $P,\dot{P}$ densities are to some extent indistinguishable. This method also allows the incorporation of further 'detail' , for example in the variation of cone angle β_0 with period, or allowing a distribution of cone angle. The final advantage of this work is it is the correct way to approach the question arising from the Candy and Blair work, 'is there a genuine minimum in the pulsewidth-age diagram', which we believe was not tackled correctly in the original papers. [See Chapter 2].

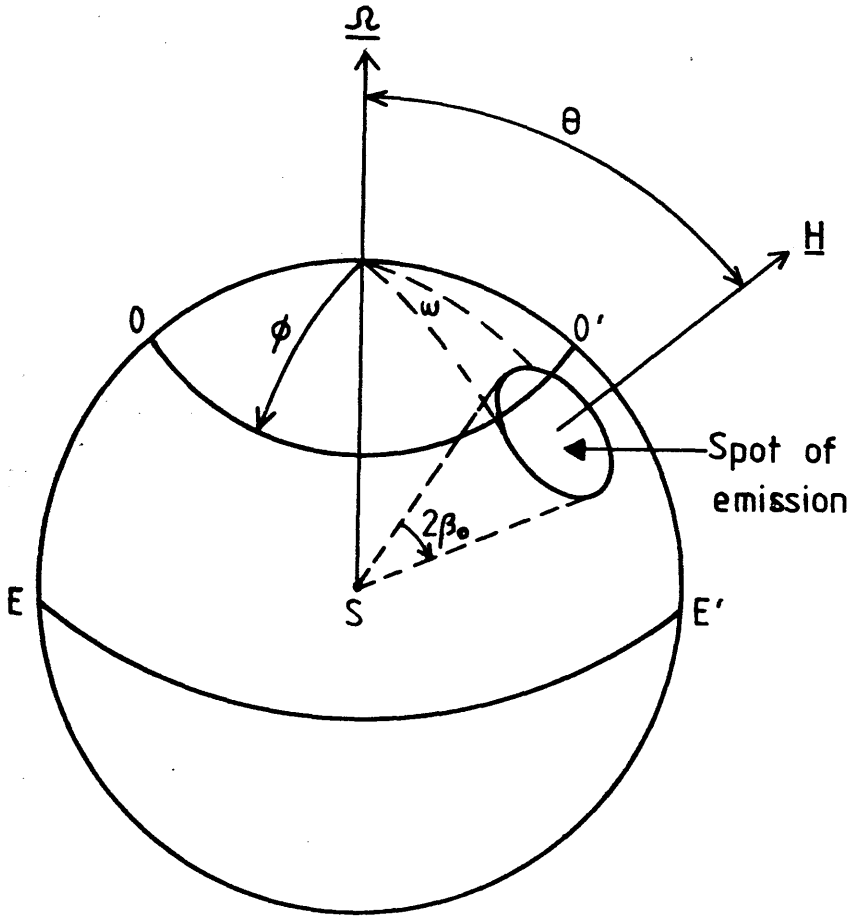

FIGURE 6.1a

The idealised geometry of pulsar emission, taken from Proszynski(1979). In our notation $2\beta_0$ is the cone angle, θ the alignment angle and Φ the angle between the rotation axes and the observer's line of sight. This gives a pulsewidth ω if the circular beam is emitting over its full extent. In our work, the angle Φ is independent of all other parameters, and does not change with time. Here Ω is the spin axis, H the magnetic dipole axis direction and OO' the path traced out by a moving observer, assuming the neutron star to be stationary.

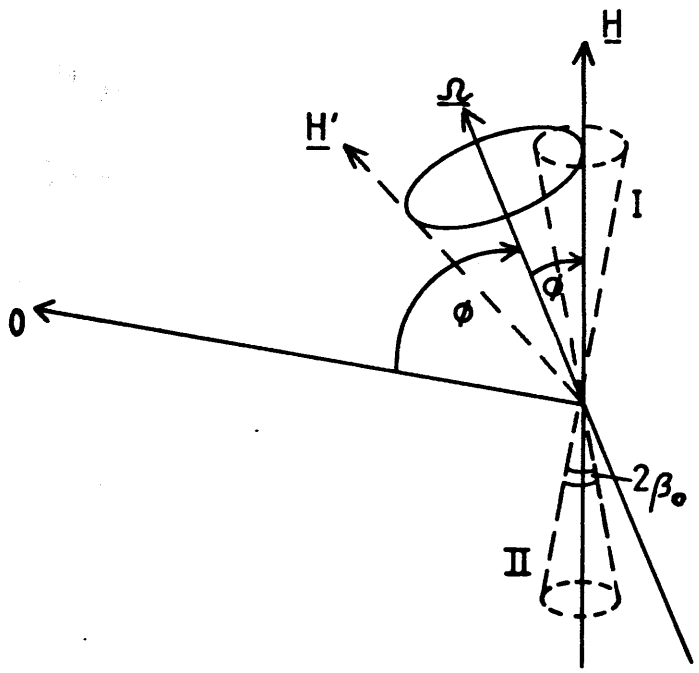

FIGURE 6.1b

The same geometry shown in Figure 6.1 (a), but showing the second identical cone of radiation from the opposite magnetic pole. The beam will sweep round the path marked HH' and not all observers O will see the pulsar.

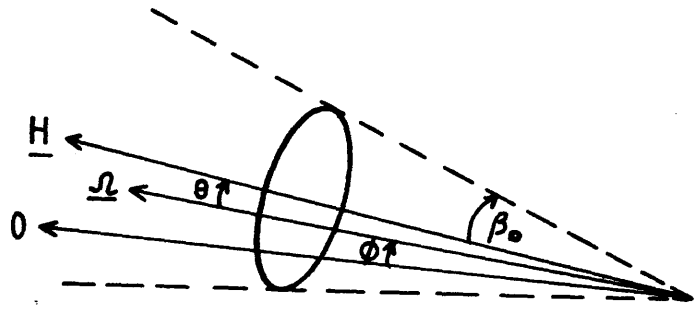

FIGURE 6.2

The required geometry for the observer always to be in the beam of the pulsar ('modulation' M in Figure 6.4). Here we can see that Φ must lie within a small angular distance of the rotation axes. See Section 6.2 for the algebraic requirements. We assume that such a pulsar will not be seen. The pulsewidth cannot be defined here.

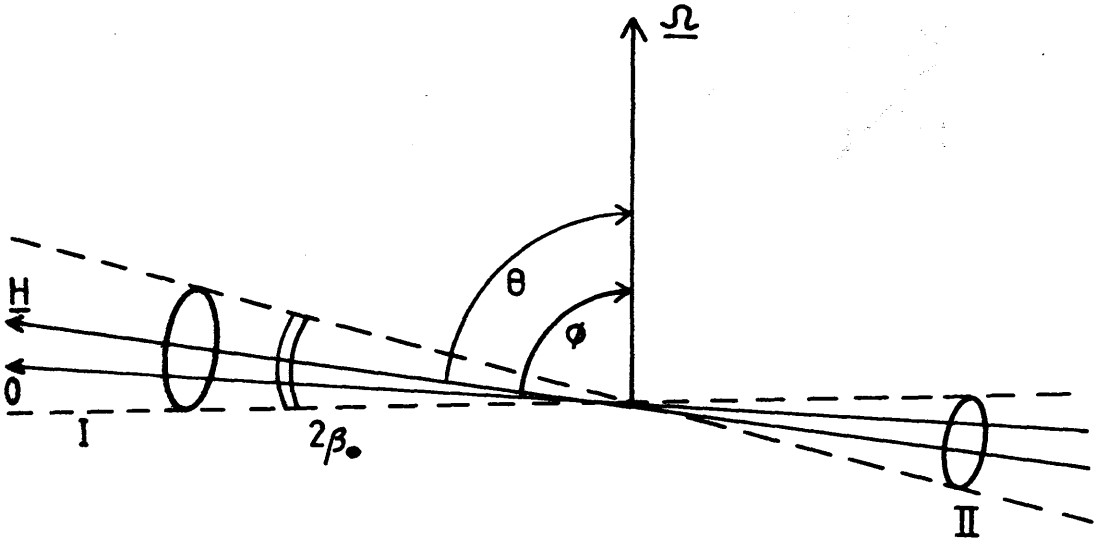

FIGURE 6.3

The required geometry for interpulses to be seen. The two beams I and II must both cross the observer's line of sight. This forces the alignment angle θ to be close to 90^0 when β_0 is small. The two pulses in this idealised case will be of identical shape and width, and in theory should be 180^o apart. Again Ω and H indicate the rotation and magnetic axes directions respectively.

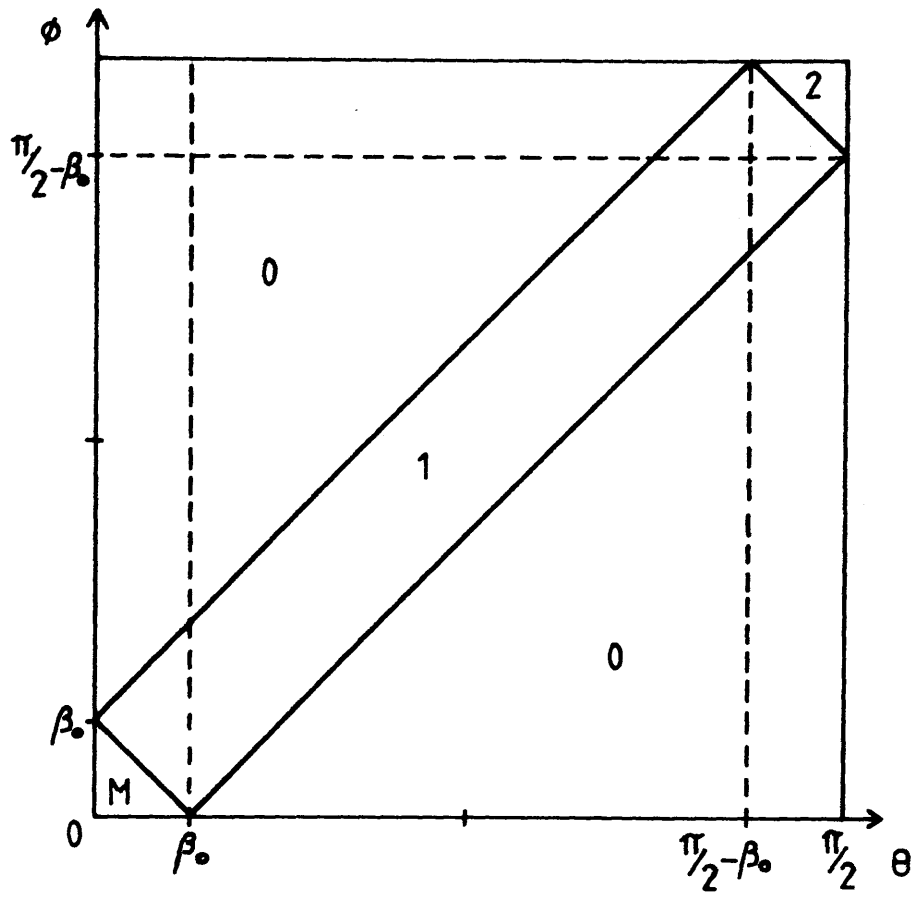

FIGURE 6.4

The 'Proszynski' diagram, adapted from Proszynski(1979). This gives the regions of the θ,ϕ plane where 0,1, or 2 pulses are seen, or where modulation (M) occurs. The diagram is symmetric in the lines $\theta = \pi/2$, $\phi = \pi/2$ and $\theta = \phi$, such that the other 'quadrants' of the θ,ϕ plane are equivalent to this, so we restrict attention to this region. The cone angle is $2\beta_0$, as usual.

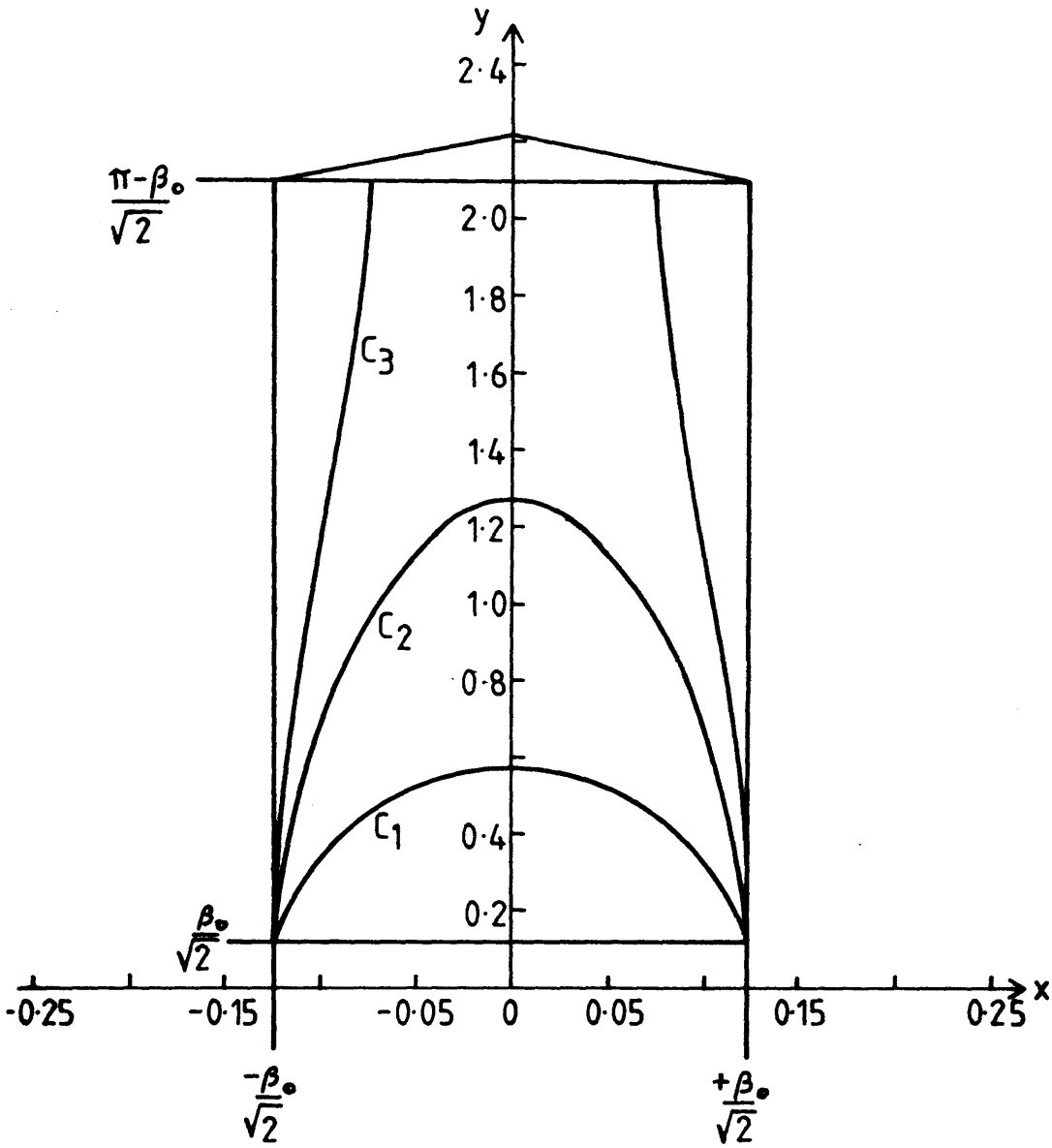

FIGURE 6.5

The rotated version of Figure 6.4, in the x,y plane, as defined by equations 6. . Three contours of constant pulsewidth are shown by the curves C_1, C_2 and C_3. The diagram is symmetrical in the y-axis.

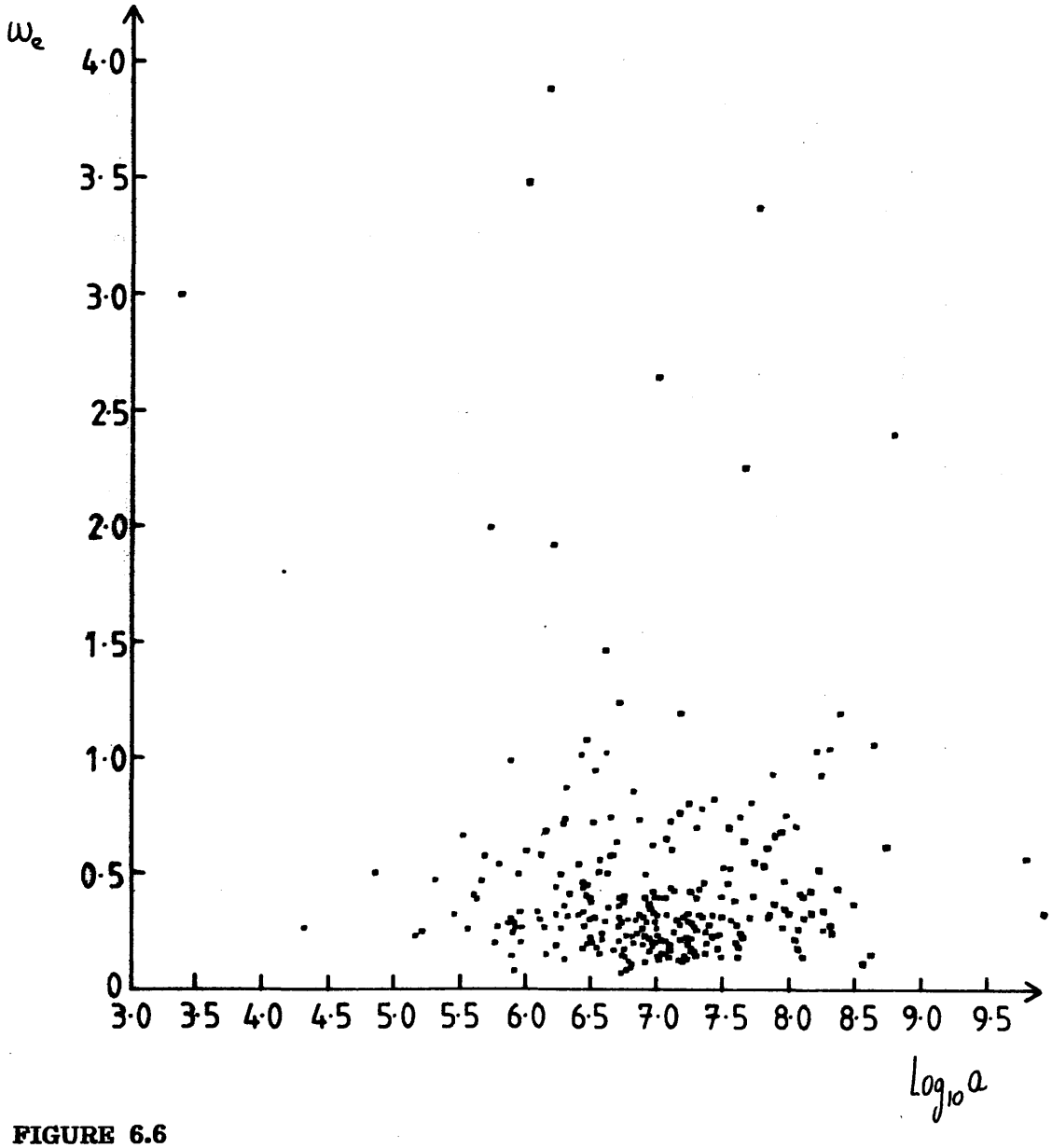

FIGURE 6.6

The scatter plot of pulsewidths against characteristic age for observed pulsars. The equivalent widths are used and characteristic age is defined as $P/2\dot{P}$, and a base-10 logarithmic scale is used, so that the range 10^3 to 10^9 years is spanned.

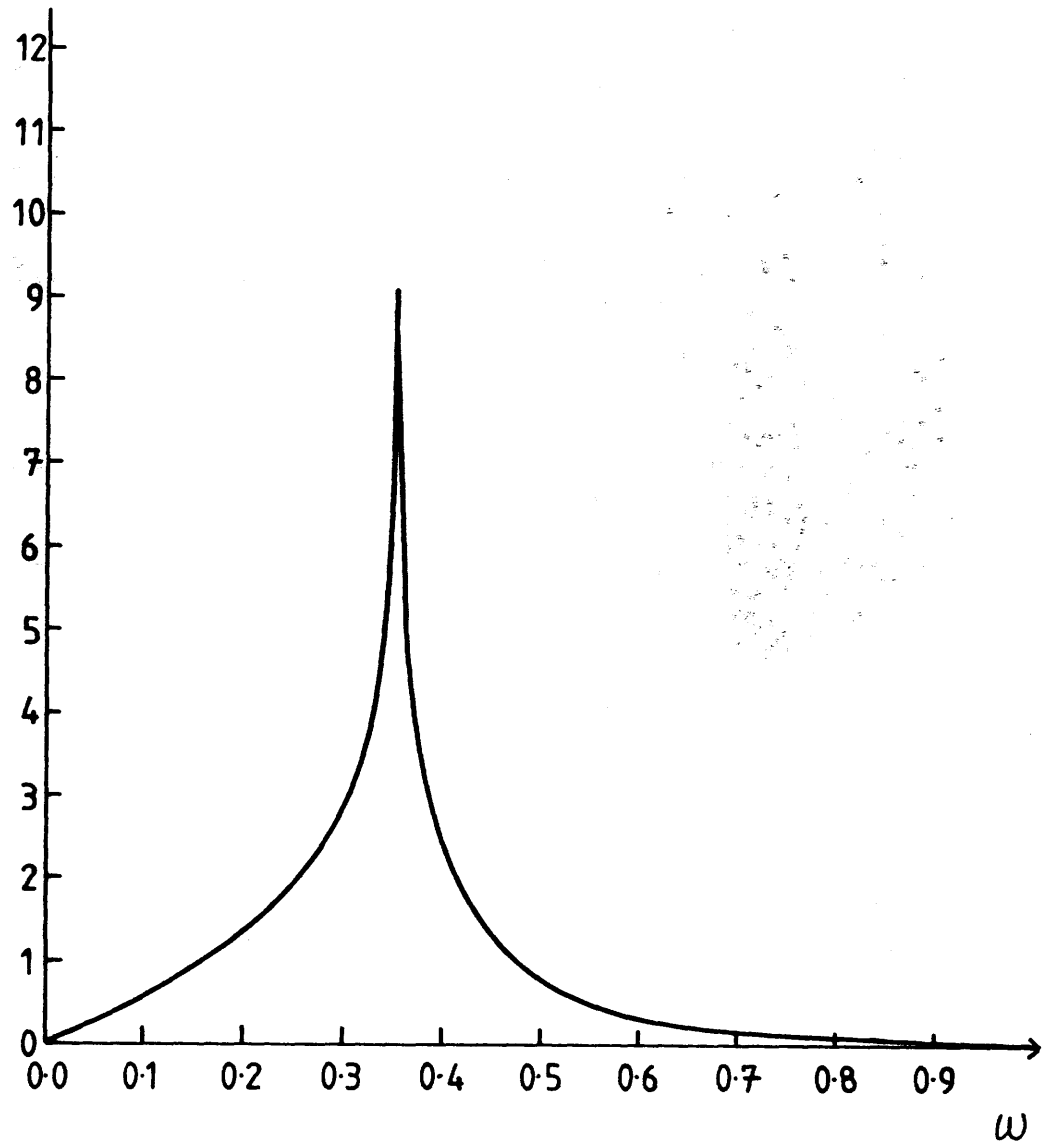

FIGURE 6.7

Distribution of pulsewidths in the non-evolving model. This is the prediction of equations 6.20 and 6.21 with parameter $\beta_0 = 0.17 \bullet 10^0$.

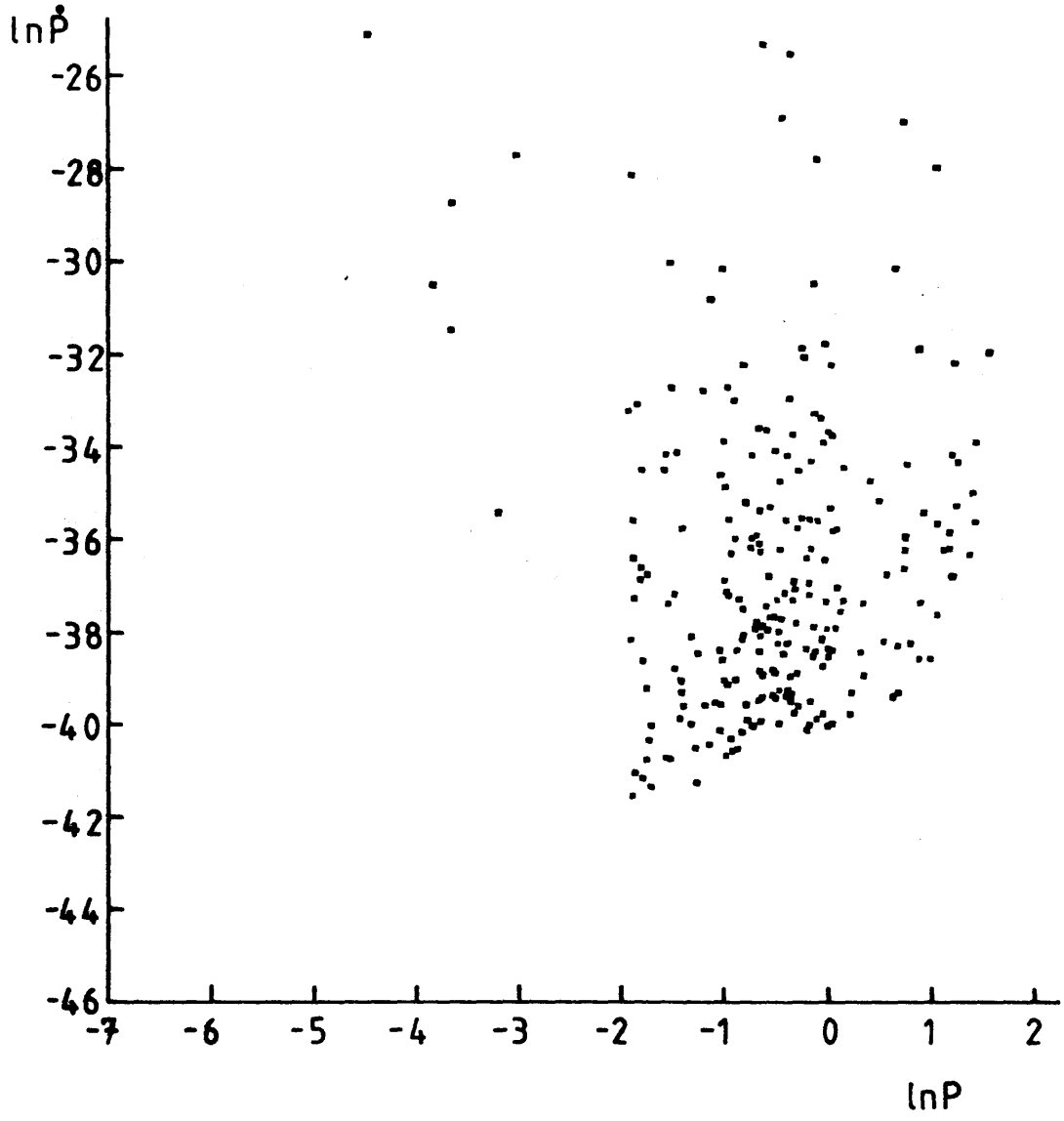

FIGURE 6.8

A simulation of the P,$\dot{P}$ diagram for the alignment model, using the parameters found from the X^2 fitting, which are given in Section 6.5.3

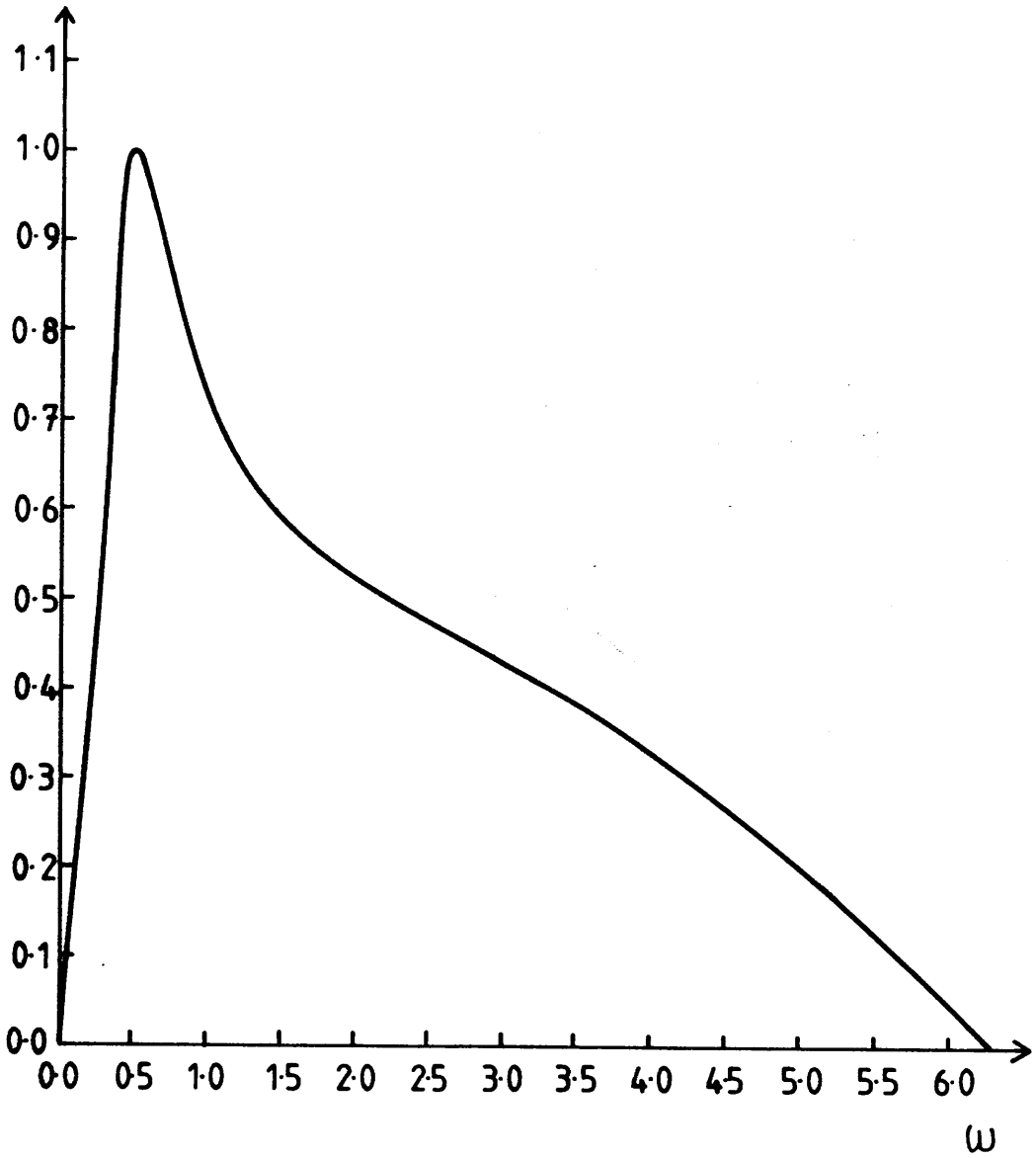

FIGURE 6.9

The distribution of pulsewidths predicted by the alignment model, using the parameters given for the optimised chi-squared fit to the $P,\dot{P}$ diagram, given in Section 6.3.1

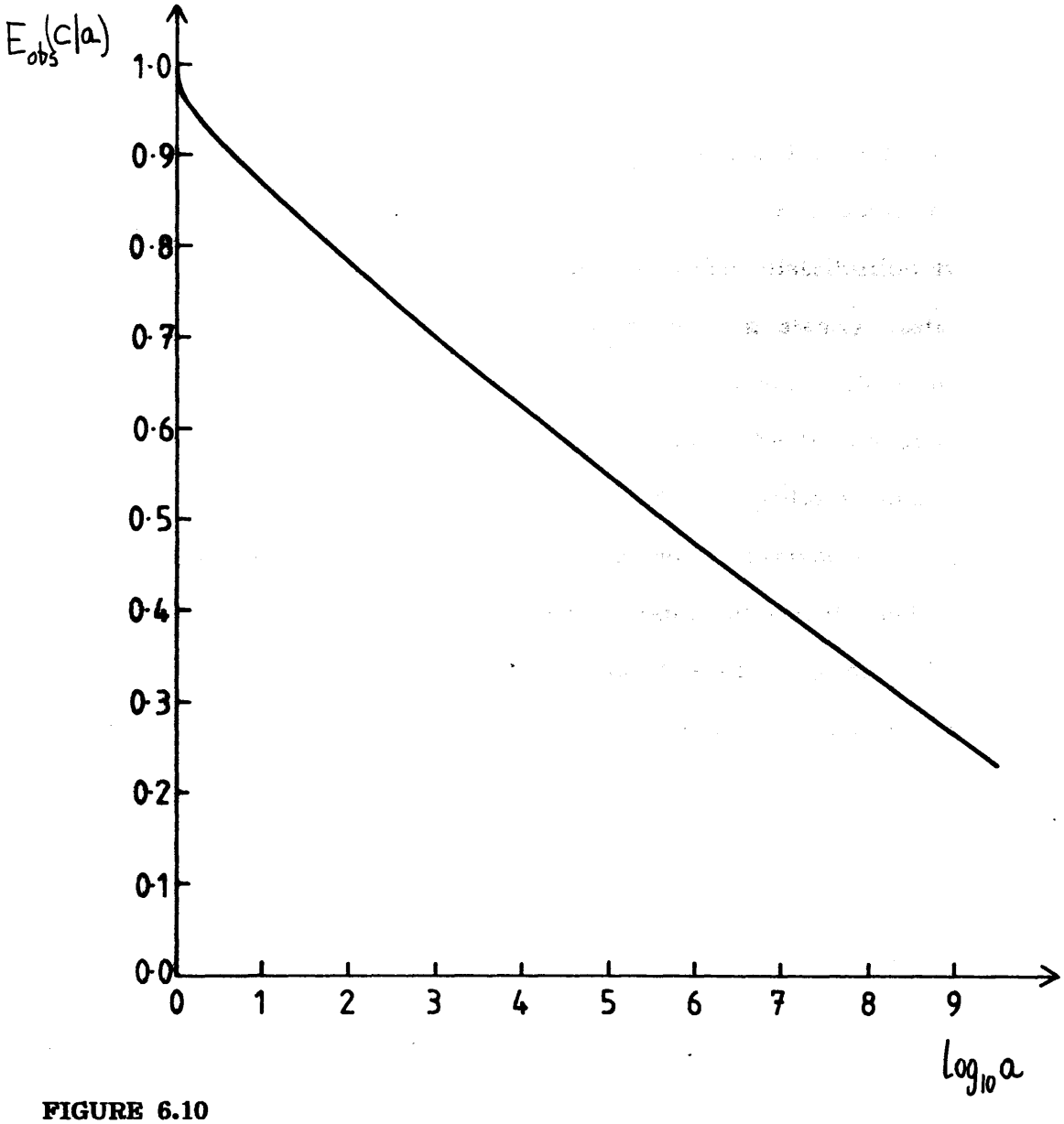

FIGURE 6.10

The expectation value of C= cos(ω/2) conditional on characteristic age a, for the alignment model. Here ω is the pulsewidth as defined in Figure 6.1a and the relation is given in equations 6.64 - 6.67.

CHAPTER 7

CONCLUSIONS AND FUTURE WORK

7.1 CONCLUSIONS

In this thesis we have presented a new method for addressing the problems of pulsar evolution. This is based on the solution of the time-dependent continuity equation in the pulsar distribution function, and does not assume a priori the existence of a steady state in the observed pulsar population. It allows the inclusion of selection effects in a logical and consistent way, allows models to be tested against the observations, and can be developed to include positional and velocity variables as well as those of periods and period derivatives.

We showed in Chapter 2 that existing 'standard' models had, in many papers, been inadequately tested against the observational data, and in some cases incorrectly dealt with the effects of selection. The most common explanation in the literature of pulsar evolution was that with magnetic field decay in the neutron star.

Thus in Chapter 3 our new method is introduced, and demonstrated on four simplistic models to show the method of solution and the consequences of abandoning the notion of stationarity, where pulsar birth and deathrates combine to keep the observed population at a constant strength. This also shows the role of selection effects, the difficulty of determining the pulsar birthrate in an unbiased way, and the importance of including a distribution in magnetic field to explain the scatter in the data.

Chapter 4 presents the first detailed model of pulsar evolution, the 'simple' model, where no field decay occurs and no alignment takes place. The time-dependent continuity equation method is used to derive the predicted observed distribution in period and period

derivative, which is then tested for goodness-of-fit against the observed data. This fit, assessed using the chi-squared statistic, is mimimised with respect to the model parameters. A level of significance is chosen at 5%, which determines the required value of χ^2 for the fit to be acceptable. The simple model fails to meet this target and is rejected as incompatible with the observed distribution of periods and period derivatives. However, it can be shown that if attention is restricted to the marginal distribution of period alone, an analogous operation produces a chi-squared fit that is well within the bounds of acceptance, showing categorically that anomalous conclusions can be drawn from analyses based primarily on the marginal of P or $\dot{P}$, and not the joint distribution of P and $\dot{P}$.

A further feature which arises in this testing procedure is the interdependence of the model parameters, such that the effective variables in the minimisation are combinations of these model parameters. This means that a 'degeneracy' exists, so that different regions of parameter space will produce identically good fits and it is not necessarily possible to identify a unique best-fit solution unless other information is used to estimate some of the values of the set of parameters. A consequence of this is that our model birthrate estimation can be uncertain since only a combination including the birthrate parameter can be determined, and so the true creation rate may remain unknown.

Chapter 5 continues with the development of the field decay model, which features an exponential decline in the magnetic field strength on timescale τ. The predicted $P,\dot{P}$ distribution is again tested in the same fashion, this time producing an acceptable fit to the data. The slightly less detailed model of Gunn and Ostriker(1970) and Lyne et al(1985)

fails to meet the required level of significance and is rejected, but it is noted that the effect of the chosen bin scheme is not immediately easy to assess, and other authors have claimed success for identical models. It is also pointed out the crucial role played by the parameter τ, which acts to enforce a steady state provided the galactic age is greater than a few decay timescales.

Thus field decay provides a possible explanation for pulsar evolution, but both of the normally discussed [Proszynski and Przybcien(1984) and Lyne et al(1985)] luminosity laws are found here to be incompatible with the fits to the $P,\dot{P}$ distribution. Identification of the compatible range of luminosity law parameters α and β is complicated by the 'degeneracy' problem already encountered in Chapter 4.

An alignment model is introduced in Chater 6. Here the magnetic axis of the pulsar tends to align with the rotation axes as the pulsar ages. This limits the ability of older pulsars to spindown beyond a 'terminal' period, similar to the field decay case. There is now the additional complication that the beaming fraction, which gives the proportion of pulsars visible through their relative orientations, now becomes dependent on period for the first time. This gives a more complicated analysis since the geometrical variables must be included. The alignment model also produces an acceptable chi-squared fit. This shows that to distinguish between field decay and alignment, further work must be carried out. The pulsewidth data offers one such possibility. The use of the pulsewidth data is explored here, and a non-evolutionary pulsewidth distribution derived to demonstrate the geometry inherent to the beam model for pulsar emission, following the work of Proszynski(1979).

The pulsewidth distribution associated with the alignment model can

be derived using the time-dependent method, and for the parameters of the best fit model, this is found, but it does not give a very close match to the observed pulsewidth distribution.

Also derived is the distribution of pulsewidth conditional on age, to show the correct approach needed for the analysis of the claim made by Candy and Blair(1983),(1986), that a distinct minimum exists in the pulsewidth-age diagram. This shows, that for the alignment model discussed, no minimum exists. Our model is not strictly compatible with the Candy and Blair model, since we deal with a cone angle that is constant, whereas Candy and Blair allow the beam to diminish in extent as the pulsar ages. However the work can be easily extended to include a distribution of cone angles, or closing of the cone angle as the pulsar evolves.

Thus the alignment model gives a second possible explanation of pulsar evolution, and to further discriminate between field decay and alignment, more analysis is necessary, with the pulsewidth data taking on a greater importance.

We have explicitly included time dependence in our method for the study of pulsar evolution. This was justified on the grounds that pulsar lifetimes were not known independent of a model, so could not be assumed short enough to ensure the observed pulsar population remained stationary. However, both the field decay and alignment models in the forms developed in this thesis give rise to fits to the $P,\dot{P}$ diagram with typical pulsar lifetimes of, say, 10^7 years which is less than the age of the galaxy and the duration of the epoch of pulsar formation, by assumption. Thus a true steady-state does arise in these cases, so the time-dependent method is not strictly necessary. We contend that the time-dependent continuity equation method is a

more direct, logical and easy-to-follow than other treatments in the literature. The stationary case of any model is retrieved by letting the age of the galaxy (parameter t_0 in earlier Chapters) tend to infinity.

It must be reiterated that not all conceivable models will necessarily give rise to a steady observed population, and the existence of a steady state can depend on the form of the luminosity law, which is an unknown, and the assumption of a uniform pulsar creation rate, which precludes the possibility of 'bursts' of formation.

7.2 FUTURE WORK- FURTHER TESTING OF MODELS

We have looked in detail at three models, in Chapters 4,5 and 6. Of interest would be other tests, of the same nature, of other models of pulsar evolution and variations on these main models. Particular cases would be a counter-alignment model, where the magnetic and rotation axes tend to become perpendicular as the pulsar spins down, and the model of Beskin(1984), which also involves counter-alignment. We show the initial stages of the development of a counter-alignment model in Section 7.8.

The Beskin model is less easy to summarise than the above models since it uses different approximations in different regimes, which are distinguished by a parameter dependent on both period and period derivative. This will give a considerably more complicated model than we have so far encountered.

Other variations would be to look at different decay laws for magnetic field, as tried by Narayan and Ostriker(1990), or different alignment laws. Observational evidence suggests that there is a dependence of beam size and possibly elongation as well, on pulsar period, such that younger objects have wider beams, thus the beaming fraction varies over period quite apart from orientational changes due

to alignment or counter-alignment [Lyne and Manchester(1988), Narayan(1987)]. It is also hoped to repeat the Candy and Blair(1983) model analysis by including a power-law cone angle dependence on period.

There is considerable scope for use of our method to test and compare competing models.

The question of parameter bounds for acceptable fits is one which has not so far been tackled. Clearly it is of importance to assess within which ranges of the model parameters acceptable fits are still obtained. This is made more difficult by the 'degeneracy' problem encountered in Chapters 4-6, since the effective parameters of a model are not physically interpretable, and involve combinations of the input parameters. However, it ought to be possible to assign bounds to e.g. mean field strength for a given luminosity law such that a particular model fits at the prescribed level of significance, and this task is one which should be tackled as future research.

7.3 FUTURE WORK- INCLUDING POSITIONAL COORDINATES

A more complete analysis would involve the inclusion of the pulsar positions and velocities, of which the former are known from observation for all pulsars, and the latter for a small sample only, as discussed in Chapter 1. The distribution of pulsar positions in the galaxy will not be that of a uniform planar density, as assumed for the models we have discussed. Including the position and velocity data would allow the migration of pulsars from the galactic plane to be modelled, which will give new selection effects to be treated, since only large proper motions can be detected.

A repeat of Hanson's (1979a and 1979b) work on proper motion distributions using the larger data sample of Cordes(1987) would be of

great interest, especially to establish if this sample is biased significantly in the same way that the proper motion data analysed by Hanson in these papers was, by the domination of the fastest transverse velocity pulsars. It is also relevant to the question raised by Stollmann and Van den Heuvel(1986) of whether the correlation between transverse velocity and inferred magnetic field that is present in the observed sample is real or induced by selection effects.

7.4 INVERSE PROBLEMS

It was shown in Chapter 3 and Appendix A7 how the time-dependent continuity equation method for pulsar evolution gives rise to inverse problems which can be in principle be solved for unknown source distributions. Some of the simplest cases are treated in Appendix A7. More realistic problems which are based on the same methods would be of interest for future research, especially when the observed pulsar sample has increasd to the extent indicated in Section 7.7.

7.5 FUTURE WORK- WHITE DWARF COOLING

The time-dependent continuity equation can be applied in other fields. The problem of white dwarf star cooling is one area which would be suited to such an approach. The observed data for white dwarf luminosities and ages give the temperature and cooling rates, and expected overall cooling times are $\triangleq 10^9$ years, approaching the galactic age, so a time-dependent method is expected to be needed. Although the sample size is small for the purposes of model-testing, the situation may improve in the future. See Shapiro and Teukolsky(1986).

7.6 FUTURE WORK- STARBURSTS

The assumption of steady creation is virtually universal in the pulsar literature. This is also the easiest scenario to work with. If we decide

to investigate the consequences of a creation rate that is time-dependent, then the continuity equation method is easily used, and indeed is the only appropriate method in this case. Of particular interest is the concept of 'bursts' of formation, concentrated period of pulsar formation which are short compared to the lifetimes of the pulsars thus created, or the interval between bursts. Such ideas are triggered by the work of Richter and Rosa(1988) who examine supernova data and conclude that in certain galaxies supernovae are more frequent than in others, and suggest this is due to bursts of star formation/supernovae in particular galaxy types.

If all pulsars are created at a single period and at a single instant, then the resulting $P,\dot{P}$ distribution will simply consist of pulsars spread along the 'deathline' from the models in Chapters 4-6. A spread in initial period will yield a different picture, creating a narrow wedge in the $P,\dot{P}$ plane where pulsars can be. A series of regular 'bursts' of formation also will give greater coverage of the $P,\dot{P}$ plane.

Of more relevance might be a 'decaying' burst, where the birthrate falls off (possibly exponentially) after turning on instantaneously. It will be clear that for a single burst it is difficult to obtain qualitatively the observed large scatter in the $P,\dot{P}$ plane, unless pulsars are created at virtually all periods, which seems unlikely. A further inversion problem could be solved in this instance, for an unknown birthrate as a function of time.

The importance of the time-dependent continuity equation approach is that it has the capability to deal with this case as well as handling steady creation, under the same formalism, a considerable improvement on existing methods.

7.7 FUTURE WORK- INCLUSION OF LUMINOSITY DATA

It was pointed out in Chapter 4 that the inclusion of the luminosity data would be desirable in the chi-squared test, but the sparseness of the data rendered this impossible at present. Once sufficient data is available, this becomes an option. For a reasonably fine grid in P, $\dot{P}$ and L, say of 26 x 5 bins = 130 bins (26 bins in the P,$\dot{P}$ plane x 5 in luminosity) we would require of the order of at least 1000 pulsars, preferably twice as many. This gives a minimum requirement of a doubling of the existing sample, which will take a major observational effort.

7.8 COUNTERALIGNMENT MODEL FOR PULSAR EVOLUTION

7.8.1 Introduction to counter-alignment.

One of the first papers to talk about pulsar counter-alignment was that of Flowers and Ruderman(1977), who argued from theoretical considerations that magnetic fields ought to decay and simultaneously the dipole moment would evolve to make a large angle with the rotation axis. We define counter-alignment to have occurred when the alignment angle between these two axes reaches 90°. The major analysis of Beskin et al(1984) also predicted counter-alignment, but as yet the consequences of this have not been fully explored. Beskin et al(1984)'s work is incomplete in that they neglect selection effects due to luminosity, and the full geometry that was introduced in Chapter 6 is also omitted. The law used by Beskin et al(1984) was, where θ is the alignment angle,

$$\sin(\theta) = \sin(\theta_0)P.P_0^{-1} \qquad (7.15)$$

such that θ rises as P increases. It is clear that now either the pulsar lifetime must be very short, or pulsars must be born with $\theta \triangleq 0^{\circ}$ to prevent $\sin(\theta)$ exceeding unity, which is non-physical. Beskin does not

apparently address this since the counter-alignment is really only a minor consequence from this paper, but there clearly will be a problem preventing this happening, which is a defect in the model. If one adopts conventional spin-down, then a typical pulsar born at P_0 = 10 msec and θ = 10° say will have a lifetime of only 10^{4-5} years before full counter-alignment takes place, and this becomes more acute for pulsars born with large values of alignment angle θ, or smaller periods. Although Beskin et al use a spindown mechanism that is significantly different in nature from the magnetic dipole radiation, we still expect it to produce similar spindown rates, (to be compatible with the $P,\dot{P}$ diagram), thus a definite problem exists.

A second problem is the predicted preponderance of interpulse pulsars which we expect in the case where alignment angles tend to 90°. Nearly all pulsars with $\theta \triangleq 90^{\circ}$ would be expected to show evidence of a second beam from the opposite pole, whereas observations suggest [e.g. Biggs(1990)] that it is primarily younger objects (such as the Crab pulsar) that seem to possess interpulses. Beskin et al(1984) claims that their analysis predicts the correct number of interpulse pulsars but we must reiterate that this work does not properly include the selection effects present e.g. in Chapter 6 above. We have started a preliminary analysis of a simple counter-alignment model, designed to be 'analogous' to the alignment model of Chapter 6 as far as possible.

7.8.2 A basic counter-alignment model.

We adopt the same spin-down law as usual:

$$\dot{P} = k.\ \sin^2(\theta)/P \qquad (7.16)$$

and the counter-alignment law:

$$\cos(\theta) = \cos(\theta_0).\exp\{\ -(t-t_0)/\tau\ \} \qquad (7.17)$$

The solution of (7.16) gives the trajectory equation, which is:

$$P^2 = P_0^2 + 2k(t-t_0) - \tau k\cos^2(\theta_0).[1-\exp[-2(t-t_0)/\tau]] \qquad (7.18)$$

The basic consequence of counter-alignment will be that no terminal period exists: the pulsar is free to spindown indefinitely as it ages, but the law (7.17) prevents θ from exceeding 90°. We adopt the same source function as in Chapter 6 for alignment, namely:

$$C(P,\theta,\phi;t) = c_0\Delta(P-Q).H(t).\sin(\theta)\sin(\phi)H(\sin\theta)H(1-\sin\theta)/4 \qquad (7.19)$$

to give random orientations of pulsars in the geometrical coordinates θ and ϕ, the alignment and observer's direction angles respectively. [See Figures 6.1,6.2 and 6.3]. We allow all pulsars to have the same magnetic torque at first, for simplicity. From (7.18) we get the Jacobian

$$J = \frac{\partial(P_0,\theta_0)}{\partial(P,\theta)} = \frac{P_0\tan(\theta_0)}{P\tan(\theta)} \qquad (7.20)$$

thus the solution to the continuity equation will be: (7.21)

$$n(P_0,\theta_0,\phi_0;t_0) = \frac{c_0P_0\tan(\theta_0)\sin(\phi_0)}{4k}\left[\frac{\cos\theta.H(t)H(\sin\theta)H(1-\sin\theta)}{\sin^2(\theta)}\right]_{P=Q}$$

Now the bracketed term is crucial. We can see from (7.18) that we are unable to solve explicitly for $t = 0$ at $P = Q$, therefore a problem exists in establishing the constraints on our distribution which are of great importance. In fact the value of the bracketed term must be found by a numerical solution, a great hindrance when compared to the analytic neatness of the previous models. This difficulty is due to the fact that our spindown law depends on $\sin(\theta)$ and the counter-alignment law on $\cos(\theta)$. Therefore a numerical solution is obligatory in this case, even for the limits of the integrals. If a

satisfactory law could be found that surmounted the problem, then this would be much easier to solve.

7.8.3 Attempts to solve the counter-alignment problem.

The first step is to be able to solve the equation (7.18) when P=Q, to give the first condition of constraint, and which enables the term in square brackets to be evaluated at t_*, say, the solution of:

$$h(t) = P_0^2 - Q^2 + 2k(t-t_0) - \tau k\cos^2(\theta_0)(1-\exp-2(t-t_0)/\tau) \quad (7.22)$$

where $h(t_*) = 0$. This can be done by a Newton-Raphson root-finding method, and thus the bracket term in (7.21) can be found, using (7.17). However, to use this information in the condition $t_* \geqslant 0$ to give an analytic constraint on P or θ is not possible. Thus we are hindered at the outset by this feature of this particular aproach to counter-alignment.

It is certainly possible to develop a pulsar evolution model with counter-alignment but unless some form can be found for the law which governs the behaviour of θ which allows the solution of (7.16) to be expressed analytically when the condition $t \geqslant 0$ is applied, then a restricted numerical solution is all that can be attempted. This is worthwhile, however, and a definite future aim is to complete this model and find the $P,\dot{P}$ distribution that it predicts, and proceed to test it against the observations.

7.9 THE BEAMING FRACTION IN THE SIMPLE MODEL

It was stressed earlier in Chapters 1 and 6 that the beaming fraction would be independent of period unless the alignment angle evolved as the pulsar spins down. This was correct for the particular application that was chosen in Chapters 4 and 5 where we treated k as a variable which effectively contained all the details from equation (2.1), the magnetic dipole spin-down law. One of these details was the $\sin^2(\theta)$

factor which resurfaced in the alignment model of Chapter 6. If we separate this from the start we get the same spindown law, but in a new guise as:

$$\dot{P} = k \sin^2(\theta)/p \qquad (7.23)$$

where now we treat k and θ as independent variables. Now however when the analysis is repeated, the beaming fraction becomes period-dependent, since θ does govern how efficiently a pulsar of given k can spin down. This is shown as follows:

We repeat the analysis of Chapter3, model 1b, with a source term:

$$C(P,k,\theta,\phi;t) = c_0.K(k).\sin(\theta)\sin(\phi)\Delta(P-Q)H(t) \qquad (7.24)$$

which gives the solution to the observed distribution of P, $\dot{P}$, θ and ϕ to be:

$$n_{obs}(P,\dot{P},\theta,\phi;t) = \frac{c_0 S P^{1+\alpha}\, \dot{P}^{\beta-1} K(P\dot{P}\mathrm{cosec}^2(\theta)\sin(\phi)H(t)}{16F_{min}\sin(\theta)}\Bigg|_{P=Q} \qquad (7.25)$$

where we choose K(k) to be the same distribution that appeaed in Chapter 3, i.e.

$$K(k) = ka^{-2}\exp(-k/a) \qquad (7.26)$$

Now we recall the Proszynski diagram (Figure 6.4) which gives the regions of the θ,ϕ plane that are consistent with a pulse being observed. To define the beaming fraction, we consider the equivalent model without any geometrical variables included, and thus :

$$\Gamma(P,\dot{P}) = \frac{n_{obs}(P,\dot{P};t)\ [\text{geometry}]}{n_{obs}(P,\dot{P};t)\ [\text{no geometry}]} \qquad (7.27)$$

where the numerator of (7.27) is the expression obtained when no consideration is made of θ and ϕ, and the denominator is from (7.25).

So, using (7.26), (7.25) and the expression from Chapter 3, (3.21)

we get

$$\Gamma(P,\dot{P}) = \frac{G(\ 1/2,\ P\dot{P}a^{-1}\tan^2(\beta_0)\ ).2\sin(\beta_0)}{2\sqrt{(P\dot{P}a^{-1})}} \qquad (7.28)$$

where G(,) is an incomplete gamma function and β_0 is the cone half-angle for the circular radiation beam, as used in Chapter 6.

By the definition of the error function erfc(x), [erfc(0) = 1], erfc(x) = G(1/2,x) so the final expression is:

$$\Gamma(P,\dot{P}) = \frac{\sin(\beta_0).\mathrm{erfc}[\tan(\beta_0).\sqrt{(\dot{P}P/a)}]}{\sqrt{(\dot{P}P/a)}} \qquad (7.29)$$

even although there is no alignment or counter-alignment, there is a beaming fraction which varies over the $P,\dot{P}$ plane. Noting the form of (7.29) we can see that along a line of constant $P\dot{P}$, which will be a straight line with slope -1 on the log-log plot in Figure 1.1, the beaming fraction as defined here will be constant. For lines 'higher up' the plane, this quantity will fall, from the form of (7.29). So in this case, it is pulsars with larger k which will be selected against. This is a small effect, but for different parameters there could be a significant biasing against faster pulsars. On this section we have omitted the contribution from the interpulse region of the Proszynski diagram, Figure 6.4, dealing only with single-pulse objects.

APPENDICES

APPENDIX A1. THE KOLMOGOROV-SMIRNOV TEST

This is a non-parametric statistical test of goodness-of-fit between the cumulative distribution functions of theory and the data sample. The standard practice in these situations is to test the null hypothesis, in this case that 'the two distributions are identical'. An unsatisfactory fit will then lead to a rejection of the null hypothesis at a particular level of significance. For a data sample of size N, say $\{x_1,x_2,...x_N\}$ then the cumulative distribution function can be constructed to be $S_N(x)$ where $S_N(x)$ is the proportion of sample values which do not exceed the value x. Thus $S_N(x)$ is a step function which increases by 1/N at each 'jump point' (i.e. the values $x_1,x_2,...$ above) over the range of the data sample. If theory provides a cumulative distribution function F(x) over the same range then the quantity D_N defined as follows:

$D_N = \max| S_N(x) - F(x) |$ over the range of the sample, is the Kolmogorov-Smirnov statistic. It is the maximum departure of the two curves from one another. Clearly, a small D_N will correspond to a close fit. This is a useful measure, since it is distribution-free in the sense that D_N does not depend on F (provided F is continuous) and its sampling distribution is known, allowing probabilities to be established for inference purposes. Kolmogorov(1933) found that the probability of a given D_N being less than a certain z was:

$$\lim_{N\to\infty} P\left[D_N < \frac{z}{\sqrt{N}}\right] = L(z)$$

where $L(z) = 1-2\sum_{i=0}^{\infty}(-1)^{i-1}e^{-2i^2z^2}$

and for larger N, the approximation becomes more exact. Thus we can proceed to test models using the Kolmogorov-Smirnov test statistic and

reject a model that fails to provide a significant fit. See Press et al(1986) and Gibbons(1971) for further details of this theory.

The Kolmogorov-Smirnov test uses ungrouped data so we are making the most complete use of the entire data sample. Another advantage is that the D_N sampling distribution is known accurately and tabulated, whereas the corresponding situation for the chi-squared test (see below in Appendix A2) is only approximate.

APPENDIX A2. THE CHI-SQUARED TEST

This is an alternative goodness of fit test, but is not restricted to cumulative distributions. It requires the data to be grouped, but can be applied to multi-variate samples, provided each bin has a sufficient occupancy to make the analysis rigorous. Usually we insist on at least 5 'points' in each bin. One has an observed sample and a theoretical prediction for the functional form of the distribution of this data. The null hypothesis to be tested is again 'the two distributions are identical'. Denoting the observed occupancy in the i^{th} by m_i, and the predicted occupancy by n_i we define

$$X^2 = \sum_{i=1}^{\nu} \frac{(m_i - n_i)^2}{n_i}$$

It can be shown, that for sufficiently high ν, that this quantity is distributed according to the chi-squared distribution with ν-1 degrees of freedom, hence the notation. By insisting that the predicted total occupancy is the same as the total sample size the number of degress of freedom is thus ν-1 instead of ν. Clearly, a large value of χ^2 will be incompatible with the null hypothesis, which would consequently be rejected. In the case of t additional free parameters of the model also being fitted the number of degrees of freedom falls by one for each additional parameter. To put this on a rigorous footing, the

probability of a χ^2 occurring by chance for a particular ν can be found and for a given level of significance α, we would reject the null hypothesis if $\chi^2 > \chi^2_{\alpha,\nu-t-1}$ or $\chi^2 < \chi^2_{1-\alpha,\nu-t-1}$. This is a one-tailed test. The associated probability $P(\chi^2|\nu)$ is a special case of the incomplete gamma function. One can also perform a so-called two-tailed test, which is more appropriate if the user is reluctant to reject the null hypothesis(Strait(1989).

The chi-squared test is distribution-free in the sense that it applies to all distributions (Strait(1989).

APPENDIX A3.

THE BIVARIATE NORMAL DISTRIBUTION.

For two random variables x and y, the bivariate normal distribution takes the form:

$$N(x,y) = (2\pi\sigma_2\sigma_3\sqrt{(1-\rho^2)})^{-1}.\ \exp\{-Q(x,y)/2(1-\rho^2)\} \qquad (A3.1)$$

where Q is a quadratic form in x and y of the form:

$$Q(x,y) = (x-\mu_x)^2/\sigma_x^2 + (y-\mu_y)^2/\sigma_y^2 - 2\rho(x-\mu_x)(y-\mu_y)/\sigma_x\sigma_y \qquad (A3.2)$$

Here μ_x, μ_y are respectively the mean values of x and y, σ_x^2 and σ_y^2 the variances in x and y and ρ the correlation parameter, which must be in the range (-1,1). The constant outside the exponential is chosen so that the distribution is normalised to unity.

Since the distribution is symmetrical in x and y, any result applying to the marginal distribution of x will equally apply to that of y, with an appropriate switch of subscripts x →y and y →x. It can be shown that the distribution of x alone, the marginal distribution, which is a univariate normal is given by

$N(x) = (2\pi\sigma_x^2)^{-1/2} \exp\{-(x-\mu_x)^2/2\sigma_x^2)\}$ independent of μ_y, σ_y and ρ.

We now wish to prove a result that is needed in Chapters 4-6. This will be called Theorem 1.

THEOREM 1.

$$\exp(\alpha x).\exp\{-(x-\mu)^2/2\sigma^2\} = \exp\left[-(x-\bar{\mu})^2/2\sigma^2\right] + \beta$$

where $\bar{\mu} = \mu + \alpha\sigma^2$ and $\beta = \alpha(\mu + \alpha\sigma^2/2)$

Proof. $$\exp(\alpha x)\exp\{-(x-\mu)^2/2\sigma^2\} = \exp\left[-(x-\mu)^2 + 2\alpha x\sigma^2/2\sigma^2\right]$$

$$= \exp\left[-(x^2-2\mu x+\mu^2-2\sigma^2\alpha x)/2\sigma^2\right]$$

$$= \exp\left[-(x-(\mu+\sigma^2\alpha))^2-2\mu\sigma^2\alpha-\sigma^4\alpha^2/2\sigma^2\right]$$

$$= \exp\left[-(x-\bar{\mu})^2/2\sigma^2 + \beta\right] \quad \text{Q.E.D.}$$

Thus by multiplying a normal distribution function in x by exp(αx) we again obtain a normal distribution in x with a new mean and a new normalisation constant.

Now a second Theorem will be proved, also required for Chapters 4-6. This gives the expression analogous to Theorem 1 for multiplying a bivariate normal distribution N(x,y) by a factor exp(εy). Here, the parameters of the bivariate normal are η and μ (means), σ_x^2 and σ_y^2 (variances) and correlation ρ. ε is a constant.

Theorem 2. $$\exp(\epsilon x).N(x,y) = \exp\left[-A^2/2 - (y-\bar{\mu})^2/\gamma\sigma_y^2 + \mu\epsilon + \rho A\sigma^2\epsilon + \gamma\sigma^2\epsilon^2/4\right]$$

where $A = (x-\eta)/\sigma_x$; $\gamma = 2(1-\rho^2)^{1/2}$; $\bar{\mu} = \mu + \frac{\sigma_y^2}{2}(\gamma\epsilon + \frac{2\rho A}{\sigma_y})$

Proof. The exponent of the bivariate part is as given above in A3.2: Combining all the exponents together we get:

$$E = \frac{A^2 + (y-\mu)^2\sigma_y^2 - 2\rho A(y-\mu)/\sigma_y - \epsilon\gamma y}{-\gamma} \qquad \text{in the above notation}$$

$$= \frac{-A^2}{\gamma} - \frac{2\rho A\mu}{\gamma\sigma_y} - \frac{(y-\mu)^2}{\gamma\sigma_y^2} + \frac{y(\epsilon\gamma+2\rho A/\sigma_y)}{\gamma}$$

Define $\bar{\mu} = \mu + \sigma_y^2(\epsilon\gamma+2\rho A/\sigma_y)/2$

Thus $$E = \frac{-A^2}{\gamma} - \frac{(y-\bar{\mu})^2}{\gamma\sigma_y^2} - \frac{2\rho A\mu}{\gamma\sigma_y} + \frac{\bar{\mu}^2 - \mu^2}{\gamma\sigma_y^2}$$

$$E = \frac{-A^2}{2} - \frac{(y-\bar{\mu})^2}{\gamma\sigma_y^2} + \mu\epsilon + \rho A\epsilon\sigma_y + \frac{\gamma\epsilon^2\sigma_y^2}{4}$$

which was the desired result.

APPENDIX A4. CORRELATION COEFFICIENTS.

Correlation is a statistical measure of association between two variables. The degree of association is usually indicated by assigning a coefficient of correlation, defined by a formula which utilises the data in pairs of the form (x_i,y_i).

A4.1 Pearson's linear correlation coefficient.

The most commonly used is Pearson's linear correlation coefficient, which is defined as:

$$r = \frac{\Sigma_i(x_i-\bar{x}).(y_i-\bar{y})}{\sqrt{\{\Sigma_i(x_i-\bar{x})^2\,\Sigma_i(y_i-\bar{y})^2\}}} \qquad (A4.1)$$

here $\bar{x}$ and $\bar{y}$ are the means of the x_i and y_i respectively, and Σ_i denotes the sum from i=1 to i=N.

The value of r indicates the degree of correlation.

(a) r = 0 → No correlation, x and y independently distributed

(b) r = +1 → Perfect positive correlation, (x_i,y_i) lie on straight line of positive gradient.

(c) r = -1 → Perfect negative correlation, $(x_i,y_i$ lie on straight line of

negative gradient.

The slope of the lines in (b) and (c) does not influence the value of r. In practice, we usually encounter values of r in the range between -1 and +1.

When a correlation is present, r gives a measure of its strength. However, it is difficult to assess the significance of a given value of r. (Press et al(1986)). r takes no account of the distributions of x and y, thus one cannot compute its distribution in the case of the null hypothesis. What can be assumed, is that for well-behaved distributions of x and y, and sufficiently large samples, r is approximately normally distributed, with a mean of zero and a standard deviation of $1/(\sqrt{N})$, for N data points. The significance then turns out to be $\mathrm{erfc}\{ |r|\sqrt{(N/2)} \}$, for the complementary error function erfc, where $\mathrm{erfc}(0)=1$. However, this renders r useful only in the case where the x and y data are not too far from being binormally distributed. Interpreting the r statistic can be meaningless if the data come from a widely different distribution.

A4.2 Spearman's correlation coefficient.

The difficulties inherent in the Pearson statistic can be circumvented by the introduction of a non-parametric correlation coefficient. This is also called rank correlation since one replaces the (x_i,y_i) pairs by their ranks which will be numbers in the range 1,2,....,N so the distribution of the ranks is perfectly known. This is the usefulness of rank correlation. There is some loss of information, since we have replaced the data by either integers or half-integers, but when a correlation is found, it is guaranteed to be real, to a sensitivity level that depends on the significance chosen [Press et al(1986)]. In statisitical parlance, it is a more robust technique, and less sensitive

to the form of the underlying distribution characterising the data. The particular case we shall use is the Spearman rank-order correlation coefficient, r_s, defined

as the linear correlation coefficient of the ranks of the x_i amd y_i. That is, if R_i and S_i are the ranks of the pair (x_i,y_i) then

$$r_s = \frac{\Sigma_i(R_i - \bar{R})(S_i - \bar{S})}{\sqrt{\{\Sigma_i(R_i - \bar{R})^2 \Sigma_i(S_i - \bar{S})^2\}}}$$

where Σ_i denotes the sum from i=1 to i=N.

The significance of a value of r_s can be found by evaluating t, where

$$t = r_s \left[\frac{(N-2)}{1-r_s^2} \right]^{0.5}$$

which is distributed approximately as Student's distribution with N-2 degrees of freedom. It is in fact a good approximation for all possible distributions of x_i and y_i.

We shall use both these measures of correlation when analysing the pulsar data. It can be seen that the non-parametric measure will give identical answers for both (x_i,y_i) and $(\ln(x_i),\ln(y_i))$ which can be useful.

APPENDIX A5. DEATHLINE TRANSFORMATIONS

In this Appendix we shall demonstrate how the role of the deathline is significant not only in the $P,\dot{P}$ diagram but for any plot of quantities depending on P and $\dot{P}$. This will apply if the deathline is a genuine cutoff for pulse production or due to selection effects, and if, as suggested by Model 1, Chapter 4, is due to the finite age of the galaxy. We represent the deathline by a power law relation between $\dot{P}$ and P, namely

$$\dot{P} = c\,P^{a} \qquad \text{(A5.1)}$$

so that $\ln(\dot{P}) = \ln(c) + a\ln(P)$ (A5.2)

For example, choose two new variables to be $X = P/\dot{P}$ and $Y = P\dot{P}$, so that X represents age and Y the field strength in the standard model. Thus:

$P = (XY)^{0.5}$ and $\dot{P} = (Y/X)^{0.5}$. So (A5.1) becomes:

$$\sqrt{(Y/X)} = c\,(XY)^{a/2} \qquad \text{(A5.3)}$$

Rearranging, we get : $\dfrac{(1-a)}{2}\ln(Y) = \ln(c) + \dfrac{(1+a)}{2}\ln(X)$

so $\ln(Y) = \ln(c') + \dfrac{(1+a)\ln(X)}{(1-a)}$ (A5.4)

This applies for $a \neq 1$. Thus the deathline transforms to a constraint in the X,Y plane. When $a = 3$, as implied by the cutoff used by Stollmann(1987b) and when $a = 5$, as discussd in Michel(1982) we get -2 and -3/2 respectively for the new gradient: e.g. when $a = 3$, $\ln(Y) \leqslant \ln(c') - 2\ln(X)$, which forces the pulsars to lie below this line. Interpreted at face value, it implies older pulsars have lower fields, but this has made no assumption as to field decay at all. Similar effects will be found if, for example, luminosity is plotted against a function of P and $\dot{P}$, so care must be taken at all times in these situations.

APPENDIX A6. PULSAR CURRENTS

In the work of Narayan and Vivekanand(1981), Narayan and Vivekanand(1981) and Narayan(1987), and elsewhere, the concept of pulsar current has been invoked to justify the idea of 'injection' of pulsars, that is the birth of pulsars at intermediate periods $\triangleq$ 0.5 secs, or equivalently, a delay in the onset of the pulsar phenomenon until

the neutron star has spundown to these periods, having been created at faster rotation rates. The claim has been made that this is a model independent argument, and does not depend on the effects of luminosity selection. We will show in this appendix that the pulsar current can peak at intermediate periods for the observed sample although all pulsars are actually created at a much shorter period, say 10 msec. This argument proceeds as follows: we adopt the simple model formalism of Chapter 4, in which pulsar fields do not decay and no alignment occurs. We choose the same source term as used elsewhere, so all pulsars are created at the same period of 10 msec. The derived observed distribution of P and $\dot{P}$ is, from Chapter 4;

$$n_{obs}(y_1,y_2;t) = \lambda e^{y_1(1+\alpha)+y_2(\beta-1)-A^2/2+\rho A\sigma_3} H(y_1-\ln(Q))H(t)\Big|_{y_1=\ln Q} \qquad (A5.1)$$

where the notation is that of Chapter 4, so $y_1 = \ln(P)$, $y_2 = \ln(\dot{P})$. The pulsar current, is by definition, [Narayan(1987)],

$$J(y_1) = \int_{y_{2min}}^{\infty} \dot{y}_1 \, n_{obs}(y_1,y_2)\, dy_2 \qquad (A5.2)$$

and represents the flow of pulsars from periods below y_1 to higher values. Here y_{2min} is the 'deathline' term, as derived in Chapter 4. The integral in (A5.2) can be found analytically to be:

$$J(y_1) = \lambda' e^{y_1(\alpha-\beta)} \operatorname{erfc}\left[\frac{y_{2min}-\mu_2+y_1-\beta\sigma_2{}^2-\rho\sigma_3\sigma_2}{\sqrt{2}.\ \sigma_2}\right] H(y_1-\ln Q) \qquad (A5.3)$$

where λ' is a constant, erfc(x) is the normal complementary error function, the parameters σ_2, σ_3, ρ and μ_2 are from the bivariate normal for k,δ in the source term and α and β from the luminosity law. It is clear from (A5.3) that if $\alpha-\beta > 0$ then this function of y_1 will reach a peak and then fall off as y_1 rises further, due to the erfc factor. This 'maximum' current can occur at different y_1 depending on

the particular parameters that are chosen. Therefore, if this model were a realistic description of the $P,\dot{P}$ diagram, (it does not matter that we now know from Chapter 4 it is not), and $\alpha-\beta$ did satisfy the condition $\alpha-\beta > 0$ (Note α and β are unknown) then pulsar injection would be inferred from the peak in the pulsar current, although the true situation is that all pulsars are actually created at fast periods. This serves to emphasise the distortions created by selection and the danger of reaching spurious conclusions from arguments that are not truly model independent, and subject to selection effects that are difficult to quantify accurately.

APPENDIX A7. INVERSE PROBLEMS

A7.1 Introduction.

This is a type of problem that can arise which is addressable by the time-dependent continuity equation method. An unknown distribution occurring within an integral which gives an observed distribution can formally be solved in some of the simplest cases by differentiating the known distribution to obtain an expression for the desired unknown density. We can observe the distribution in period, or find a suitable analytic form to describe the data. This, algebraically, in the simple case, is the solution of

$$f(x) = \int_{-\infty}^{h(x)} g(y)\, dy \qquad (A7.1)$$

for the unknown function g(y), which is obtained by differentiation:

$$\frac{df(x)}{dx} = g[\, h(x)\,] \qquad (A7.2)$$

Here, h(x) is a limit found from the analyses as above e.g.

$P_{max}(k,t) = \sqrt{(2kt)}$ in the simple model. See Craig and Brown(1982) for a review of inverse problems in the astrophysics context,

and the difficulties inherent in their solution in the presence of noisy data.

As an illustration of the potential application of the inverse problem strategy to pulsar evolution, we will look at two particular problems of solving for the source function, given the observed period distribution. The first problem is to find an unknown distribution in the birth-periods of pulsars (relevant to the injection arguments of Chapter 2), the second to obtain the unknown distribution in magnetic field, which is often assumed to be a gaussian in the logarithm of B, the field strength.

A7.2 Inversion to find unknown period distribution.

We assume that pulsars are born with a single value of magnetic torque, k but with periods according to the distribution C(P), which is to be determined. For simplicity, we look at the simple model of pulsar spindown, as outlined in Chapter 4. This is not expected to be a realistic description of the data, but is intended to show the method of solution and the possible use for more complicated and descriptive models.

For convenience we use the variable $z = P^2$, since from equation 4.1, with $n = 3$, the constant of motion is P^2-2kt. We assume a source function of the form:

Source term = $C(z)\,H(t)$ (A7.3)

where C(z) is the distribution to be found, and, as before, H(t) is a Heaviside step function which allows pulsar birth to commence at t = 0. The spindown law is now

$\dot{z} = 2k$ such that $z = z_0 + 2k(t-t_0)$, (A7.4)

where k is the universal value of magnetic torque. The continuity equation gives the solution:

$$n_{obs}(z) = \frac{\varsigma z^{\alpha}}{2k} \int_{0}^{z_0} C(z)\, dz \qquad 0 \leqslant z_0 \leqslant 2kt_0$$

$$n_{obs}(z) = \frac{\varsigma z^{\alpha}}{2k} \int_{z_0-2kt_0}^{z_0} C(z)\, dz \qquad z_0 > 2kt_0 \qquad \text{(A7.5)}$$

for a luminosity law $L = \varsigma P^{\alpha}$, for index α, which has to be assumed known for this problem. It is easiest to group all the known terms on the left-hand side, into a function $f(z_0)$ which is defined as:

$$f(z_0) = n_{obs}(z_0) \cdot 2kz^{-\alpha}/\varsigma = \int C(z)\, dz \qquad \text{(A7.6)}$$

where the limits depend on z_0 and $2kt_0$ as in (A7.5), and f is known.

So, formally, $f'(z_0) = C(z_0)$ when $0 \leqslant z_0 \leqslant 2kt_0$ (A7.7)

and $f'(z_0) = C(z_0) - C(z_0 - 2kt_0)$ when $z_0 > 2kt_0$ (A7.8)

where $f'(z_0)$ is the derivative of f with respect to z_0.

So, in general, $C(z_0) = \sum_{i=0}^{\infty} f'(z_0 - i.\, 2kt_0)\, H(z_0 - i.2kt_0)$ (A7.9)

where H again is the Heaviside step function. (Interestingly, this is identical to the solution found by MacKinnon and Brown(1989) for a solar physics problem of nonthermal hard X-ray source models.) There are two possible strategies that can be adopted: one is to use an analytic form for the function f that matches the observed data to at least an approximate level, the second retains the discrete nature of our knowledge of f and inverts to give the desired C(z) in similar discrete form. In both cases the 'parameter' $2kt_0$ must be determined, as this governs the difference between the two expressions for integral limits. If $2kt_0$ turns out to be small, say less than 1 sec, then pulsar birth at long periods is inevitable. We can estimate $2kt_0$ by proceeding to use solution (A7.7) until the derived C(z) goes negative,

which indicates z has exceeded $2kt_0$, so the analysis restarts from the first estimate of $2kt_0$ and uses the new values of f'(z) to proceed.

In practice, applying this to the real data yields no satisfactory solution. The derived C(z) does not tend to fall with larger periods, as one would expect. The lack of short-period pulsars gives poor knowledge of f(z) and consequent poorer certainty on its derivative. The most likely reason for this is that the simplicity of the model is such that it is not consistent with the observed data. This should not deter us from realising the potential of the inverse problem approach, but we note the reservations of Phinney and Blandford(1981), who studied pulsar evolution using the continuity equation and showed that a direct determination of the source term was impossible from the existing data sample, although they did not appear to acknowledge the importance of selection effects in their work.

A7.3 Inversion to find the magnetic torque distribution.

A second problem of a similar nature is to establish the source term which gives the distribution of initial torques, K(k) in the notation of Chapter 3. Again we will restrict attention to the simple model spindown law. From equation (3.21) we get :

$$N(P,k,t) = c_0 k^{-1} P\, K(k)\, H(P-Q) H(t)\big|_{P=Q} \qquad (A7.10)$$

for the intrinsic distribution in P and k. We assume a luminosity law of $L = \mathcal{E}P^{\alpha}$, so that the observed period distribution is:

$$N_{obs}(P,\, t) = \frac{c_0 B.\, P^{1+\alpha}}{4F_{min}} \int_{k_{min}}^{\infty} K(k)\, dk \qquad (A7.11)$$

where B is the beaming fraction and is constant, and k_{min} is the lowest value of k compatible with a given P and t, namely:

$$k_{min} = \frac{P^2 - Q^2}{2t} \qquad (A7.12)$$

and is a consequence of time-dependence. We regroup all the known factors on the left-hand side as before, so getting:

$$G(P) = \frac{4F_{min}N_{obs}(P)}{Bc_0 \varepsilon P^{\alpha}} = \int_{k_{min}}^{\infty} K(k)\, dk \qquad (A7.13)$$

Thus we differentiate (dash' notation) with respect to P to get:

$$G'(P) = - K(k_{min})\, k_{min}^{-1}.P/t \qquad (A7.14)$$

Thus using (A7.12) in (A7.14) we get the distribution for k. Again, to get a practical solution requires the analytic knowledge of G(P). This is again subject to the same problems as the first problem, namely our ignorance of accurate values for G'(P), which is a major drawback.

REFERENCES

Ables,J.G., McConnell,D., Jacka,C.E., McCulloch,P.M., Hall,P.J. and Hamilton,P.A. 1989 Nature,**342**,6246,158

Allakhverdiyev,A.O.,Guseinov,O.H. and Yusifov,I.M. 1987 Aust. J. Phys. ,**40**,837

Alpar,M.A., Cheng,A.F., Ruderman,M.A. and Shaham,J.A. 1982 Nature, **300**,728

Anderson,B. and Lyne,A.G. 1983, Nature, **303**,597

Applegate,J.H., Blandford,R.D. and Hernquist,L. 1984 in 'Proceedings of Green Bank Workshop on millisecond pulsars', Ed. by Reynolds,S. and Stinebring,D.R.

Arnaud,M. and Rothenflug,R. 1981 Astron. and Astrophys.,**103**,263

Arnett,W.D. and Bowers,R.L. 1977 Astrophys. J. Supp. **33**,415

Arnett,W.D. and Lerche,I. 1981 Astron. and Astrophys.,**95**,308

Baade,W. and Zwicky,F. 1934 Phys. Rev. **45**,138

Backer,D.C. 1976 Astrophys. J.,**209**,895

Backer,D.C., Kulkarni,S.R., Heiles,C., Davis,M.M. and Goss,M. 1982 Nature,**300**,675

Baym,G. and Pethick,C.J. 1979 Ann. Rev.Astron. Astrphys., **17**,415

Baym,G. , Pethick,C.J. and Sutherland,P. 1971 Astrophys. J.,**170**,307

Becker,R.H. 1987 pp91-97 in IAU Syposium No. **125**, Ed. by Helfand,D. and Huang,J.H. [Reidel]

Beskin,V.S., Gurevich,A.V. and Istomin,Ya.N. 1983 Sov.Phys JETP. **58**,2

Beskin,V.S., Gurevich,A.V. and Istomin,Ya,N. 1984 Astrophys.Sp.Sci, **102**,301

Bethe,H. and Brown,G. 1988 in Scientific American, **252**,5,60

Bethe,H. and Johnson,A. 1974 Nucl. Phys. **A230**,1

Biggs, J.D. 1990 Non. Not. Roy. Astron. Soc.,**245**,3,514

Biggs, and Lyne,A.G. 1988 Mon. Not. Roy. Astron. Soc., **235**,1,255

Blandford,R.D., Applegate,J.H. and Hernquist,L. 1983 Mon. Not. Roy. Astron. Soc., **204**,1025

Blandford,R.D. and Romani, 1988 Mon. Not. Roy. Astron. Soc.,**234**,3,57

Boynton,P., Groth,E., Hutchinson,D., Partridge,R. and Wilkinson,D. 1972, Astrophys. J. **175**, 217

Brecher,K. and Chanmugam,G. 1983 Nature,**302**,5904

Candy,B.N. and Blair,D.G. 1983 Mon.Not.Roy.Astron.Soc.,**205**,281

Candy,B.N.,and Blair,D.G. 1987 Astron. and Astrophys.,**183**,L17

Candy,B.N. and Blair,D.G. 1986 Astrophys.J.,**307**,535

Canuto, V. 1970 Astrophys. J. **159**,641

Chau,W.Y. and Henriksen,R.N. 1970 Astrophys. J. **161**,L137

Cheng,A.F. 1985 Astrophys.J.,**299**,917

Cheng,A.F. 1989 Astrophys.J. **337**,803

Chevalier,R.A. and Emmering,R.T. 1986 Astrophys.J.,**304**,140

Clifton,T.R. and Lyne,A.G. 1986 Nature,**320**,43

Cordes,J.M. 1986 Astrophys.J.,**311**,183

Cordes,J.M. 1987 in IAU Symposium No. **125**, pp35-46, Ed. by D.Helfand and J.-H. Huang, [Reidel].

Craig, I.J.D. and Brown, J.C. 1986 'Inverse problems in Astronomy' (Adam Hilger)

Damashek,M., Taylor,J.H., Backus,P.R. and Burkhardt,R. 1982 Astrophys. J. Lett. **253**,L57

Davis,M.M., Taylor,J.H., Weisberg,J.M., and Backer,D.C. 1985 Nature **315**,547

Davis,L. and Goldstein,M. 1970 **159**,L81

De Jager,O.C. and Nel,H.I. 1988 Astron. and Astrophys.,**190**,87

Dewey,R.J., Stokes,G.H., Segelstein,D.J., Taylor,J.H. and Weisberg,J.M.

1984 in 'Proceedings of Green Bank Workshop on millisecond pulsars', Ed. by Reynolds,S. and Stinebring,D.R.

Dewey,R.J., Taylor,J.H.,Maguire,C.M. and Stokes,G.H. 1988 Astrophys.J., **332**,762

Emmering,R.T. and Chevalier,R.A. 1989 ,Astrophys.J.,**345**,931

Ewart,G.M., Guyer,R.A. and Greenstein,G. 1975 Astrophys.J.,**202**,238

Fitzpatrick, R. and Mestel, L. 1988a Mon. Not. Roy. Astron. Soc. **232**,2,277

Fitzpatrick, R. and Mestel, L. 1988b Mon. Not. Roy. Astron. Soc. **232**,2,303

Flowers,E. and Ruderman,M.A. 1977 Astrophys.J.,**215**,302

Fokker,A.D. 1987 Astron. and Astrophys.,**182**,41

Friedman,J.L. 1983 Phys.Rev.Lett.,**51**,1

Friedman,J.L. and Schutz,B.F. 1975 Astrophys.J. **199**,L157

Friedman,J.L., Ipser,J.R. and Parker,L. 1986 Astrophys.J. **304**,115

Friedman,J.L. and Pandharipande,V.R. 1981 Nucl. Phys. **A361**,502

Fujimara.F.S. and Kennel,C.F. 1980 Astrophys. J., **236**,245

Gailly,J.L., Lequeux,J. and Masnou,J.L. 1978 Astron. and Astrophys.,**70**,L15

Gibbons,J.D. 1971 'Nonparametric statistical inference', McGraw-Hill Inc.

Glendenning,N.K. 1988 Phys. Rev. C, **37**,6,2733

Gold,T. 1968 Nature,**218**,731

Goldreich,P. and Julian,W.H. 1969 Astrophys.J.,**157**,869

Goldreich,P. and Julian,W.H. 1970 Astrophys,J.,**160**,L11

Gunn,J.E. and Ostriker,J.P. 1969 Nature, **302**,5904

Gunn,J.E. and Ostriker,J.P. 1970 Astrophys.J.,**160**,979

Greenstein,G. 1972 Astrophys. J.,**177**,251

Greenstein,G. 1981 in IAU Symposium No.**95**, p291 Ed. by Sieber,W.

and Wielibinski,R.[Reidel]

Greiner,J. and Wiebicke,H.J. 1990 Astro. Lett and Communications, Vol **27**, pp381-384

Groth,E.J. 1975a Astrophys.J. **200**,278

Groth,E.J. 1975b Astrophys.J. Suppl.,**29**,453

Hanson,R.B. 1979a Mon.Not.Roy.Astron.Soc.,**186**,2,357

Hanson,R.B. 1979b Mon.Not.Roy.Astron.Soc.,**186**,3,875

Harding,A.K. 1984 in 'Proceedings of Green Bank Workshop on Millisecond Pulsars',pp,Ed. by Reynolds,S. and Stinebring,D.R.

Harding,A.K. and Harding,D.S. 1982 Astrophys.J.,**257**,603

Heintzmann,H. 1981 Nature,**292**,811

Helfand,D.J. and Tademaru,E. 1977 Astrophys.J.,**216**,842

Henry,G.R. and Paik,H.-J. 1969 Nature,**224**,5225

Hewish,A., Bell,S.J., Pilkington,J.D.H., Scott,P.F. and Collins,R.A. 1968 Nature **217**,709

Hills,J.G. 1978 Astrophys.J.,**221**,973

Hulse,R.A. and Taylor,J.H. 1975 Astrophys.J. Lett., **195**,L51

Jones,P.B. 1976 Astrophys. J.,**209**,602

Jones,P.B. 1980 Astrophys.J. **231**,661

Kassim,N.E. and Weiler,K.W. 1990 Nature, **343**,6254,146

Krishnamohan,S. 1985 Mon.Not.Roy.Astron.Soc,**214**,15P

Krolak,A. 1988 in 'Proceedings of NARW on Gravitational Wave Data Analysis' at Cardiff, 1987, ed. by B.F. Schutz [Kluwer]

Krolak,A. and Schutz,B.Z. 1988 Gen. Rel. Gravit., **19**,1163

Kulkarni,S.R. 1985 Astrophys.J. **306**,L85

Kulkarni,S. and Narayan,R. 1988 Astrophys.J.**335**,755

Kundt,W. 1981 Astron. and Astrophys.,**98**,207

Kundt,W. 1988 Comments. Astrophys.,Vol. **12**,3

Lamb,F.K. 1981 in IAU Symposium No **95**, pp303-319 Ed. by Sieber,W. and Wielibinski,R. [Reidel]

Large,M.I. 1971 p165 in IAU Symposium No. 46 on the Crab Nebula, Ed. by Davies,R.D. and Smith,F.G.

Large,M.I. and Vaughan,A.E. 1977 Mon. Not. Roy. Astron. Soc. **151**,277

Lee,L.C. and Jokipii,J.R. 1976 Astrophys. J.,**205**,735

Lindblom,L. 1987 Astrophys. J. **303**,146

Lorrain,P. and Corson,D. 1970 in 'Electromagnetic fields and waves', pub. by Freeman, New York.

Lyne,A.G. 1987 pp23-34 in IAU Symposium No. **125**, Ed. by Helfand,D. and Huang,J.-H. [Reidel]

Lyne,A.G. 1989a in IAU Symposium No**140**, pp41-44, Ed. by Beck,R., Kronberg,P.P. and Wielebinski,R. [Reidel]

Lyne,A.G. 1989b in 'Proceedings of the NARW on gravitational wave data analysis', Cardiff, 1987. Ed. by Schutz,B.F. [Kluwer]

Lyne,A.G. 1989c Nature,**342**,6246,128

Lyne,A.G. 1989d Nature **337**,510

Lyne,A.G., Anderson,B. and Salter,M.J. 1982 Mon. Not, Roy. Astron. Soc., **201**,503

Lyne,A.G. and Manchester,R.N. 1988 Mon. Not. Roy. Astron. Soc. **234**,3,477

Lyne,A.G., Manchester,R.N. and Taylor,J.H. 1985 Mon. Not. Roy. Astron. Soc. ,**213**,613

Lyne,A.G., Ritchings,R.T. and Smith,F.G. 1975 Mon. Not. Roy. Astron. Soc, **188**,675

Lyne,A.G. and Smith,F.G. 1979 Mon. Not. Roy. Astron. Soc. **188**,675

Mackinnon,A.L. and Brown,J.C. 1989 Solar Physics,**122**,303

Macy,W.M. 1974 Astrophys.J.,**190**,153

Malofeev,V. and Shitov,Yu.P. 1981 Astrophy.Space. Sci.,**78**,45

Manchester,R.N. and Taylor,J.H. 1977 in 'Pulsars', Pub. by Freeman

Manchester,R.N., Lyne,A.G., Taylor,J.H., Durdin,J.M., Large,M.I. ,Little,A.G. 1978 Mon. Not. Roy. Astron. Soc. **185**,409

Matteuci,F. and Brocato,E. 1990 preprint

Mestel, L. and Ray, T.P. 1985, Mon. Not. Roy. Astron. Soc.,**212**,275

Mestel, L., Robertson, J.A., Wang, Y.-M. and Westfold, K.C. 1985 Mon. Not. Roy. Astron. Soc.,**217**,443

Michel,F.C. 1975 Astrophys.J. **195**,L69

Michel,F.C. 1982 Rev.Mod.Phys.,vol **54**,no.1

Michel,F.C. and Tucker,W.H. 1969 Nature,Vol. **223**,277

Miller,G.E. and Scalo,J.M. 1979 Astrophys.J. Suppl.**41**,513

Mood,A.M. and Graybill,F.A. 1963 'Introduction to the theory of statistics', McGraw-Hill.

Morini,M. 1981 Astron. and Astrophys.,**104**,75

Narayan,R. 1987 Astrophys.J.,**319**,162

Narayan,R. and Ostriker,J.P. 1990 Astrophy.J., **352**,222

Narayan,R. and Vivekanand,M. 1981 Nature,**290**,571

Narayan,R. and Vivekanand,M. 1983 Astron. and Astrophys.,**122**,45

Narayan,R. and Radhakrishnan,V. 1983 Current Sci.,**52**,2

Nelder, S.A. and Mead,R. 1965 Computer Journal, Vol.**7**,308

Neshpor,Yu.I. 1985 Astron. Zh. **62**,408

Nowakowski,L.A. 1983a Astron. and Astrophys.,**118**,29

Nowakowski,L.A. 1983b Astron. and Astrophys.,**127**,259

Ostriker,J.P. and Gunn,J.E. 1969 Astrophys. J.,**157**,1395

Ostriker,J.P.,Richstone,D.O. and Thuan,T.X. 1974 Astrophys.J.,**188**,L87

Pacini,F. 1968 Nature,**219**,145

Pandharipande,V.R. and Smith,R.A. 1975 Nucl. Phys. **A175**,225

Papaliolos,C., Carleton,N.P., and Horowitz,P. 1971 IAU Circ. No**2368**

Phinney,F.S. and Blandford,R.D. 1981 Mon. Not. Roy. Astron. Soc.,**194**,137

Pineault,S. 1986 Astrophys. J. **301**,145

Pines,D. and Alpar,M.A. 1984 in 'Proceedings of Green Bank Workshop on Millisecond Pulsars' Ed. by Reynolds,S. and Stinebring,D.R.

Press,W.H., Flannery,B.P., Teukolsky,S.A. and Vetterling,W.T. 1986 in 'Numerical Recipes', Cambridge University Press

Proszynski,M. 1979 Astron. and Astrophys,**79**,8

Proszynski,M. and Przybcien,D. 1984 in 'Proceedings of Green Bank Workshop on Millisecond Pulsars', Ed by Reynolds,S. and Stinebring,D.R.

Radhakrishnan,V. 1982 in Contemp. Physics Vol.**23**,3

Radhakrishnan,V. 1986 in 'Highlights of Astronomy', ed. by S.-P. Swings pp3-26

Radhakrishnan,V. and Cooke,D.J. 1969 Astrophys.Lett,**3**,225

Radhakrishnan,V. and Manchester,R.N. 1969 Nature,**222**,228

Radhakrishnan,V. and Shukre,C.S. 1987 Bull. Astron. Soc. India, **15**,1,32

Radhakrishnan,V. and Srinivasan,L. 1981 in IAU Symposium No.**95**, p417

Rankin,J. 1990 Astrophys. J.,**352**,250

Reichley,P.E. and Downs,G.S. 1969 Nature, **222**,229

Reichley,P.E. and Downs,G.S. 1970 Nature Phys. Sci. **234**,48

Richter,O.G. and Rosa,M. 1988 Astron. and Astrophys.,**206**,2,219

Roberts,D.H. and Sturrock,P.A. 1972 Astrophys. J.,**173**,L33

Rocca-Volmerange,B. and Schaeffer,R. 1989 preprint

Ruderman,M. 1979 pp427-476 in Ann.Rev.Astron.Astrophys. 1979

Ruderman,M.A. and Sutherland,P.G. 1975 Astrophys. J.,**196**,51

Salvati,M. and Pacini,F. 1987 p77 in IAU Symposium No **125**,Ed. by

Helfand,D. and Huang,J.-H. [Reidel]

Sang,Y. and Chanmugam,G. 1987 Astrophys.J. **323**,L61

Scalo,J.M. 1979 Fund.Cosmic.Phys., **11**,1

Scargle,J. and Pacini,F. 1971 Nat. Phys. Sci. **232**,144

Schutz,B.F. 1987 from text of talk to International Symposium on Experimental Gravitational Physics.

Schutz,B.F. 1989 in 'Proceedings of the N.A.R.W. on Gravitational Wave Data Analysis' , ed. by Schutz,B.F. [Kluwer]

Shapiro,S.L. and Teulolsky,S.A. 1986 in 'Highlights of Modern Astrophysics', (Wiley Interscience)

Shipman,H.L. and Green,R.F. 1980 Astrophys.J.,**239**,L111

Solinger, A. 1969 Astrophys. J. **164**,553

Stokes,G.H., Segelstein,D.J., Taylor,J.H. and Dewey,R.J. 1986 Astrophys.J.,**311**,694

Stollmann,G.M. 1986a Astron. and Astrophys.,**162**,87

Stollmann,G.M. 1986b Astron. and Astrophys.,**170**,48

Stollmann,G.M. 1987a Astron. and Astrophys.,**171**,152

Stollmann,G.H. 1987b Astron. and Astrophys.,**178**,143

Stollmann,G.H. and Van Den Heuvel,E.P.J. 1986 Astron. and Astrophys., **162**,87

Strait,P.T. 1989 'Probability and Statistics with applications', 2nd edition, [Harcourt Brace Jovanovich]

Taam,R.E. and Van den Heuvel,E.P.J. 1986 Astrophys.J.,**305**,235

Taylor,J.H. 1987 pp467-477 in 'Proceedings of 13th Texas Symposium on Relativistic Astrophysics', Ed. by M.P. Ulmer, World Scientific

Taylor,J.H. and Stinebring,D.R. 1986 pp285-328 in Ann. Rev. Astron. and Astrophys.,Vo**124**.

Tinsley,B.M. 1980 Fund. Cosmic. Physics ,**5**,287

Trumper, J., Pietsch, W., Reppin,C., Voges, W., Staubert,R. and Kendizzora,E. 1978 Astrophys.J. Lett. **219**, L105

Van den Bergh,S., McClure,R.D. and Evans,R. 1987 Astrophys.J. **323**,1,44

Van den Bergh,S. 1988 in Proceedings of the ESO Workshop on SN1987A at Garching, Ed. by I.J. Danziger

Vivekanand,M. and Narayan,R. 1981 J. Astrophys. Astr **2**,315

Vivekanand, M. and Narayan, R. 1982 J. Astrophys. Astron.,**3**,399

Vivekanand,M., Narayan,R. and Radhakrishnan,V. 1982 J. Astrophys. Astron.,**3**,237

Wang,Y.-M. and Robnik,M. 1982 Astron. and Astrophys.,**107**,222

Wolszczan,A., Kulkarni,S.R., Middleditch,J., Backer,D.C., Fruchter,A.S. and Dewey,R.J. 1989 Nature,**337**,510

Woosley,S. and Weaver,T. 1989 Scientific American,**261**,2,24

Xinji,Wu and Leahy,D.A. 1989 Acta Astronomica Sinica,**9**,3